8-2017

Robust Geotechnical Design Optimization of Retaining Walls and Levees

Parishad Rahbari
Clemson University, parishadrahbari@gmail.com

ROBUST GEOTECHNICAL DESIGN OPTIMIZATION OF RETAINING WALLS AND LEVEES

A Dissertation
Presented to
the Graduate School of
Clemson University

In Partial Fulfillment
of the Requirements for the Degree
Doctor of Philosophy
Civil Engineering

---

by
Parishad Rahbari
August 2017

Accepted by:
Dr. Nadarajah Ravichandran, Committee Chair
Dr. C. Hsein Juang
Dr. Abdul Khan
Dr. Weichiang Pang

ABSTRACT

This dissertation presents a robust geotechnical design optimization framework for retaining walls with sand backfill and lightweight shredded tire backfill subjected to earthquake load, and I-wall levee systems supported by sand foundation and clay foundation subjected to flood. The responses of retaining walls and levee systems are highly uncertain especially when subjected to natural disasters such as earthquake and flooding. The variations in the response of these systems are caused by the uncertainties associated with not only the soil properties, but also the loads induced by earthquake and flood. These critical systems must show satisfactory performance under these uncertainties because their failure may result in loss of life and property as noted in the past events. Therefore, in this study, the uncertainties in engineering properties of soils (backfill in retaining walls, levee fill and foundation in I-wall levee systems) were considered systematically along with the uncertainty in the external loads (earthquake in retaining walls and flooding in I-wall levee systems). The key design variables of these two systems were determined and based on their ranges several design cases were generated. Fully coupled finite element analyses were performed for computing responses of concern accurately, and appropriate response surfaces were developed for the respective responses of concern. Using the response surface and via a genetic algorithm code, the designs of these systems were optimized to cost and robustness while satisfying the safety constraints. Sets of preferred designs, known as Pareto fronts, were captured through the bi-objective robust optimizations that can be used as a decision-making tool for selecting the suitable design in engineering practice.

DEDICATION

To my parents and my sisters,

for their unconditional love.

ACKNOWLEDGMENT

I would like to express my deepest gratitude to my advisor, Dr. Nadarajah Ravichadran, for his excellent support, guidance, patience and constructive comments throughout my PhD program at Clemson University. I would like to thank my co-adviser, Dr. C. Hsein Juang for his support and invaluable guidance in robust design in Geotechnical Engineering. I am also thankful to committee members, Dr. Abdul Khan and Dr. Weichiang Pang, for their time, feedback and assistance.

I wish to sincerely thank Glenn Department of Civil Engineering for providing consistent support for the Robust Design project without which I would not have been able to complete my dissertation research. Finally, I would like to thank my family and friends at Clemson University, or miles apart, for their kindness and support during my time here.

TABLE OF CONTENTS

TABLE OF FIGURES

TABLE OF TABLES

CHAPTER 1

INTRODUCTION

1.1 OVERVIEW AND MOTIVATION

The response of retaining walls and levee systems is highly uncertain especially when subjected to natural disasters such as earthquake and flooding. The uncertainties associated with these systems exist not only in soil properties, but also in the loads induced by earthquake and flood. Moreover, such critical systems must represent satisfactory performance under these uncertainties because their failure may result in serious consequences such as failures that occurred in levee system of New Orleans during Hurricane Katrina. The long-distance levee systems as those along Mississippi river and Sacramento river are displayed in Figure 1.1, indicating that in addition to massive losses due to the failure of these systems, the cost of construction and rehabilitation is also of great concern.

Therefore, seismic geotechnical design of retaining walls and geotechnical design of I-wall levee systems are of great importance in geotechnical engineering practice. The variation in uncertain input parameters leads to variation in the response of the system (Phoon and Kalhawy 1999). In conventional deterministic design approaches, to cope with these uncertainties and prevent the failure, the concept of factor of safety is adopted and the uncertainties are not included explicitly in the design procedure. On the other hand, in general, in probabilistic design approaches the uncertainties associated with the

system properties and load are considered explicitly and the safety constraints are satisfied using allowable probability of failure or target reliability index.

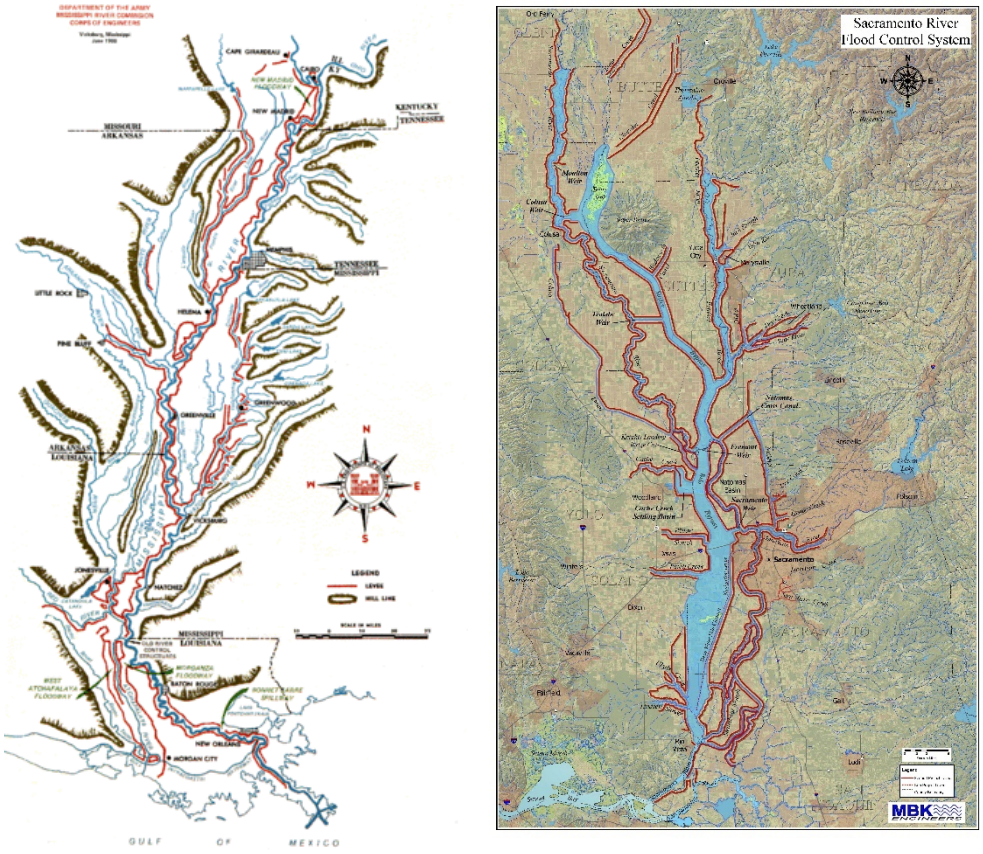

Figure 1.1 The levee systems along Mississippi river on the left, and along Sacramento river on the right

In design optimization process, cost of construction or material usage per unit length for long distance geotechnical structures such as retaining walls and I-wall levee systems is one of the major objectives to be minimized. To avoid underdesign for saving cost or overdesign for satisfying safety performing robust design optimization can be an effective solution.

A robust design which is the least sensitive design to the effect of uncertainties has the response with the least uncertainty. The concept of robust design which was originally presented in field of industrial engineering by Taguchi (1986) has been recently applied in geotechnical engineering. Implementation of robust design in geotechnical engineering was first introduced by Juang et al. (2012). In robust probabilistic design optimization, the design is optimized to robustness and cost considering safety constraints, while deterministic design optimization focuses on optimizing the design to safety and cost and the design robustness is not considered.

In this dissertation, a framework is presented for performing the robust geotechnical design of retaining walls and I-wall levee systems. It should be noted that depending on the geotechnical system response of concern, measure of robustness and safety constraints may differ. In this study, the responses of concern for cantilever retaining walls and I-wall levee systems were assumed to be wall tip deflection (serviceability criteria) and factor of safety of the system (safety criteria), respectively. The measures of robustness for cantilever retaining walls and I-wall levee systems were considered as standard deviation of wall tip deflection and standard deviation of probability of failure of the system, respectively.

1.2 OBJECTIVES

The objectives of this study are to (1) develop a robust geotechnical design optimization framework for retaining walls subjected to earthquake load and I-wall levee system subjected to flood loading by systematically taking into account the uncertainties

while satisfying safety and cost requirements, (2) propose response surfaces for retaining walls and I-wall levee systems to integrate coupled advance finite element analysis with the bi-objective design optimization (3) demonstrate the application of this approach for two type of geotechnical retaining systems: cantilever retaining walls with sand backfill and lightweight shredded tire backfill, and I-wall levee systems supported by sand foundation and clay foundation.

1.3 DISSERTATION ORGANIZATION

The dissertation consists of six chapters. The introduction is presented in current chapter, Chapter 1, to introduce and organize the entire dissertation. Chapters 2 and 3 present the robust geotechnical design optimization framework for cantilever retaining wall with conventional backfill and shredded tire backfill. In Chapters 4 and 5, robust geotechnical design optimization frameworks are presented for I-wall levee systems resting sand foundation and clay foundation. The summary and conclusion of the dissertation is presented in Chapter 6.

In Chapter 2, a robust geotechnical design framework is introduced and applied for the design of cantilever retaining wall subjected to earthquake load in which the robustness against uncertainty in earthquake load is also incorporated, in addition to uncertainty in the granular soil backfill properties. This chapter includes initial design of cantilever retaining wall, determining safe ranges for design variables, selection of uncertain parameters which are friction of sand backfill and peak ground acceleration (PGA) of earthquake load, preparing finite element models for dynamic analysis,

response surface development and validation considering maximum wall tip deflection as the response of concern, optimizing design to cost and robustness and determining final design. In addition to standard deviation of response as robustness measure, signal-to-noise ratio was also considered as robustness measure to examine the optimal final design using Pareto fronts.

In Chapter 3, the robust geotechnical design framework is presented and applied for the design of cantilever retaining wall with lightweight shredded tire backfill subject to earthquake load. Utilizing shredded tire as backfill for cantilever retaining wall is found to be a beneficial approach for recycling wasted tires. This sustainable lightweight backfill is also considered as an economical alternative for conventional soil backfill. Chapter 3 includes determining ranges for design variables performing initial design of cantilever retaining wall with shredded tire backfill, considering friction angle and cohesion of shredded tire and PGA of earthquake load as uncertainties in the system, estimating statistical characterization of shredded tire properties based on survey through existing reports, response surface development using finite element analysis results, optimizing design to cost and robustness along with safety constraints and determining final design.

Chapter 4 presents an uncertainty-based probabilistic framework for design optimization of I-wall levee systems resting on sand foundation. The chapter consists of selection of representative design variables with the ranges and considering friction angle of sand foundation, undrained shear strength of clay levee fill and flood water level as

uncertain parameters, investigating on stability analysis methods and performing limit equilibrium and finite element analysis, evaluating the effect of uncertainties on overall stability of the system, developing response surface for factor of safety, computing probability of failure, performing robust and non-robust design optimization and obtaining final optimal design.

In Chapter 5 the probabilistic design optimization framework is presented for I-wall levee systems resting on clay foundation. The chapter consists of selection of representative design variables with the ranges and considering undrained shear strength of clay foundation and clay levee fill, and flood water level as uncertain parameters, performing limit equilibrium and finite element analysis, evaluating the effect of uncertainties on overall stability of the system, developing response surface for factor of safety, computing probability of failure, performing robust and non-robust design optimization and obtaining final optimal design.

REFERENCES

Phoon, K. K., & Kulhawy, F. H. (1999). “Evaluation of geotechnical property variability.” *Canadian Geotechnical Journal*, *36*(4), 625-639.

Taguchi, G. (1986). *Introduction to quality engineering: designing quality into products and processes*.

Juang, C. H., Wang, L., Atamturktur, S., & Luo, Z. (2012). Reliability-based robust and optimal design of shallow foundations in cohesionless soil in the face of uncertainty. *Journal of GeoEngineering*, *7*(3), 75-87.

CHAPTER 2

RESPONSE SURFACE-BASED ROBUST GEOTECHNICAL DESIGN OF RETAINING WALL SUBJECTED TO EARTHQUAKE LOAD

ABSTRACT

Seismic geotechnical design of retaining walls should consider the uncertainties not only in soil properties such as friction angle of the backfill but also in earthquake load such as peak ground acceleration (PGA). When the uncertainties are incorporated in the design, the robustness which is a measure of sensitivity of a design to uncertain parameters must be considered and evaluated for obtaining suitable design and corresponding construction cost. This paper presents a response surface-based robust geotechnical design approach for cantilever retaining wall subjected to earthquake load. First, the upper and lower bounds of the design variables were determined through dynamic retaining wall design using Mononobe-Okabe method for possible variations in the uncertain parameters. Then, dynamic finite element analyses were performed on a subset of designs by applying El Centro earthquake motions with varying PGA for computing the maximum wall tip deflection which is considered as the serviceability indicator. A response surface for the wall deflection was developed as a function of uncertain and design variables and validated. Finally, a design optimization was performed considering cost and robustness index as the objectives. Two robustness indices, standard deviation of the response and signal to noise ratio were used in this

study and the results were compared. The optimization yielded a set of preferred designs, known as Pareto front, and the knee point concept was used to select the final optimal design.

Key words: Uncertainty; Dynamic load; Retaining wall; Response surface; Robust design; Design optimization;

2.1 INTRODUCTION

Cantilever retaining walls are known as the simplest and the most commonly-used earth retaining structures in seismic prone areas (Coduto 2001). However, there is no well-established dynamic design procedure available for cantilever retaining walls that considers uncertainties in soil and seismic loading. Therefore, the design of these structures should be carefully performed to ensure that the structure can withstand various earthquake loads under various soil conditions. Generally, the conventional trial-and-error procedure is used to obtain the possible safe designs and the least costly design is selected as the final design. Using this procedure, the geotechnical design of cantilever retaining walls is performed evaluating the stability of wall against sliding, overturning, bearing capacity failure and eccentricity. However, there may be a great number of combinations for design parameters of wall that satisfy the stability requirements. To avoid the time-consuming task of seeking the optimal design from a pool of feasible designs, optimization techniques can be used in the design procedure. Various design optimization approaches have been performed on cantilever retaining walls under static condition in the past in which the objectives were limited to the cost or the weight of wall and the uncertainties in the system were managed implicitly using the concept of factor of

safety (FS) (Saribas and Erbatur 1996; Ceranic et al. 2001; Yepes et al. 2008; Khajehzadeh et al. 2008; Camp and Akin 2011). Out of the existing optimization techniques, the genetic algorithm has been found to be useful in managing design optimization of cantilever retaining walls and generally problems with many design variables and complex constraints (Pei and Xia 2012; Juang et al. 2013). Coupling the genetic algorithm with finite element analysis, Papazafeiropoulos et al. (2013) optimized the cross-sectional area of a cantilever retaining wall subjected to earthquake, assuming constant values for loading and soil properties. Thus, the conventional design of retaining walls optimized to their cost or cross-sectional area often involves the use of deterministic FS-based design where the uncertainties in the system are not incorporated explicitly into the criteria. However, the uncertainties in the properties of soil and loading can lead to uncertainty in the performance of the system (Phoon and Kalhawy 1999). Therefore, a robust design optimization method involving uncertainties in backfill material and seismic loading can be a remarkable contribution towards the conventional design of the cantilever retaining wall. A robust design is referred to the least sensitive design to the unexpected variations in the surrounding uncertainties.

A reliability-based robust design approach is an effective method for considering the uncertainties in optimization process and constraining the system to a specified level of reliability. For example, in the robust design optimization of a cantilever retaining wall performed by Juang et al. (2013), the standard deviation of reliability index (as a measure of robustness) and the cost were considered as objectives of optimization and the target reliability was used as the safety constraint. Comparably, Liu et al. (2013) used an

example of cantilever retaining wall under static loading condition to demonstrate a confidence level-based robust design approach. In that study, the confidence level which is the probability of satisfying the target reliability and the cross-sectional area of the wall (as a measure of cost) were deemed as t optimization objectives. Different indices can be defined as robustness measures (e.g. standard deviation of reliability index, standard deviation of probability of failure, and standard deviation of system response), out of which the latter was adopted by Wang et al. (2014) in the robust design optimization of braced excavations using genetic algorithm. These previous studies focused mostly on the performance of geotechnical structures under static loading conditions in which the uncertainties are usually limited to soil properties. Nevertheless, while performing seismic designs of the geotechnical structures, the results are highly impacted by the variation in site specific seismic parameters (such as peak ground acceleration, frequency content, and duration of seismic loading) which are difficult to control. To overcome the sensitivity of response to the variation of those seismic parameters, the uncertainties in dynamic loading must be considered along with those in the soil.

In this study, the response surface method was used to avoid simulating a large number of designs which required time-consuming analysis. The response surface method, pioneered in the field of geotechnical engineering by Wong (1985), is the most effective approach for approximating the behavior of geotechnical structures (Massih and Soubra 2008; Guharay and Baidya 2015). In this paper, first the initial seismic geotechnical design procedure of cantilever retaining wall is introduced which is used to offer different design cases. Numerical models were developed for each of these design

cases in the finite element software, PLAXIS 2D. Then, the finite element analysis and response surface method, which involves the development of the response function as a representative of response are discussed. Subsequently, the robust design optimization is described in which the geotechnical design of retaining wall is optimized to cost and robustness, meeting the safety requirements. Finally, the optimal final design is sought through a selection procedure, which is described in this paper.

2.2 RESPONSE SURFACE-BASED ROBUST DESIGN OPTIMIZATION APPROACH

This section describes the major steps of the approach implemented for the geotechnical dynamic design optimization of cantilever retaining wall. The current approach consists of the initial geotechnical design of wall, finite element (FE) simulation, response surface development, and robust design optimization. A flowchart detailing the framework of the study is illustrated in Figure 2.1.

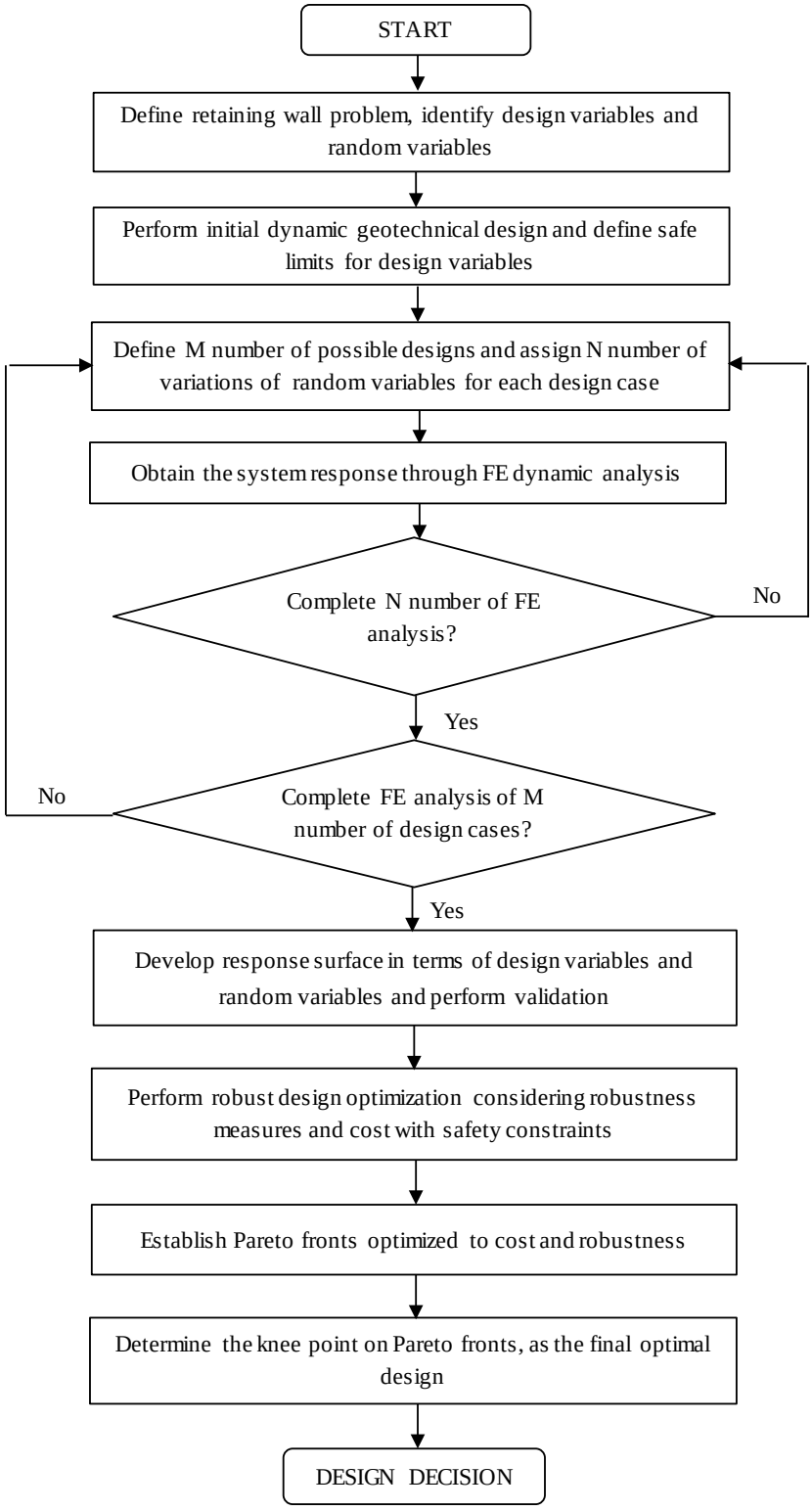

Figure 2.1 Flowchart illustrating the framework of the study

2.2.1 Initial Geotechnical Design of Retaining Wall Subjected to Earthquake Load

2.2.1.1 Problem and the variables

In this study, a typical cantilever retaining wall with the height of 6 m and embedded 1 m (at the toe side) into the soil having cohesion of 30 kPa and friction angle of 28° was used to demonstrate the proposed approach. The wall was assumed to have a horizontal sand backfill. As shown in Figure 2.2, the geometrical parameters of the wall considered in the study are footing width (X_1), toe length (X_2), footing thickness (X_3), and stem thickness (X_4). The varying parameters of the study can be categorized into two groups: random variables (i.e. uncertain parameters) and design variables. Out of various properties of soil in the system, the friction angle of the sand backfill (ϕ) was chosen as the soil-related random variables, and the unit weight and stiffness of soil were calculated based on varying friction angle. It should be noted that the in-situ soil can also involve uncertainties which can be considered in future studies. Another random variable considered in this study along with ϕ was coefficient of peak ground acceleration (k_{PGA}) in terms of gravitational acceleration (g = 9.81 m/s^2) of the acceleration-time history of the seismic load. It should also be noted that the effect of mean period which is another indicator of the characteristics of ground motion was not considered in this study. A mean value and a standard deviation of 34° and 1.36° were assumed for ϕ with desirable range of 30°-38° and a mean value and a standard deviation of 0.3 and 0.1 were assumed for k_{PGA} with desirable range of 0.1-0.5. On the other hand, X_1, X_2, X_3, and X_4 were assumed as the design variables of the study. Although X_1 is the most effective design variable on meeting the stability requirements of a retaining wall, the factor of safety also

varies with a variation in X_2. In addition, X_3 and X_4 both can control the structural design of cantilever retaining wall. The initial ranges of design variables are tabulated in Table 2.1 using minimum value for footing width equal to 0.5H as suggested in Das (2011).

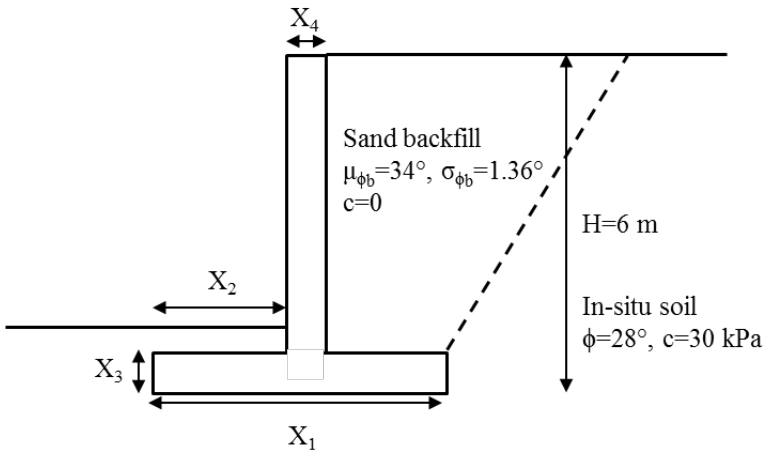

Figure 2.2 The sample retaining wall

Table 2.1 Initial ranges of design variables

Design variable	Suggested range	Range (m)
X_1	$0.5H < X_1 < 1.5H$	3 - 9
X_2	$0.1 < X_2 < X_1 - X_4$	0.1 - 8.6
X_3	$H/14 < X_3 < H/10$	0.42 - 0.6
X_4	$H/14 < X_4 < H/10$	0.42 - 0.6

2.2.1.2 Initial design optimization considering factors of safety

The initial geotechnical dynamic design optimization of retaining wall was conducted considering the wall stability against sliding, overturning, bearing capacity failure, and eccentricity. The dynamic resultant force on the wall was calculated based on pseudo-static analysis using Mononobe-Okabe method (Das 1993) which is the extension of Coulomb theory. In this study, a genetic algorithm named NSGA-II (Non-dominated

Sorting Genetic Algorithm) developed by Deb et al. (2002) was used as the optimization tool. In the optimizations, material usage of the wall (volume per unit length) as a measure of cost and the probability of failure (P_f) of the retaining wall were considered as the objectives of optimization as expressed below:

Objective function1: $y_1 = P_f$ (2.1)

Objective function 2: $y_2 = Cost\left(m^3/m\right) = X_1X_3 + (H - X_3)X_4$ (2.2)

The probability of failure (P_f) of retaining wall by each failure modes of sliding, overturning and bearing capacity failure was computed using Monte Carlo simulation. N =10000 numbers were generated for the random variables, and therefore N number of factors of safety (FS) were calculated. Assuming minimum acceptable FS of 1 and m as the number of factors of safety less than 1, probability of failure was calculated as below:

$$P_f = \frac{m}{N} \quad (2.3)$$

The results of initial bi-objective optimization were demonstrated in plots known as Pareto fronts. The Pareto fronts based on sliding failure, overturning failure and bearing capacity failure are displayed in Figures 2.3-2.5 and a trade-off relationship between cost and probability of failure is observed, in which increasing the cost of retaining wall causes probability of failure to decrease. To obtain the safe design ranges for the rest of the study, the lower limit of footing width (X_1) was increased gradually to reach the zero probability of failure of the retaining wall based on each failure mode. The narrowest range which includes the maximum lower limit was selected as the final range

for the footing width. Figures 2.3(a)-2.3(d) show the effect of footing width on cost and probability of failure by sliding. It is shown that the maximum probability of failure decreases from more than 0.2 to 0 by increasing the lower limit of footing width from 3 m to 6 m. Therefore, to satisfy the safety criteria against sliding failure the range of footing width should be narrowed to 6 m-9 m.

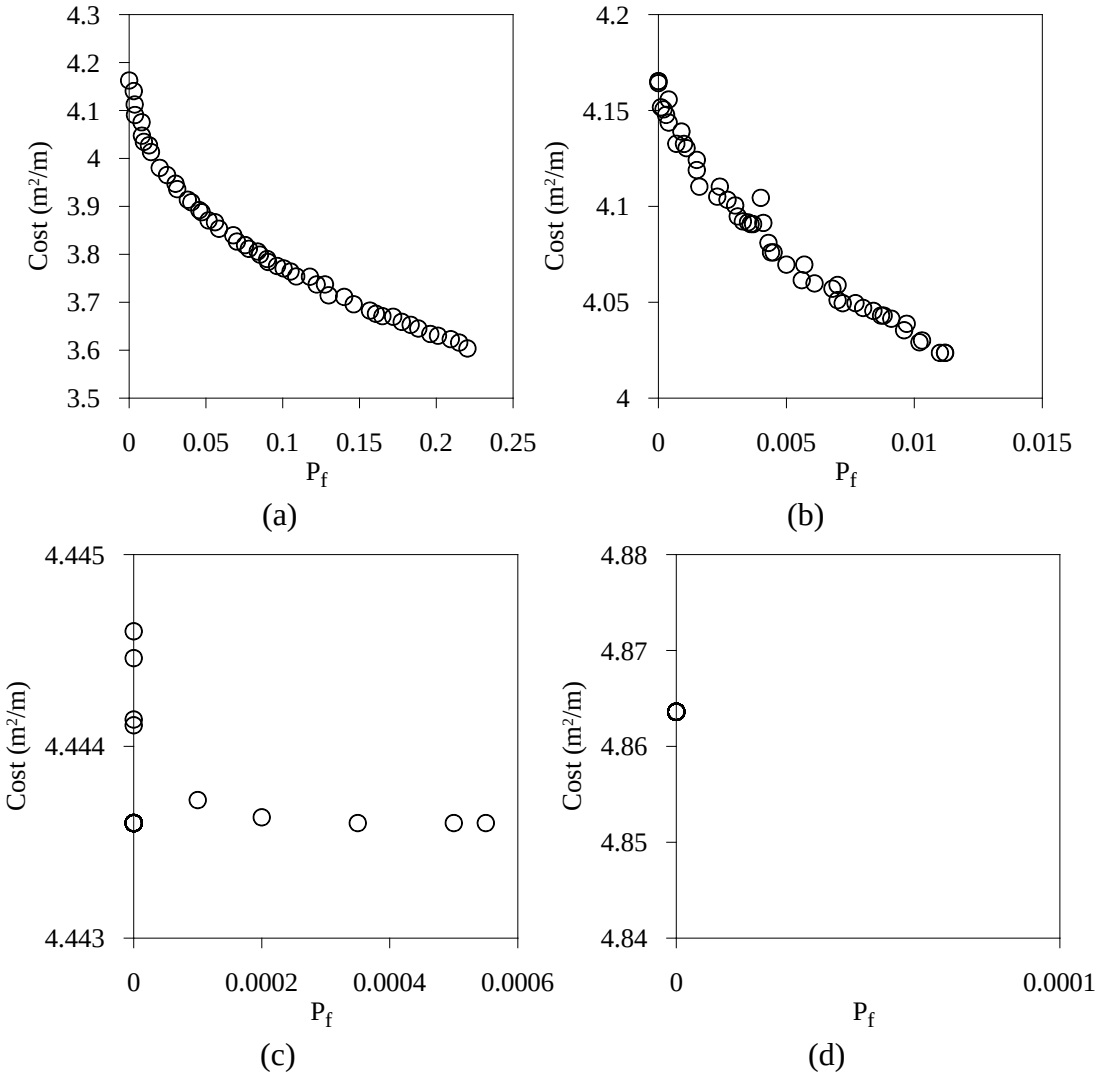

Figure 2.3 Pareto fronts based on FS against sliding for (a) min X_1=3 m, (b) min X_1=4 m, (c) min X_1=5 m and (d) min X_1=6 m

The Pareto front based on overturning failure is shown in Figure 2.4 and the effect of footing width was evaluated on cost and probability of failure by overturning. It can be observed from Figures 2.4(a)-2.4(c) that the maximum probability of failure decreases from more than 0.4 to 0 by increasing the lower limit of footing width from 3 m to 5 m. Based on the safety criteria against overturning failure, the range of footing width should be narrowed to 5 m-9 m. Moreover, shown in Figure 2.5 a zero probability of bearing capacity failure was obtained from Pareto front assuming 3 m for minimum value of footing width. Therefore, a range of 3 m-9 m for footing width will result in safe designs against bearing capacity failure.

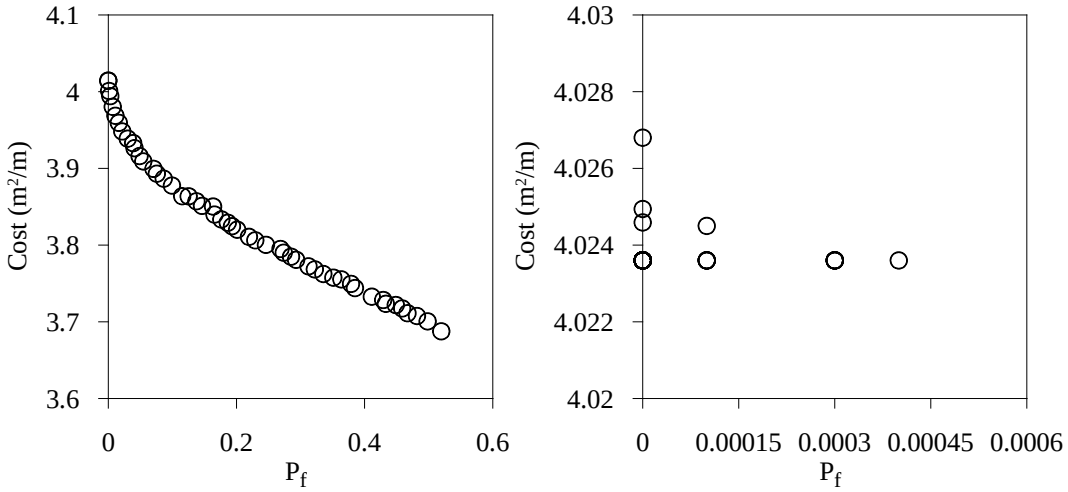

(a) (b)

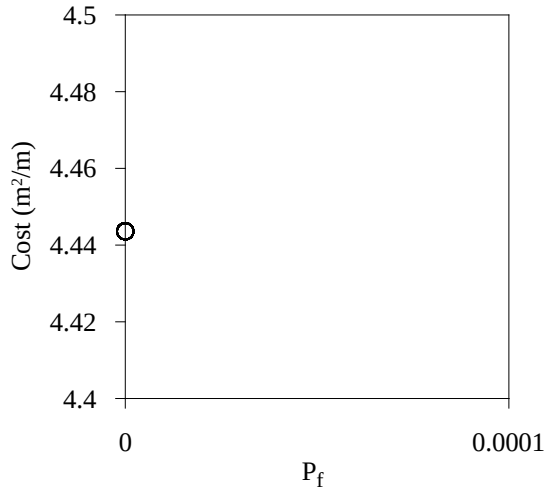

(c)

Figure 2.4 Pareto fronts based on FS against overturning for (a) min X_1=3 m, (b) min X_1=4 m, (c) min X_1=5 m

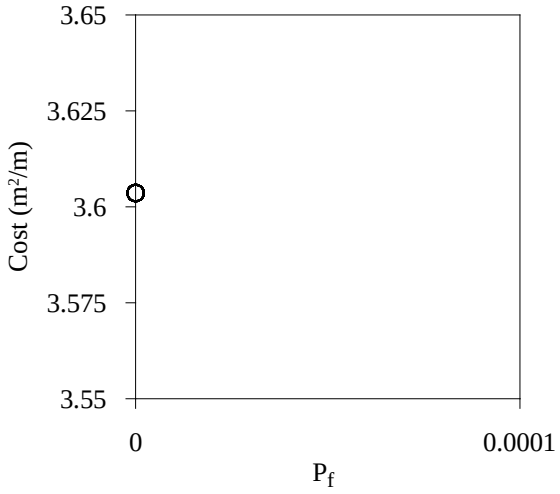

Figure 2.5 Pareto front based on FS against bearing capacity failure for min X_1=3 m

2.2.1.3 Safe design ranges for optimization based on finite element analyses

Based on these outcomes, the final range for footing width (X_1) was considered equal to min{(6 m-9 m), (5 m-9 m), (3 m-9 m)}=(6 m-9 m) and the safe upper and lower limits of the design variables were determined as shown in Table 2.2.

Table 2.2 Final ranges of design variables

Design variable	Range (m)
X_1	6 - 9
X_2	0.1 - 8.6
X_3	0.42 - 0.6
X_4	0.42 - 0.6

Based on the ranges determined above, ten different design cases as listed in Table 2.3 were selected to be implemented in dynamic FE simulations. The geometric properties of design cases are selected in such a way that will cover the full range of variables. For instance, in design case 1 the design variables X_1, X_3, and X_4 are at their lower limit while X_2 is at its upper limit. Similarly, design case 2 was created using the lower limits of all design variables while the upper limits were used in design case 5.

Table 2.3 Design cases of retaining wall selected for finite element simulation

Design case	X_1 (m)	X_2 (m)	X_3 (m)	X_4 (m)
1	6	5.58	0.42	0.42
2	6	0.1	0.42	0.42
3	7.5	3.5	0.51	0.51
4	9	0.1	0.6	0.6
5	9	8.4	0.6	0.6
6	6.5	2	0.55	0.45
7	8	3.75	0.45	0.55
8	7	4	0.48	0.52
9	8.5	3	0.6	0.42
10	6.5	5	0.58	0.58

2.2.2 Dynamic FE Analysis of Retaining Wall

2.2.2.1 FE model generation

The FE models of the subset designs were generated using PLAXIS 2D, which is a FE-based commonly used software in geotechnical engineering and selected for this study (Ravichandran and Huggins 2013; Shrestha et al. 2016). It should be noted that the accuracy of the computer simulation results may affect the robust design outcome and several steps must be taken to eliminate/reduce the user controllable errors in the simulations. The steps include evaluation of the simulation domain, the mesh size and the stress-strain behavior of the material, and boundary condition for dynamic analysis. Therefore, a size sensitivity analysis was carried out to determine the size of the simulation domain. For this purpose, the width of the model was varied until the computed response (wall tip displacement-time history in this study) converged to prevent the simulation domain size from affecting the computed results. A similar procedure was followed to obtain a suitable mesh size to eliminate the mesh dependency of the computed results. Specifically, the fineness of the mesh was increased from a coarse mesh until the computed results converged, which in turn yielded simulation domain dimensions (Figure 2.6) with a very fine mesh consisting of 1700 to 2000 15-node triangular elements.

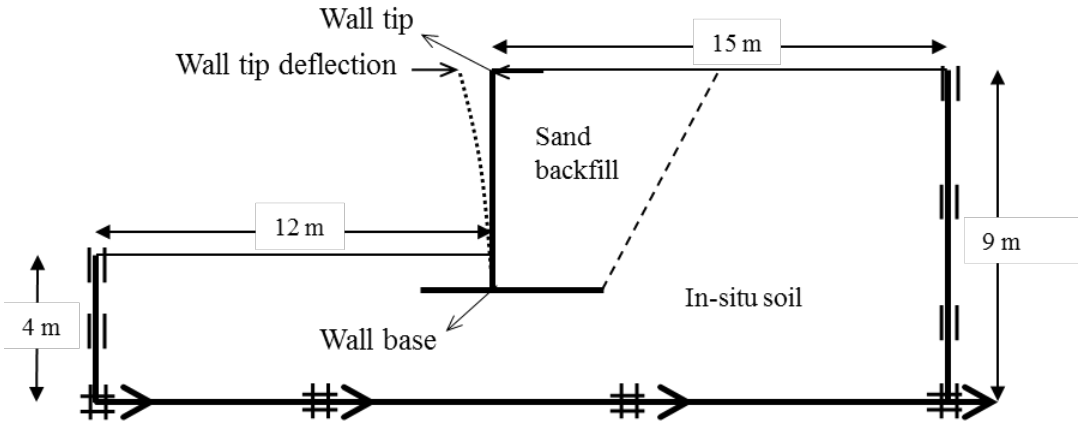

Figure 2.6 Schematic of the simulation domain

To apply the regular boundary conditions to the model, the vertical sides of the simulation domain were fixed to prevent horizontal translation and the base of the domain was fixed against both horizontal and vertical movements. The standard earthquake boundary condition suitable for dynamic analysis was applied at the bottom and the vertical sides of the model to ensure that the earthquake waves propagating from the bottom of the model are properly represented. The stress-strain behavior of both the backfill and the in-situ soils were represented by the nonlinear elastoplastic Hardening Soil (HS) material model available in PLAXIS 2D. It is worth noting that linear elastic and Mohr-Coulomb models are usually preferred in static analysis due to determination of few numbers of model parameters but these models might not be suitable for dynamic analysis. Thus, the HS model which takes into account the modulus reduction with strain increase and the small-strain damping, was implemented in this study. The schematic of the stress-strain curve of the HS material model is displayed in Figure 2.7, and the values of the key HS model parameters are listed in Table 2.4 for both in-situ and backfill materials for the selected variations. The HS model parameters can be better calibrated if

triaxial test results are available for the soil. The wall components (stem and footing) were represented by plate elements and the linear elastic material model was used as the constitutive model of these plates. In addition, the geometrical parameters of the plate wall components were calculated for each design case. Moreover, the accurate modeling requires the consideration of interaction between the wall and the soil which was applied through interface elements in the simulations of this study.

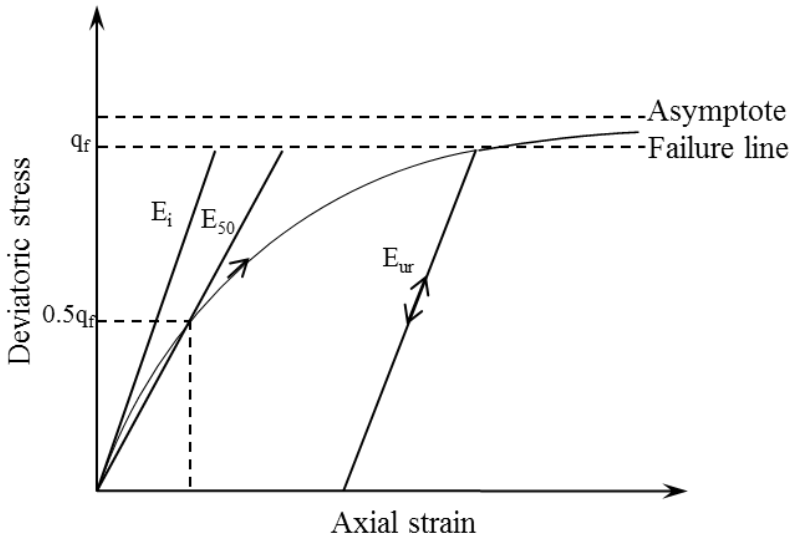

Figure 2.7 Stress-strain curve for Hardening Soil model

Table 2.4 Hardening soil input parameters for model

Soil	Variation	ϕ (°)	c (kPa)	E_{50}^{ref} (kPa)	E_{oed}^{ref} (kPa)	E_{ur}^{ref} (kPa)	m	ψ	γ (kN/m^3)
In-situ soil	-	28	30	40150	51154	120450	1	0	18
Sand Backfill	μ_ϕ	34	0	47760	60577	143280	0.5	4	18
	$\mu_\phi + 3\sigma_\phi$	38.08	0	62650	77450	187950	0.5	8.08	18
	$\mu_\phi + 2\sigma_\phi$	36.72	0	57800	72325	173400	0.5	6.72	18
	$\mu_\phi + \sigma_\phi$	35.36	0	52250	67307	156750	0.5	5.36	18
	$\mu_\phi - \sigma_\phi$	32.64	0	42100	53846	126300	0.5	2.64	18
	$\mu_\phi - 2\sigma_\phi$	31.28	0	36610	47115	109830	0.5	1.28	18

μ_ϕ - 3σ_ϕ	29.92	0	32040	40385	96120	0.5	0	18

Note: E_{50}^{ref} = secant stiffness in standard drained triaxial test; E_{oed}^{ref} = tangent stiffness for primary oedometer loading; E_{ur}^{ref} = unloading/reloading stiffness from drained triaxial test; m = the power for stress-level dependency of stiffness; K = hydraulic conductivity and ψ is the dilatancy angle.

2.2.2.2 Seismic loading

The first ten seconds of the acceleration-time history of El Centro 1940 earthquake, as shown in Figure 2.8(a), was adopted for dynamic FE simulations. This record, with the PGA of approximately 0.3 g, is often used as the reference earthquake motion in the seismic design and analysis of current structures and geotechnical systems. To apply the variations of k_{PGA} in the FE analyses, the El Centro 1940 acceleration-time history was scaled to PGA of 0.1 g, 0.2 g, 0.4 g, and 0.5 g and used as the ground motion. The sample acceleration-time history with PGA of 0.1 g is shown in Figure 2.8(b). As mentioned earlier, mean and standard deviation of k_{PGA} were assumed to be 0.3 and 0.1, respectively in the robust design optimization procedure.

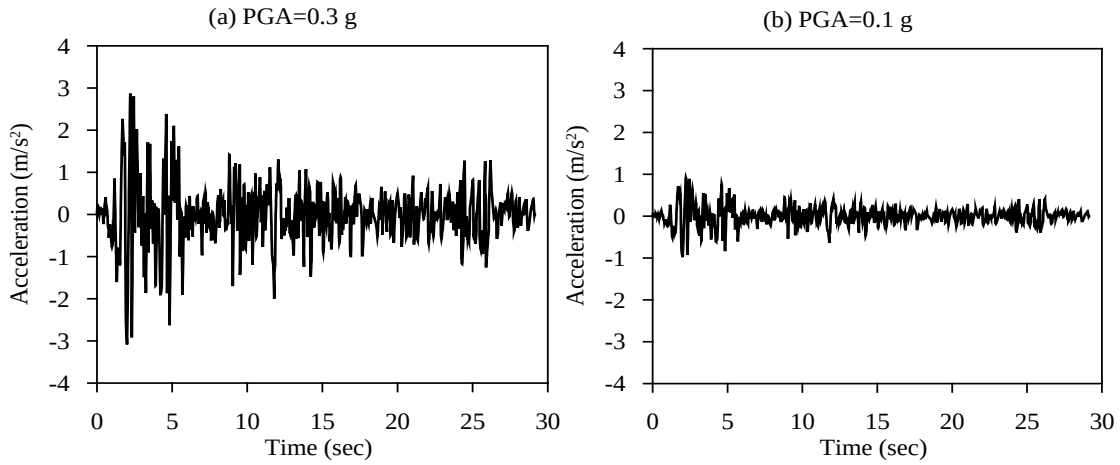

Figure 2.8 El Centro acceleration-time history with (a) PGA = 0.3 g and (b) PGA = 0.1 g.

2.2.2.3 Results

The primary outcomes of PLAXIS 2D models are the wall displacement, shear

force, and the bending moment. Using the wall displacement output, the wall tip deflection-time history was obtained by subtracting the wall base displacement-time history from wall tip displacement-time history. The sample wall tip deflection-time histories for design cases 2 and 7 are shown in Figure 2.9. Then the maximum wall tip deflection (d_{max}) was determined from wall tip deflection-time history and considered as the response of concern in this study. It should be noted that the wall tip deflection controls the safety and stability of the system and is also easily measured while shear force and bending moment can be easily manipulated via reinforcement in the structural design. The representative of input variables and response for one design case is tabulated in Table 2.5 as a sample simulation table and was applied to all selected design cases.

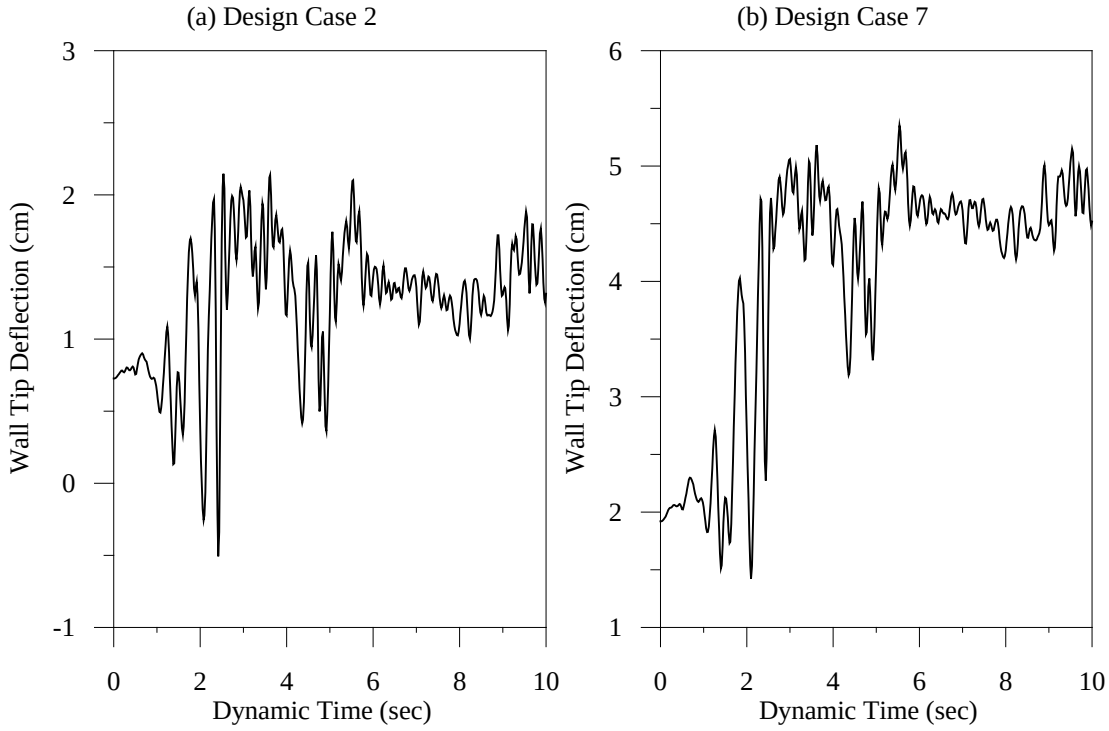

Figure 2.9 Wall tip deflection-time history of (a) design case 2 and (b) design case 7

Table 2.5 Sample simulation table for one design case

Design Variables				Random Variables		Response
(X_1)	(X_2)	(X_3)	(X_4)	ϕ	k_{PGA}	d_{max}
Values of the design case				μ	μ	d_1
				$\mu + 3\sigma$	μ	d_2
				$\mu + 2\sigma$	μ	d_3
				$\mu + \sigma$	μ	d_4
				$\mu - \sigma$	μ	d_5
				$\mu - 2\sigma$	μ	d_6
				$\mu - 3\sigma$	μ	d_7
				μ	$\mu + 2\sigma$	d_8
				μ	$\mu + \sigma$	d_9
				μ	$\mu - \sigma$	d_{10}
				μ	$\mu - 2\sigma$	d_{11}

2.2.3 Response Surface Development

Using results obtained from the FE dynamic analysis, the response surface method was then implemented to model the system response. The response surface was developed via regression analysis between the input variables (ϕ, k_{PGA}, X_1, X_2, X_3, and X_4), and the response (d_{max}). Among the models commonly used in the response surface method, the logarithmic regression model, expressed in Eq. 2.4, which fitted the data points reasonably well was used in this study.

$$y = \exp\left(b_0 + \sum_{i=1}^{n} b_i Ln\left(x_i \right) \right) \tag{2.4}$$

where y and x denote the response and input variables respectively and b_0 and b_i are the coefficients. Using the abovementioned model and determining the model coefficients, the response surface of the study was constructed as displayed below with R^2 (coefficient of determination) equal to 0.93.

$$d_{\max} = \exp\begin{pmatrix} 1.543 - 0.717Ln(\phi) + 0.419Ln(k_{PGA}) + \\ 0.389Ln(X_1) - 0.169Ln(X_2) - 1.735Ln(X_3) - 0.62Ln(X_4) \end{pmatrix} \quad (2.5)$$

The response surface presented in Eq. 2.5, as the serviceability indicator of the cantilever retaining wall, represents the system response in terms of maximum wall tip deflection considering wall geometry and uncertainties in backfill and dynamic loading. In other words, approximate behavior of retaining wall with sand backfill, specific height, and specific in-situ soil properties can be predicted by considering uncertainties of the system. This methodology obviates the usual need for thousands of time-consuming analyses, thus greatly accelerating the process. However, performing the design optimization based on the established response surface is first predicated on evaluating the validity and rating the performance of the response surface.

To conduct the validation procedure, twenty random design sets combined with twenty random values for random variables within their specified ranges were generated and modeled in PLAXIS 2D. Subsequent results compared with those obtained from the response surface, as shown in Figure 2.10, show that the points are closely adjacent to the line y = x. and a close agreement between the two sets of results is observed.

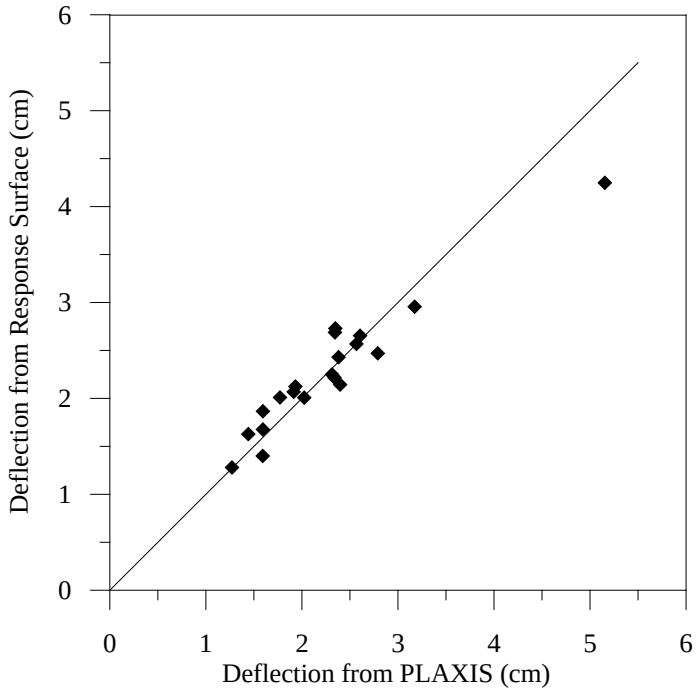

Figure 2.10 Graph of wall tip deflection obtained by PLAXIS 2D and response surface

However, this visual method of validation may be insufficient for finalizing the response surface. To assess the accuracy of the regression in a quantitative manner, additional indicators may need to be applied. Moriasi et.al (2007) recommended three quantitative statistics for evaluating the simulation results per the observed results: the Nash-Sutcliffe efficiency (NSE), the percent bias (PBIAS), and the ratio of the root mean square error to the standard deviation of measured data (RSR) described respectively in Eqs. 2.6, 2.7, and 2.8.

$$NSE = 1 - \left[\frac{\sum_{i=1}^{n} \left(Y_i^{obs} - Y_i^{sim} \right)^2}{\sum_{i=1}^{n} \left(Y_i^{obs} - Y_i^{mean} \right)^2} \right] \tag{2.6}$$

$$PBIAS = \left[\frac{\sum_{i=1}^{n} \left(Y_i^{obs} - Y_i^{sim} \right) * 100}{\sum_{i=1}^{n} Y_i^{obs}} \right] \tag{2.7}$$

$$RSR = \frac{\left[\sqrt{\sum_{i=1}^{n} \left(Y_i^{obs} - Y_i^{sim} \right)^2} \right]}{\left[\sqrt{\sum_{i=1}^{n} \left(Y_i^{obs} - Y_i^{mean} \right)^2} \right]} \tag{2.8}$$

where Y^{obs} is the observation, Y^{sim} is the simulated value and Y^{mean} is the mean of observed data. Here, the response resulted from PLAXIS 2D model and from response surface are considered as Y^{obs} and Y^{sim}, respectively. These validation statistics were then computed and evaluated based on Table 2.6 to estimate the precision of the obtained values from the response surface. The statistics values shown in Table 2.7 demonstrate that the performance of response surface ranged from good to very good and the overall performance can be described conservatively as good. In sum, the combination of both visual technique and quantitative statistics were utilized to validate the response surface and ensure its reliability for use in the design optimization process.

Table 2.6 Performance ratings for recommended statistics (After Moriasi et al. 2007)

Performance rating	RSR	NSE	PBIAS[a]
Very good	0-0.5	0.75-1	<±15
Good	0.5-0.6	0.65-0.75	±15 - ±30
Satisfactory	0.6-0.7	0.5-0.65	±30 - ±55
Unsatisfactory	>0.7	<0.5	> ±55

[a]Ranges were problem-dependent and the average one is considered here.

Table 2.7 Response surface validity

Statistics	Value	Performance
RSR	0.347	Very Good
NSE	0.653	Good
PBIAS	0.309	Very Good

2.2.4 Design Optimization of Retaining Wall

To first acquire a set of preferred designs and then a single optimal design, an optimization algorithm was used to define, implement and then minimize a set of objective functions. Therefore, the authors applied NSGA-II for the robust design optimization of the retaining wall. In this study, the robust design optimization involved minimizing the cost (material usage) of the wall and maximizing the robustness of the system. Concurrent with ensuring that the optimization is both robust and economical, constraints are also used to meet the safety requirements of defined target reliability, allowable wall tip deflection, and toe length limit. In this study, two robustness indices suitable for adaptation into the robust design procedure were standard deviation of response and signal-to-noise ratio of the system. Here, maximizing the robustness of the system means desensitizing the response of the system to various uncertainties, by either minimizing the standard deviation of the response or by maximizing the signal-to-noise ratio of the system. Computing these robustness indices requires defining the performance function of the system, as expressed in Eq. 2.9, using the response surface discussed in previous section, and considering an allowable deflection for the wall tip,

$$g(\theta, X) = d_{all} - d(\theta, X) \tag{2.9}$$

where θ and X are the respective symbols of the random and design variables; $g(\theta,X)$=performance function, d_{all}= the allowable wall tip deflection, and $d(\theta,X)$= the response surface of d_{max}. Standard deviation of the response (SD) can be computed using First Order Second Moment (FOSM) method, as expressed in Eq. 2.10, assuming there is no correlation between ϕ and k_{PGA}.

$$SD = \sigma\left(d\left(\theta, X\right)\right) = \sqrt{\left(\frac{\partial d\left(\theta, X\right)}{\partial \phi}\right)^2 \sigma_{\phi}^2 + \left(\frac{\partial d\left(\theta, X\right)}{\partial k_{PGA}}\right)^2 \sigma_{k_{PGA}}^2} \tag{2.10}$$

Another measure of design robustness that has been used in quality engineering is the signal-to-noise ratio (SNR). Maximizing the SNR of a system leads to identify the most robust design from a pool of designs. This robustness measure is defined as following (Phadke 1995):

$$SNR = 10Log_{10}\left(\frac{\mu^2\left(g\left(\theta, X\right)\right)}{\sigma^2\left(g\left(\theta, X\right)\right)}\right) \tag{2.11}$$

where $\sigma(g(\theta, X))$= the standard deviation of the performance function (numerically equal to the SD), and $\mu(g(\theta,X))$= the mean value of performance function obtained using Eq. 2.12,

$$\mu\left(g\left(\theta, X\right)\right) = g\left(\mu_{\theta}, X\right) \tag{2.12}$$

where μ_{θ} is the mean value of random variables.

In this study, the robust design optimization, was performed twice first using SD as first objective and then using SNR while keeping cost as the second objective in both optimizations. It should be noted that 1/SNR was used as the objective so that by minimizing 1/SNR the designs of the higher SNR are obtained. For cost (the second objective) the volume of the retaining wall per unit length was adopted in optimization setting. The objective functions of the study are summarized as below:

Objective function 1: $y_1 = SD$ or $y_1 = 1/SNR$ (2.13)

Objective function 2: $y_2 = Cost\left(m^3/m\right) = X_1 X_3 + (H - X_3) X_4$ (2.14)

To manage the screened designs in the design optimization process, a target reliability index (β_t) equal to 3 was considered as constraint to prevent inclusion of designs of lower reliability into the set of suitable designs. The mean value and standard deviation of performance function as shown in Eq. 2.15 was then used to compute the reliability index of system (β), which is expressed as:

$$\beta = \frac{\mu\left(g\left(\theta, X\right)\right)}{\sigma\left(g\left(\theta, X\right)\right)} \tag{2.15}$$

It is also possible to constrain the optimization setting by limiting the toe width to approximately half of the footing width; this constraint is considered as a justification for typical engineering preferences. Generally, depending on the properties on both sides of the retaining wall and wall ownership, the extension of the toe can be limited. For example, if the upstream neighbor is assumed to be the wall owner and responsible for all

wall repairs, the downstream neighbor will be responsible for all toe repairs (as the wall toe is located within the downstream property), and will not face an unacceptable charge if the constraint is applied to the wall.

Based on the design optimization setting in this study as shown in Figure 2.11, a set of preferred designs were obtained and displayed in a curve, also known as a Pareto front, from which the optimum final design can be extracted. The Pareto fronts established through the NSGA-ii algorithm consist of a number of data points, each representing a suitable design case, with values of computed objectives.

Find:	Design parameters $X=\{X_1, X_2, X_3, X_4\}$
Objectives:	Maximizing design robustness: (i) minimizing SD (ii) maximizing SNR Minimizing cost
Subject to:	$X \in$ safe design range $\beta > \beta_T$

Figure 2.11 Robust design optimization setting of the study

2.3 DESIGN OPTIMIZATION RESULTS AND DISCUSSION

Following the response surface-based robust design optimization in this study, the designs within the safe design domain were screened based on the optimization settings and demonstrated collectively in Pareto front. A clear trade-off relationship between the cost and the robustness index can be inferred from the obtained Pareto front as shown in

Figure 2.12. In other words, either decreasing the standard deviation or increasing the SNR which desensitized the system towards uncertainties in turn yielded retaining walls that had a greater volume per unit length, which were represented in a costlier design. This incompatibility in the relationship between two objectives required an investigation of the main characteristics of the established Pareto front, particularly the knee point concept to determine the best trade-off solution, or final optimal design.

As clearly indicated in Figure 2.12, the Pareto front based on case (i) in optimization setting, the variation of the standard deviation of wall tip deflection as a representative of variation of system response was between 0.1 cm and 0.4 cm. Also, the volume per unit length, which simply represents the cost of materials used in the construction of the wall, decreased from approximately 7 m^3/m to 4.5 m^3/m with an increase in the standard deviation. Each point in the following set of Pareto fronts is a demonstration of a design case with its specific value of cost (volume per unit length) and a standard deviation of wall tip deflection. The optimal design is assumed as a point at which both objectives remain at the minimum condition.

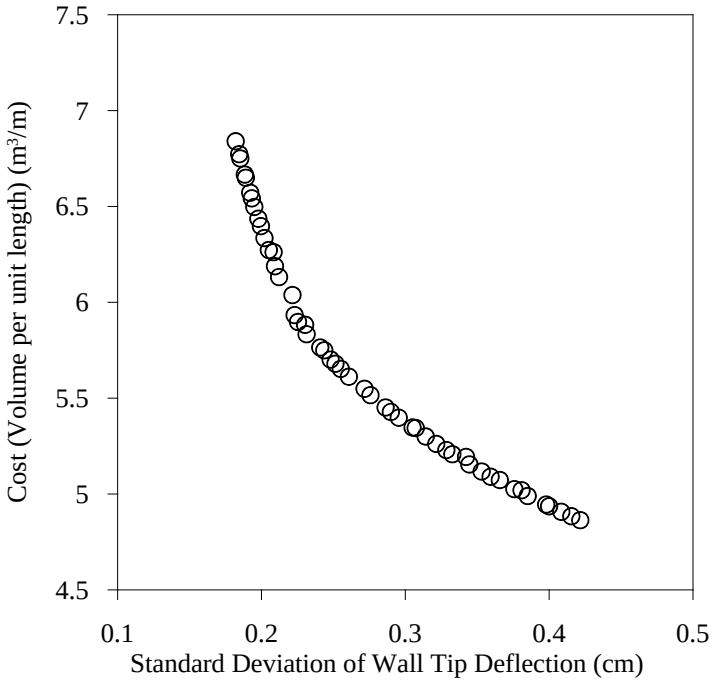

Figure 2.12 Pareto front optimized to both cost and robustness (SD)

A second Pareto front, as shown in Figure 2.13, was also established based on case (ii) of the optimization setting which was examination of the 1/SNR as another robustness measure for the design optimization. Similar to the first case, the results show a trade-off relationship in which a decrease in the volume of wall causes a corresponding increase in the 1/SNR and reduction in SNR and thus in robustness.

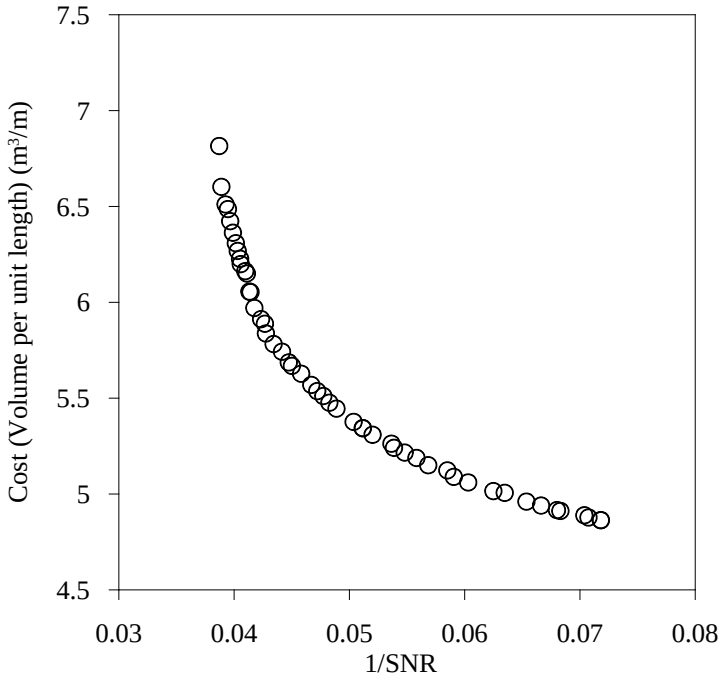

Figure 2.13 Pareto front optimized to cost and robustness (1/SNR)

In order to determine the optimal design with respect to cost and robustness, the normal boundary intersection (NBI) (Das and Dennis, 1998) approach was used to compute the knee points on the two Pareto fronts. As shown in Figure 2.14, for each point of the Pareto front, the distance from the boundary line, which connects the highest point of the Pareto front to the lowest point, is computed in the normalized space of Pareto front. Then, the point with maximum distance from the boundary line is sought and selected as the knee point which corresponds to the optimal design of the study.

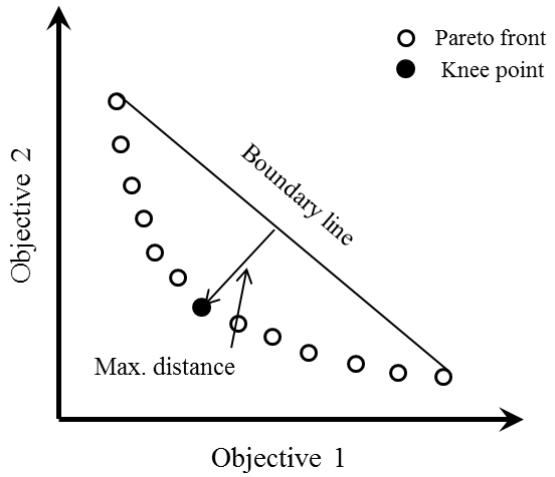

Figure 2.14 Normal boundary intersection approach

The results of final optimal design using both robustness measures are summarized in Table 2.8, which holds the design parameter values of the retaining wall obtained from the properties of the knee points of both Pareto fronts. The consistency of both sets of results can be interpreted as different robustness measures yielded similar design sets and also as evidence of the appropriateness of the developed response surface. The obtained design parameters from knee points indicate that the final optimal design, which is identified as the most cost-efficient and the most robust design simultaneously, includes minimum footing width, maximum footing thickness, and minimum stem thickness based on the limiting values of the design range.

Table 2.8 Summary of final optimal designs properties

Robustness measure	X_1 (m)	X_2 (m)	X_3 (m)	X_4 (m)
SD	6	2.96	0.59	0.42
SNR	6	2.97	0.54	0.42

Both Pareto fronts can also be used to obtain the final design based upon the engineering preferences and available sources (e.g. a specific budget). These provide an option for designers to choose a desired level of robustness for determining the final design that corresponds to a specific level of optimization. Moreover, the expertise of engineer, can be applied to inform the addition of constraints to the optimization setting. These features that increase the flexibility of the current methodology are advantageous in ensuring the robust design optimization.

When comparing the Pareto front with a conventional design, the design with the least cost, which corresponds to the least robust design on the Pareto front, is considered as the final design in conventional practices. In the current approach, safety is the common requirement shared between the robust design and conventional designs, which is applied in the initial design step and serves as an initial constraint in the design optimization.

2.4 CONCLUSION

In this paper, the authors presented a framework of response surface-based robust geotechnical design of a retaining wall backfilled with sand subjected to earthquake load. The adopted approach which is conducted through the coupling of FE dynamic analysis and response surface development linked to bi-objective optimization considers safety, robustness, and cost simultaneously in the geotechnical design of a retaining wall. The robustness of the design was satisfied by minimizing the standard deviation of response and maximizing the SNR in two attempts. The safety of design was ensured by

performing stability analysis of the initial design and then defining target reliability index and allowable wall tip deflection. It should also be noted that the sources of system uncertainties, mainly identified in backfill material and in seismic loading, were considered as random variables to reduce the variation in system response along with carefully adjusting the design variables.

This approach can be introduced as a beneficial tool for the geotechnical dynamic design of retaining structures with which designers may work with more efficient designs to prevent an overdesign because of safety satisfactions or an under-design, which results from cost concerns. Moreover, the concept of knee point can be utilized based on the obtained Pareto fronts from design bi-objective optimizations to aid in the selection of the final optimal design from a series of safe designs.

REFERENCES

Basudhar, P.K., Lakshman, B. and Dey, A. (2006). "Optimal cost design of cantilever retaining walls." *India: IGC, Chennai*, 14-16.

Camp, C.V. and Akin, A. (2011). "Design of retaining walls using big bang–big crunch optimization." *Journal of Structural Engineering*, 138(3), 438-448.

Ceranic, B., Fryer, C. and Baines, R.W. (2001). "An application of simulated annealing to the optimum design of reinforced concrete retaining structures." *Computers & Structures*, 79(17), 1569-1581.

Coduto, D. P. (2001). *Foundation design: principles and practices*. Prentice Hall.

Das, B.M. (1993). *Principles of Geotechnical Engineering*, 3rd ed., PWS Publishing, Boston.

Das, B. M. (2011). *Principles of foundation engineering*, Cengage Learning.

Das, I., and Dennis, J. E. (1998). "Normal-boundary intersection: A new method for generating the Pareto surface in nonlinear multi-criteria optimization problems." *SIAM Journal on Optimization*, *8*(3), 631-657.

Deb, K., Pratap, A. and Agarwal, S. (2002). "A fast and elitist multiobjective genetic algorithm NSGA-II." *Evolutionary Computation*, 6(2), 182-197.

Guharay, A. and Baidya, D. K., (2015). "Reliability-based analysis of cantilever sheet pile walls backfilled with different soil types using the finite-element approach." *International Journal of Geomechanics*, 15(6), p.06015001.

Juang, C. H., Liu, Z. and Atamturktur, H. S. (2013). "Reliability-based robust geotechnical design of retaining walls." *Sound Geotechnical Research to Practice*, 514-524.

Khajehzadeh, M., Taha, M.R., El-Shafie, A. and Eslami, M. (2010). "Economic design of retaining wall using particle swarm optimization with passive congregation." *Australian Journal of Basic and Applied Sciences*, 4(11), 5500-5507.

Liu, Z., Juang, C. H. and Atamturktur, S. (2013). "Confidence level-based robust design of cantilever retaining walls in sand." *Computers and Geotechnics*, 52, 16-27.

Moriasi, D.N., Arnold, J.G., Van Liew, M.W., Bingner, R.L., Harmel, R.D. and Veith, T.L. (2007). "Model evaluation guidelines for systematic quantification of accuracy in watershed simulations." *Transactions of the ASABE*, 50(3), 885-900.

Papazafeiropoulos, G., Plevris, V. and Papadrakakis, M. (2013). “Optimum design of cantilever walls retaining linear elastic backfill by use of genetic algorithm”. *Proc., 4th ECCOMAS Thematic Conference on Computational Methods in Structural Dynamics and Earthquake Engineering*, Greece.

Pei, Y. and Xia, Y. (2012). “Design of reinforced cantilever retaining walls using heuristic optimization algorithms.” *Procedia Earth and Planetary Science*, 5, 32-36.

Phadke, M. S. (1995). “Quality engineering using robust design.” *Prentice Hall PTR*.

Phoon, K. K., & Kulhawy, F. H. (1999). “Evaluation of geotechnical property variability.” *Canadian Geotechnical Journal*, *36*(4), 625-639.

Ravichandran, N. and Huggins, E.L. (2013). “Seismic response of gravity-cantilever retaining wall backfilled with shredded tire.” *Geotechnical Engineering*, 44(3), 14-24.

Saribas, A. and Erbatur, F. (1996). “Optimization and sensitivity of retaining structures.” *Journal of Geotechnical Engineering*, 122(8), 649-656.

Shrestha, S., Ravichandran, N., Raveendra, M. and Attenhofer, J.A. (2016). “Design and analysis of retaining wall backfilled with shredded tire and subjected to earthquake shaking”. *Soil Dynamics and Earthquake Engineering*, *90*, 227-239.

Wang, L., Juang, C. H., Atamturktur, S., Gong, W., Khoshnevisan, S. and Hsieh, H. S. (2014). “Optimization of design of supported excavations in multi-layer strata.” *Journal of Geoengineering*, Vol. 9, 1, 1-12.

Wong, F.S. (1985). “Slope reliability and response surface method.” *Journal of Geotechnical Engineering*, 111(1), 32-53.

Yepes, V., Alcala, J., Perea, C. and González-Vidosa, F. (2008). A parametric study of optimum earth-retaining walls by simulated annealing." *Engineering Structures*, 30(3), 821-830.

Youssef Abdel Massih, D.S. and Soubra, A.H., (2008). "Reliability-based analysis of strip footings using response surface methodology." *International Journal of Geomechanics*, 8(2), 134-143.

CHAPTER 3

ROBUST GEOTECHNICAL DESIGN OF RETAINING WALL BACKFILLED WITH SHREDDED TIRE AND SUBJECT TO EARTHQUAKE LOAD

ABSTRACT

A new robust design optimization methodology is presented in this study for cantilever retaining wall backfilled with shredded tire and subjected to earthquake load. Regarding the merits of application of shredded tire backfill in seismically active areas, the uncertainties in properties of this material (e.g. friction angle and cohesion) as well as uncertainties in earthquake load (e.g. peak ground acceleration) necessitates examining the robustness of design along cost efficiency in geotechnical design procedure. The wall tip deflection was treated as the response of concern for which a response surface was developed based on the design and random (uncertain) variables. Coupling with Monte Carlo simulation, the optimization in terms of cost and standard deviation of response as a measure of robustness yielded a set of preferred designs, or Pareto front, and the final optimal design was determined via selection procedures.

Keywords: Shredded tire; design optimization; robust design; retaining wall; earthquake load; uncertainty

3.1 INTRODUCTION

Recent studies show that a beneficial method for recycling waste tires is utilizing the shredded tire in civil engineering purposes such as embankment, road beds, soil improvement, drainage in landfill and backfill for retaining structures (Eldin and Senouci

1992; Bosscher et al. 1997; Reddy et al. 2009; Humphrey et al. 1993; Cesich 1996; Tweedie et al. 1998; Lee et al. 1999). The applicability of shredded tire as an economical alternative for conventional soil backfill of retaining walls has been previously examined under dynamic loading condition compared to conventional backfill (Ravichandran and Huggins 2013; Reddy and Krishna 2015; Shrestha et al. 2016). The experimental study by Reddy and Krishna (2015) also indicated that horizontal displacements can decrease to half when adding tire chips to sand backfill. Performing finite element dynamic analysis of various cases of cantilever retaining wall, Shrestha et al. (2016) showed that using shredded tire as backfill results in considerable reduction in wall tip deflection and structural demand. It was also reported that shredded tire backfill provides cost-efficiency in design of cantilever retaining wall, causing significant reduction in total cost of construction.

In this study, the design optimization of cantilever with shredded tire backfill was performed under dynamic loading condition. Generally, in the conventional design procedure the least costly design that meets the safety criteria is selected as final design. However, selecting the final design out of a great number of combinations of design parameters can be achieved through optimization methods. Various optimization approaches based on the limit equilibrium method have been used for the design of cantilever retaining wall in the past and cost (or weight) of wall was considered as the only objective of optimization (Saribas and Erbatur 1996; Ceranic et al. 2001; Yepes et al. 2008; Camp and Akin 2011). The genetic algorithm has been found to be a promising approach in design optimization when there are many design variables and multiple

constraints, as in a retaining wall problem (Pei and Xia 2012, Papazafeiropoulos et al. 2013). In the above-mentioned studies, all properties of soil and loading were used as deterministic parameters. Using target reliability as safety constraint and considering uncertainties in soil properties, Babu and Basha (2008) performed a reliability based design optimization of cantilever retaining wall under static loading condition and reported a significant cost reduction in the procedure compared to conventional design optimizations. Thus, along with cost optimization to identify the least sensitive design to uncertainties and reduce the variation of system response due to high variability of uncertain parameters, concept of robust design was examined in the current work.

Properties of shredded tire (as a pure material or as supplementary material for soil) such as friction angle, cohesion, unit weight, permeability, and elasticity have been studied experimentally in the past for civil engineering goals. As the variability of soil parameters is required to be considered in geotechnical design (Phoon and Kalhawy 1999), the use of this lightweight material as an alternative to soil backfill also involves uncertainties which may affect the system response such as wall tip deflection, shear force and bending moment introduced in the wall. Moreover, in seismic geotechnical design, uncertainties are not only limited to material properties, but also include earthquake loading properties. Robust design of geotechnical structures has been proved to be beneficial in dealing with hard-to-control uncertain parameters of the geotechnical systems such as retaining walls and reducing the sensitivity of design to these parameters (Juang et al. 2012; Liu et al. 2013; Juang et al. 2013; Wang et al. 2014;). A reliability-based robust design optimization was performed by Juang et al. (2013) for a cantilever

retaining wall under static loading condition considering uncertainties in backfill. In their study, cost and standard deviation of reliability index as the measure of robustness were considered as the objectives of optimization along with target reliability as the safety constraint. Other indices can also be used as the measure of robustness. Liu et al. (2013) performed a robust design of cantilever retaining wall using confidence level (the probability of meeting the target reliability index) as robustness measure. Moreover, standard deviation of response has been found to be an appropriate indicator of robustness so as the smaller variation in response results in a more robust design (Wang et al. 2014).

In this study, regarding that seismic design responses are highly affected not only by the backfill properties but also by the characteristics of the seismic loading, a new procedure is presented to incorporate the variations in seismic load through robust design optimization. In this procedure, dynamic finite element analysis was conducted using computed statistical properties of random variables and limiting values of design variables and a response surface was developed based on wall tip deflection results. Then, the genetic algorithm-based optimization was performed to identify the final seismic geotechnical design of cantilever retaining wall with shredded tire backfill based on performance requirement and cost limitation.

3.2 UNCERTAINTY IN SHREDDED TIRE PROPERTIES

The shear strength and behavior of shredded tire must be evaluated to apply the material as backfill for retaining walls. In order to identify the key properties of shredded tire as uncertain parameters (also known as random variables) in this study, a literature

review was performed based on past experimental studies on shredded tire material properties as displayed in Table 3.1. The material characteristics are collected in the table, and the suitability of this material for retaining wall backfill is determined based on tire size. Regarding FHWA report prepared by Balunaini et al. (2009), several researchers have investigated the properties of tire derived aggregates (TDA) for application in various geotechnical projects. In that report, the range of optimum size appropriate for backfill is mentioned as 50 mm-300 mm and the larger size tires are emphasized to be more economical in constructions.

Table 3.1 Properties of shredded tire

Source	Tire Size (mm) /Suitability		Unit Weight (kN/m^3)	Friction Angle (deg)	Cohesion (kPa)	E (kPa)	Poisson's Ratio
Bressette (1984)	25-64	OK	4.6	21	25.85	--	--
	25-64	OK	5.96	14	31.6	--	--
Humphrey et al. (1993)	38*	OK	6.1	25	8.6	770	0.32
	51*	OK	6.3	21	7.7	1130	0.28
	76*	OK	6.1	19	11.5	1120	0.20
Gharegrat (1993)	50*	OK	6.3	21	7.6	--	--
Ahmed & Lovell (1993)	13**	N.A	6.2	11.6	22.7	--	--
	25**	OK	6.3	12.6	25.4	--	--
	25**	OK	6.4	14.6	22.1	--	--
	25**	OK	6.8	14.3	24.6	--	--
Ahmed & Lovell (1993)	13***	N.A	6.2	20.5	35.8	--	--
	25***	OK	6.3	22.7	37.3	--	--
	25***	OK	6.4	25.3	33.2	--	--
	25***	OK	6.8	24.7	39.2	--	--
Edil & Bosscher (1994)	51-76	OK	--	40	--	--	--
Black & Shakoor (1994)	Max. 1	N.A	--	30	4.79	--	--
	1-4	N.A	--	31	3.35	--	--
	4-7	N.A	--	27	6.22	--	--
Duffy (1995)	51	OK	--	27	7.18	--	--
Cosgrove (1995)	38	OK	--	38	3.3	--	--
	76	OK	--	32	4.3	--	--
Cecich et al.	12.5	N.A	5.7	27	7.04	--	--

(1996)	--	N.A	6.97	22	5.75	--	--
Andrews & Guay (1996)	25-51	OK	--	27.5	3.83	--	--
Foose et al. (1996)	50, 100, 150[+]	OK	5.7	30	3	--	--
Masad et al. (1996)	4.6*	N.A	6.18	6	NA	--	--
	4.6**	N.A	6.18	11	NA	--	--
	4.6***	N.A	6.18	15	NA	--	--
Wu et al. (1997)	Max. 38	OK	5.89	--	--	--	--
	Max. 19	N.A	5.69	54	0	--	--
	Max. 9.5	N.A	5.42	50.5	0	--	--
	Max. 2	N.A	5.69	45	0	--	--
Gebhardt (1997)	38-1400	OK	14.45	38	3.11	--	--
	38-1400	OK	14.45	38	0 (NA)	--	--
Tweedie et al. (1998)	Max. 38	OK	6.97	25	8.6	--	--
	Max. 76	OK	6.77	19	11.9	--	--
	Max. 76	OK	6.97	21	7.7	--	--
Tatlisoz et al. (1998)	--	N.A	5.9	30	0	--	--
Lee et al. (1999)	50	OK	6.3	21	17.5	3394.4	--
Yang et al. (2002)	10*	N.A	5.7	32	0	1129	0.28
	10**	N.A	5.7	11	21.6	1129	0.28
	10***	N.A	5.7	18.8	37.7	1129	0.28
Youwai & Bergado (2003)	16	N.A	7.05	30	--	--	0.33
Moo-Young et al. (2003)	50	OK	6.25	15	0.39 (NA)	--	--
	50-100	OK	7.25	32	0.37 (NA)	--	--
	100-200	OK	6.5	27	0.37 (NA)	--	--
	200-300	OK	6.25	29	0.35 (NA)	--	--
Shalaby & Khan (2005)	75	OK	6.38	22	9.5	1100	0.3
Warith et al. (2004)	75	OK	7.3	--	--	--	--
Hataf & Rahimi (2006)	--	N.A	5.8	23	0	--	--
Average input values w.r.t suitability			6.99	--	--	1502.88	0.275

[+]Direct Shear Test at 10% strain

*Triaxial Test at 10% strain, **Triaxial Test at 15% strain, ***Triaxial Test at 20% strain

Generally, TDAs may be categorized into two types of tire chips (A) and tire shreds (B). Type A of approximately 12 mm-50 mm size and type B of 50 mm-305 mm

size are considered as classifications of TDA. It should be noted that the lightweight materials of backfill are mostly taken from type B TDA and larger size tires of type A TDA. Therefore, the size range which is considered suitable for application as retaining wall backfill is assumed to be greater than 25 mm. Out of these properties, friction angle and cohesion of shredded tire backfill were considered as random variables in this study. To determine the statistical properties of these variables, the suitable data of friction angle and cohesion was examined for fitting distribution and the lognormal distribution was deemed to be the most appropriate one. The probability plots of both data for the lognormal distribution are shown in Figure 3.1 and Figure 3.2. The lognormal parameters of the properties were determined from the linear trendline of which slope and interception are the scale (ξ) and location (λ) parameters of the lognormally distributed variable. In the current work, the lower and upper limits of the random variables were defined as $\exp(\lambda-\xi)$ and $\exp(\lambda+\xi)$, respectively. Based on the obtained parameters, the limiting values for friction angle are 16.6° and 33.87°, and for cohesion are 4.5 kPa and 28.12 kPa.

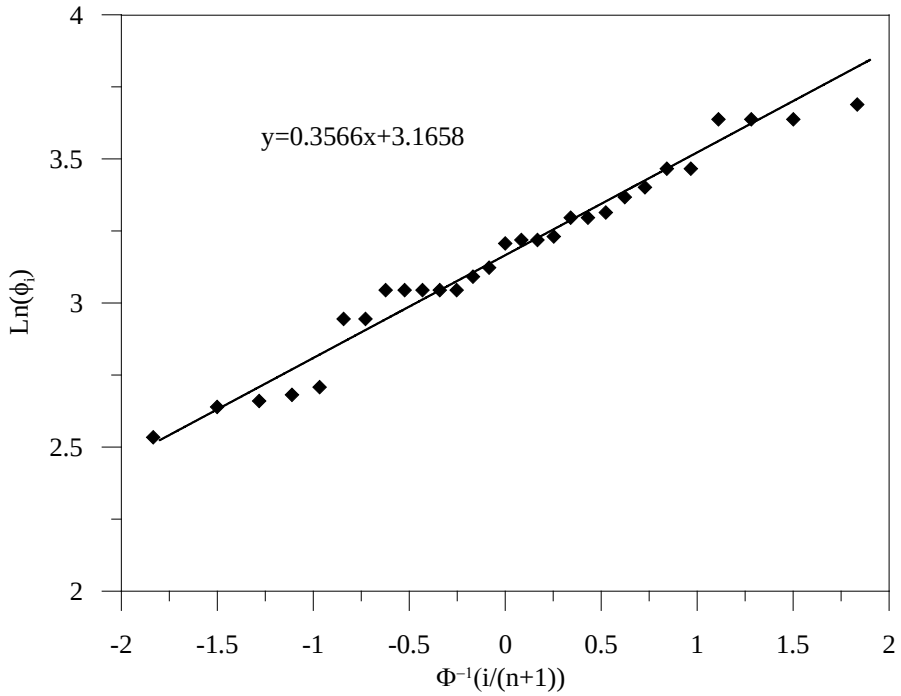

Figure 3.1 Probability plot for friction angle (ϕ) data of shredded tire

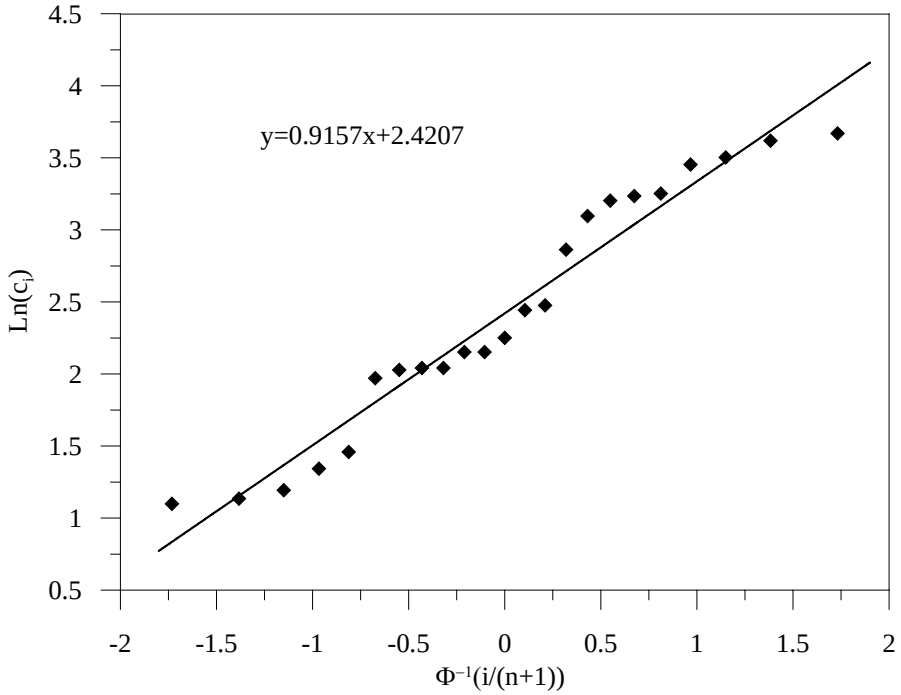

Figure 3.2 Probability plot for cohesion (c) data of shredded tire

3.3 UNCERTAINTY IN EARTHQUAKE LOAD PROPERTIES

To conduct a robust geotechnical design with presence of seismic loading, identifying the key uncertainties in strong motion parameters (such as amplitude parameters and frequency content) is of great importance. Out of these parameters, the peak ground acceleration (PGA) of the earthquake was examined in this study and the coefficient of PGA (k_{PGA}) in terms of g was considered as random variable. Assuming that this variable is lognormally distributed with unit of g, the statistical parameters can be determined using the attenuation relationship by Cornell et al. (1979) as expressed below:

$$Ln(PGA) = -0.152 + 0.859M - 1.803Ln(d_h + 25) \tag{3.1}$$

$$d_h = \sqrt{z^2 + d_e{}^2} \tag{3.2}$$

where M is the earthquake magnitude, d_h is the hypocentral distance (site-to-source), z is the depth of earthquake and d_e is the epicentral distance as shown in Figure 3.3. The standard deviation of Ln(PGA) based on Cornell relationship is 0.57 which can be considered as the scale parameter (ξ) of lognormal distribution. Assuming a magnitude of 7 for the earthquake and hypocentral distance of 30 km, Ln(PGA) is obtained equal to -1.365 which can be assumed as location parameter (λ) of the lognormally distributed k_{PGA}. To this aim, a survey was conducted through more than thirty earthquakes with maximum PGA value of 0.25 g-0.35 g, as shown in Table 3.2. The average depth of earthquakes and average epicentral distance were obtained about 12 km and 27 km, respectively which indicates an average hypocentral distance of 30 km (Eq. 3.2) for an average magnitude of 7 for the surveyed earthquakes. Based on the obtained statistical

parameters, the lower limit (exp(λ-ξ)) and upper limit (exp(λ+ξ)) for k_{PGA} were obtained equal to 0.14 and 0.45, respectively.

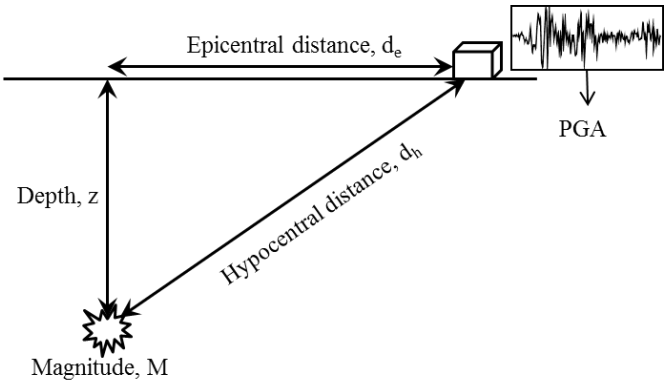

Figure 3.3 Demonstration of earthquake location

Table 3.2 Earthquakes data

Earthquake	M	PGA (g)	z (km)	d_e (km)	Earthquake	M	PGA (g)	z (km)	d_e (km)
Sierra El Mayor	7.2	0.27	10	22	Loma Prieta	6.9	0.29	18	64
Sierra El Mayor	7.2	0.27	10	34	Loma Prieta	6.9	0.32	18	40
Landers	7.3	0.29	1	11	Ferndale	6.5	0.35	29.3	31
Landers	7.3	0.3	1	24	Coalinga	6.5	0.28	10	30
hector mine	7.1	0.32	23.6	13	Coalinga	6.5	0.27	10	38
Northridge	6.7	0.34	18	3	Kyushu, Japan	7	0.35	10	10
Imperial valley	6.5	0.31	12	8	Kocaeli, Turkey	7.6	0.32	15	5
Imperial valley	6.5	0.26	12	15	El Centro 1940	7	0.3	16	13
Imperial valley	6.5	0.27	12	17	Chi-Chi, Taiwan	7.3	0.33	8	20
Imperial valley	6.5	0.29	12	20	Chi-Chi, Taiwan	7.3	0.29	8	35
Imperial valley	6.5	0.26	12	30	Chi-Chi, Taiwan	7.3	0.3	8	40
Petrolia	7.1	0.3	15	15	Chi-Chi, Taiwan	7.3	0.26	8	30
Petrolia	7.1	0.32	15	25	Denali	7.9	0.24	5	56
Petrolia	7.1	0.26	15	30	Denali	7.9	0.24	5	66
Loma Prieta	6.9	0.35	18	18	Morgan hill	6.2	0.31	8.4	10
Loma Prieta	6.9	0.28	18	52	Morgan hill	6.2	0.29	8.4	38
Average	**6.96**	**0.29**	**12.18**	**26.97**					

3.4 DESIGN PARAMETERS OF THE STUDY

The key design parameters of this study, as shown in Figure 3.4, are footing width, toe width, footing thickness and stem thickness, denoted as X_1, X_2, X_3 and X_4, respectively. In order to determine the limiting values of key design parameters, the stability of the retaining wall was checked using Mononobe-Okabe method for overturning, sliding, bearing capacity and eccentricity. Considering the limiting values of ϕ, c and k_{PGA}, the lower and upper limits of design variables to be implemented in defining some design cases are obtained as following:

$4.5 < X_1 < 6.1$; $3 < X_2 < 6.1$; $0.5 < X_3 < 0.87$; $0.3 < X_4 < 0.61$

As it can be observed, the range of X_2 is not consistent with typical dimension of toe in retaining walls. This long toe is due to the low unit weight of shredded tire backfill which caused difficulties in meeting eccentricity requirements. For satisfying these requirements, the toe length was increased to have a longer moment arm. Based on the obtained upper and lower limits for design variables, six different design cases were defined for conducting dynamic finite element simulations for the variations of random variables as listed in Table 3.2.

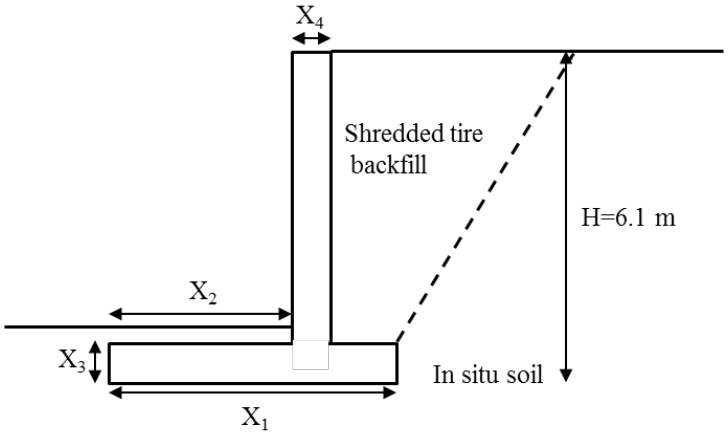

Figure 3.4 Illustration of the example retaining wall

Table 3.3 Design cases selected for finite element simulation

Design variables	Design 1	Design 2	Design 3	Design 4	Design 5	Design 6
X_1 (m)	4.5	6	6	5.5	5	4.5
X_2 (m)	3	5.4	3	4	3.2	4
X_3 (m)	0.5	0.87	0.5	0.7	0.6	0.5
X_4 (m)	0.3	0.6	0.6	0.45	0.4	0.5

3.5 DYNAMIC FINITE ELEMENT ANALYSIS

The dynamic finite element (FE) simulations of retaining wall-backfill-in situ soil system were conducted using PLAXIS 2D for the defined design cases. Each design case was analyzed for various combinations of random variables, using values of exp(λ), exp(λ-ξ) and exp(λ+ξ) for each random variable while keeping other variables at exp(λ). Thus, 7 simulations were performed for each design case and 42 simulations were carried out in total. Since the accuracy of the FE analysis results will affect the optimization results, a number of steps were taken to reduce the errors in the computed response. First, the size of the simulation domain and corresponding finite element mesh size were obtained from parametric studies following the procedure presented in Ravichandran and

Huggins (2013) to ensure that the computed response, wall tip deflection in this study, is independent of mesh size and simulation domain size.

The parametric study resulted in the model size presented in Figure 3.5 with Very Fine mesh which consists of 1800 to 2000 15-node triangular elements. The standard earthquake boundary condition was applied to the model to ensure that the earthquake waves propagating from the bottom of the model are properly represented. In addition, to accurately account the interaction between the structural components and backfill and in situ soils, interface elements were used. Finally, the stress-strain behavior of the backfill and in situ soils were represented by the Hardening Soil (HS) model which is a nonlinear elastoplastic model suitable for cyclic nonlinear analysis. Comparing to Mohr-Coulomb and linear elastic models, HS is a superior model for dynamic analysis that considers soil modulus reduction and small-strain damping. The HS model input parameters, as shown in Table 3.4, were obtained by calibrating the HS model with Mohr-Coulomb model. Although the accuracy of the procedure followed in this study may not result in the best HS model parameters, this procedure and the model parameters were considered reasonable to demonstrate the proposed procedure.

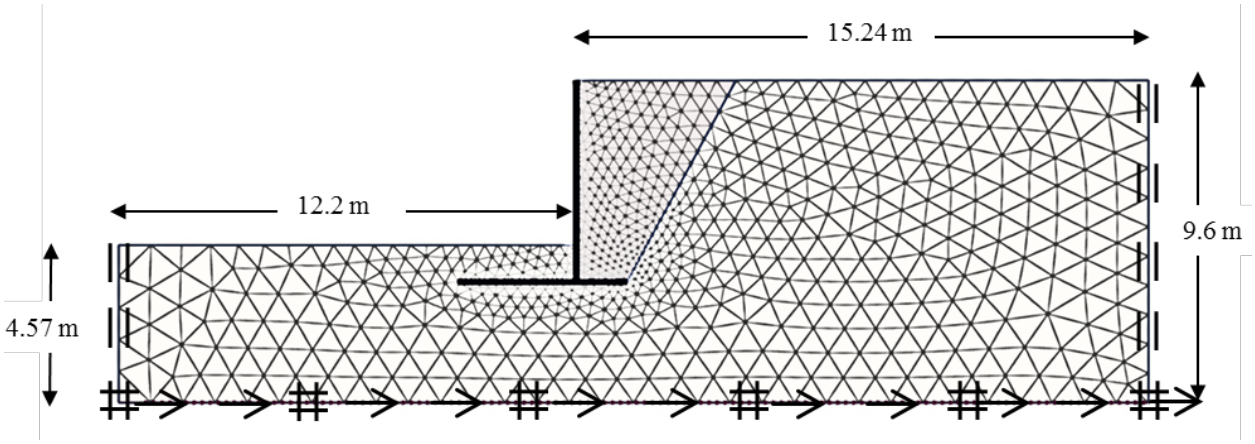

Figure 3.5 Schematic of the simulation domain and finite element mesh

Table 3.4 Hardening Soil input parameters of shredded tire

ϕ (°)	c (kPa)	E_{50}^{ref} (kPa)	E_{oed}^{ref} (kPa)	E_{ur}^{ref} (kPa)	m	ψ
23.71	11.25	1600	2026.84	4800	1	0
33.87	11.25	1621	2026.84	4863	1	3.87
16.6	11.25	1576	2026.84	4728	1	0
23.71	28.12	1516	2026.84	4548	1	0
23.71	4.5	1645	2026.84	4935	1	0

Note: E_{50}^{ref} is secant stiffness in standard drained triaxial test, E_{oed}^{ref} is tangent stiffness for primary oedometer loading, E_{ur}^{ref} is unloading/reloading stiffness from drained triaxial test, m is the power for stress-level dependency of stiffness, and ψ is the dilatancy angle

The computer models for each combination were analyzed by applying the first ten seconds of the El Centro 1940 earthquake acceleration-time history shown in Figure 3.6(a). The PGA of the motions is approximately 0.3 g. This record is often used as the reference earthquake motion in seismic analysis of geotechnical systems. The acceleration-time history scaled to PGAs of 0.14 g, 0.25 g and 0.45 g was used as the ground motion for the finite element analyses. Sample scaled acceleration-time history for PGA = 0.14 g is shown in Figure 3.6(b). The computed wall tip deflection-time histories for design cases 1 and 2 with mean ϕ, c and k_{PGA} are shown in Figure 3.7. The

wall tip deflection was computed by subtracting the wall base deflection-time history from the wall tip deflection-time history. The maximum wall tip deflections were then determined from the deflection-time histories for developing response surface.

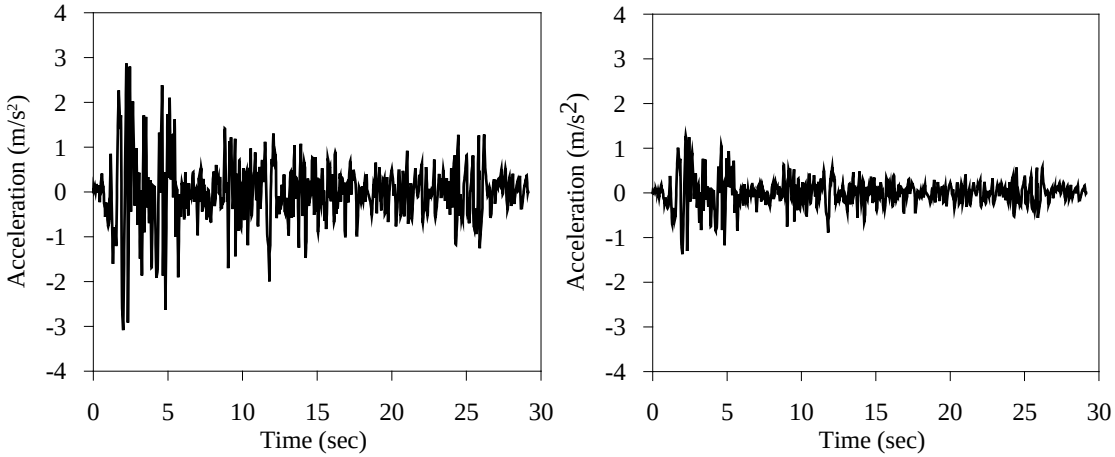

Figure 3.6 El Centro 1940 earthquake acceleration-time history

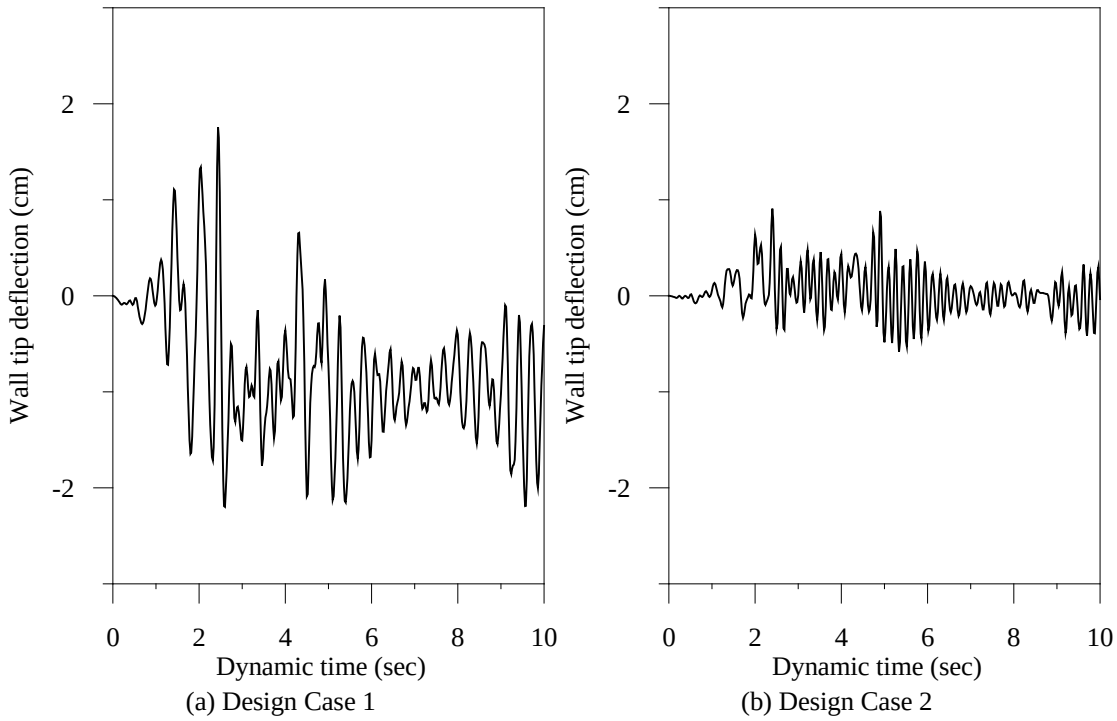

Figure 3.7 Wall tip deflection-time histories

3.6 RESPONSE SURFACE DEVELOPMENT

Using response surface method, the results obtained from finite element dynamic analysis were utilized to establish a functional relationship between independent variables and the dependent variables. Thus, in this study, a response model was developed between seven (input) variables, including three random variables (ϕ, c, k), four design variables (X_1, X_2, X_3, X_4), and the deflection (d) as response, by performing nonlinear regression analysis (Khuri and Mukhopadhyay 2010). Among common models applied in response surface method, here the logarithmic regression fitted data points reasonably well and the validity of function was also evaluated. The logarithmic model adopted to express the response is as follows:

$$y = \exp\left(b_0 + \sum_{i=1}^{n} b_i Ln\left(x_i\right) \right) \tag{3.3}$$

where y and x denote the response and variables respectively and b_0 and b_i are the coefficients. Using this model, which brings a good interpretation of data, the response surface *d* shown in Eq. 3.4 was proposed in terms of random variables (ϕ, *c*, k_{PGA}) and design variables (X_1, X_2, X_3 and X_4) with R-squared value of 0.941.

$$d = \exp\begin{pmatrix} 1.377 - 0.123Ln\left(\phi\right) + 0.037Ln\left(c\right) + 0.921Ln\left(k_{PGA}\right) - \\ 0.653Ln\left(X_1\right) + 0.385Ln\left(X_2\right) - 0.417Ln\left(X_3\right) - 1.03Ln\left(X_4\right) \end{pmatrix} \tag{3.4}$$

This relationship represents the response of the system in terms of deflection regarding the uncertain parameters and geometrical parameters. In other words, the approximate behavior of retaining wall system backfilled with lightweight material like shredded tire with specific height can be predicted considering uncertain properties and design parameters. This methodology provides an opportunity to perform the design optimization avoiding thousands of time-consuming analyses.

Moreover, the validity and performance rate of the response surface need to be evaluated. For this purpose, 20 random design sets combined with 20 random values for random variables were generated and modeled in PLAXIS 2D and the results were compared with those obtained from the response surface. Figure 3.8 shows that the points are fairly adjacent to the line y=x and demonstrates a good agreement between two sets of results. However, this method of visual qualitative validation may not be adequate to guarantee the validity of response surface; additional indicators may need to be applied to quantitatively evaluate the accuracy of regression. Recommended by Moriasi et.al

(2007), three quantitative statistics were computed based on FE simulation results and observation results of response surface.

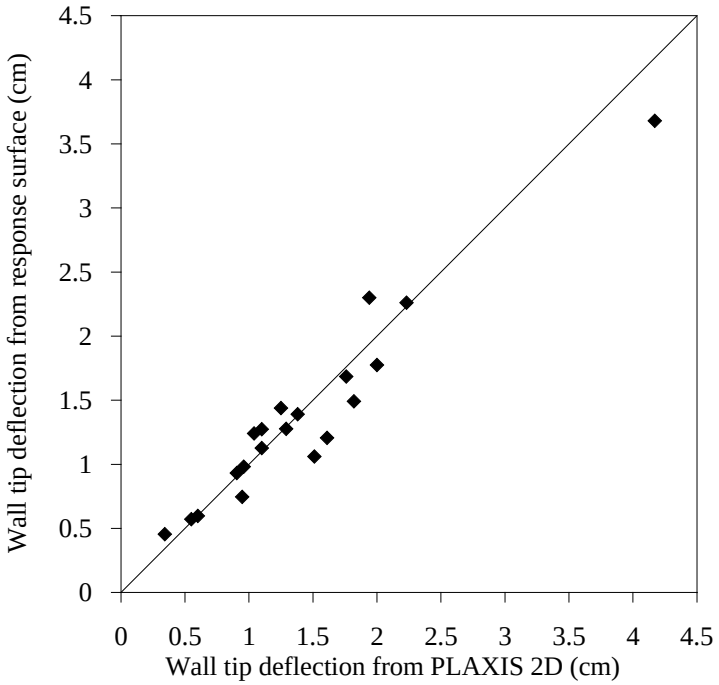

Figure 3.8 Graph of deflection obtained by PLAXIS 2D and response response

Nash-Sutcliffe efficiency (NSE), percent bias (PBIAS) and ratio of the root mean square error to the standard deviation of measured data (RSR) are expressed as in Eqs. 3.5, 3.6 and 3.7 and categories of performance rating are listed as per Table 3.5:

$$NSE = 1 - \left[\frac{\sum_{i=1}^{n} \left(Y_i^{obs} - Y_i^{sim} \right)^2}{\sum_{i=1}^{n} \left(Y_i^{obs} - Y_i^{mean} \right)^2} \right] \tag{3.5}$$

where Y^{obs} is the observation, Y^{sim} is the simulated value and Y^{mean} is the mean of observed data. Here, the response resulted from PLAXIS 2D model and from response surface are considered as Y^{obs} and Y^{sim}, respectively.

$$PBIAS = \left[\frac{\sum_{i=1}^{n} \left(Y_i^{obs} - Y_i^{sim} \right) * 100}{\sum_{i=1}^{n} Y_i^{obs}} \right] \tag{3.6}$$

$$RSR = \frac{RMSE}{STDEV_{obs}} = \frac{\left[\sqrt{\sum_{i=1}^{n} \left(Y_i^{obs} - Y_i^{sim} \right)^2} \right]}{\left[\sqrt{\sum_{i=1}^{n} \left(Y_i^{obs} - Y_i^{mean} \right)^2} \right]} \tag{3.7}$$

Table 3.5 Performance ratings for recommended statistics

Performance rating	**RSR**	**NSE**	**PBIAS***
Very good	0-0.5	0.75-1	<±15
Good	0.5-0.6	0.65-0.75	±15 - ±30
Satisfactory	0.6-0.7	0.5-0.65	±30 - ±55
Unsatisfactory	>0.7	<0.5	> ±55

*Ranges were problem-dependent and the average one is considered here.

The computed statistics shown in Table 3.6 indicate that the overall validity of response surface is classified as “very good”. In sum, a combination of visual technique and dimensionless statistics were utilized to validate the response surface and ensure its reliability to be used in design optimization process.

Table 3.6 Response surface validity performance

Statistics	**Value**	**Performance**
RSR	0.29	Very Good
NSE	0.92	Very Good
PBIAS	3.58	Very Good

3.7 DESIGN OPTIMIZATION OF RETAINING WALL BACKFILLED WITH SHREDDED TIRE

To capture a set of preferred designs, a set of objective functions were defined to be implemented in optimization algorithm, NSGA-ii (Non-dominated Sorting Genetic Algorithm) (Deb et al. 2002; Song 2011). Cost and robustness were treated as objectives in this work along with specified safety constraint. Standard deviation of response was considered as the robustness index. Minimizing the standard deviation of response corresponds to maximizing the robustness of the system and making the system less sensitive to the uncertainties involved. The objectives of design optimization of current study are described in the following.

3.7.1 Objective Function 1: Cost

The cost function derived for the retaining wall, as expressed Eq. 3.8, considers the cost of concrete used for construction of the retaining wall, the cost of earth excavation and tire shredding. The cost of concrete, excavation and tire shredding were assumed 75, 10 and 40 USD/m^3, respectively. The cost of shredded tire was estimated based on prices suggested by companies or used in relevant reports as listed in Table 3.7.

$$y_1 = \left(X_1X_3 + (H - X_3)X_4\right)\times\left(75\text{USD/m}^3\right) + \left(\left(\left(X_1 - X_2 - X_4\right)\times 2 + H\right)\times H/2\right)\times(10\text{USD/m}^3) + \left(\left(\left(X_1 - X_2 - X_4\right)\times 2 + H\right)\times\left(H - X_3\right)/2\right)\times(40\text{USD/m}^3) \quad (3.8)$$

Table 3.7 Shredded tire cost

Source	Size	Price (USD)	(USD/m3)
recycle.net	mix	80 /ton	63.0

	mix	45/ton	35.4
	<3"	40/ton	31.5
	mix	64/ton	50.3
	<4"	40/ton	31.5
	<2"	28/ton	22.0
vecoplanllc.com	2"	25-50 /ton	20-40
Head et al. (2001)	--	--	12
Dwyer (2008)	--	--	80-90
Average ~	--	--	**40**

3.7.2 Objective Function 2: Standard Deviation of Response

Standard deviation of response was computed using two methods: Monte Carlo (MC) and Taylor Series Finite Difference (TSFD). MC method involves generating random samples of the input random variables based on the lognormal distributions of the variables, computing the response for each set of variables, repeating the procedure for N number of samples and then calculating the mean value and standard deviation of response. While in TSFD method, standard deviation of response can be expressed using the relationship below:

$$\sigma_d = \sqrt{\left(\frac{d^+ - d^-}{2}\right)_\phi^2 + \left(\frac{d^+ - d^-}{2}\right)_c^2 + \left(\frac{d^+ - d^-}{2}\right)_{k_{PGA}}^2} \tag{3.9}$$

where σ_d= standard deviation of wall tip deflection, d^+= wall tip deflection corresponding to exp(λ+ξ) of random variable and d^-= wall tip deflection corresponding to exp(λ-ξ) of random variable. Therefore, using either method for computing the second objective function, we have:

$$y_2 = \sigma_d = f(X_1, X_2, X_3, X_4) \tag{3.10}$$

3.7.3 Safety Constraint

For screening designs in the design optimization process, a target reliability index (βt) equal to 3 was defined as a constraint based on serviceability limit state. This constraint prevents the designs of lower reliability from involving in the set of suitable designs. To compute the reliability index of the system, defining performance function of the system is required using the response surface and considering an allowable deflection for wall tip as below,

$$g\left(\theta, X\right) = d_{all} - d\left(\theta, X\right) \tag{3.11}$$

where θ and X indicate random variables and design variables, respectively, g(θ, X)= performance function, d_{all}= allowable wall tip deflection and d(θ, X)= response function. Mean value, standard deviation of performance function and reliability index were then calculated using Eqs. 3.12, 3.13 and 3.14, respectively.

$$\mu_g = g\left(\mu_\theta, X\right) = d_{all} - d(\mu_\phi, \mu_c, \mu_{k_{PGA}}, X_1, X_2, X_3, X_4) \tag{3.12}$$

$$\sigma_g = \sigma_d \tag{3.13}$$

$$\beta = \frac{\mu_g}{\sigma_g} \tag{3.14}$$

3.8 DESIGN OPTIMIZATION RESULTS AND DISCUSSION

The Pareto fronts established through NSGA-ii consist of the computed objectives of all populations in the last generation, in which population size is equal to the number of designs dominated by other designs. Generally speaking, in NSGA-II

a population of candidate solutions (design cases) of an optimization problem is developed to better solutions. The evolution, which is an iterative process, usually starts from a population of randomly generated individuals, and the whole population in each iteration is called a generation. In each iteration, after combining the populations of parents and the children, values of objective functions are evaluated, and the best individuals are sorted and selected from the current population. The new population plays the role of parents and is used for selection, crossover, and mutation to create the children population. The next generation consists of the combination of parents and children, again. Commonly, the algorithm terminates when a maximum number of generations has been produced, or the population has reached a satisfactory level. (Deb et al. 2002)

In this study, a clear trade-off relationship between cost and the robustness index was inferred from the resulted Pareto fronts. In other words, decreasing the standard deviation of wall tip deflection which helps the system to perform in a more robust manner resulted in retaining walls of more costly designs. Using MC method in optimization, as demonstrated in Figure 3.9, the computed standard deviation of deflection increased from about 0.4 cm to 0.65 cm while cost per unit length of wall decreased from 900 USD to more than 600 USD, as is shown in Figure 3.10. Each point in the following set of Pareto fronts is a demonstration of a design case with its specific value of cost (per unit length) and standard deviation of wall tip deflection. Using TSFD method, another Pareto front was resulted from optimization as shown in Figure 3.11. As it is observed, the range of variations of cost and standard deviation are in good agreement with the variations in Figure 3.10.

The resulted Pareto fronts can be judged by designers and the final design can be selected based on engineering preferences and available resources such as project budget. Also, a higher robustness level may be considered by designers, and a final design corresponding to that level of robustness can be determined without cost concerns. However, considering both objectives (cost and robustness level) simultaneously, the optimal final design can be determined from Pareto front using knee point concept.

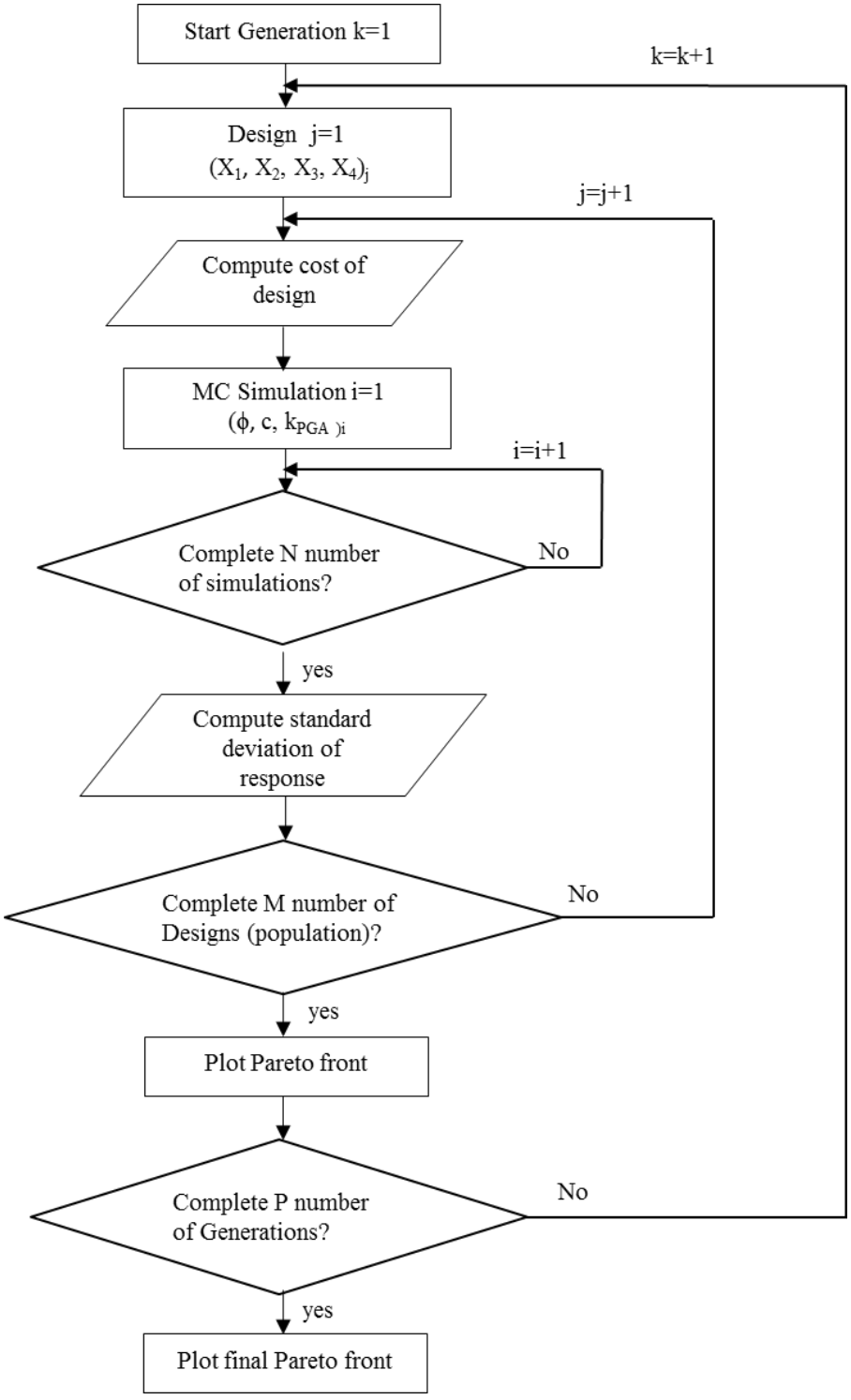

Figure 3.9 Flowchart of optimization using NSGA-ii coupling with MC method

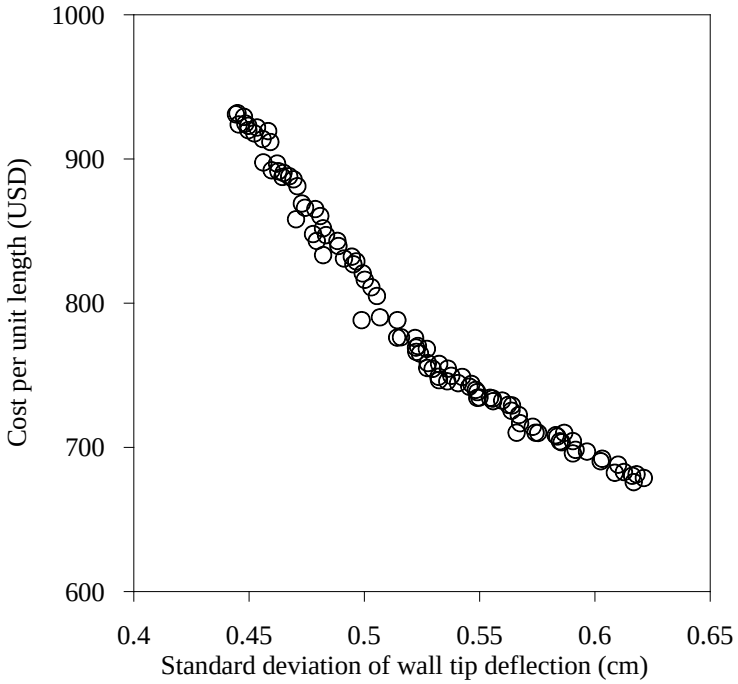

Figure 3.10 Pareto front optimized to cost and standard deviation using MC method

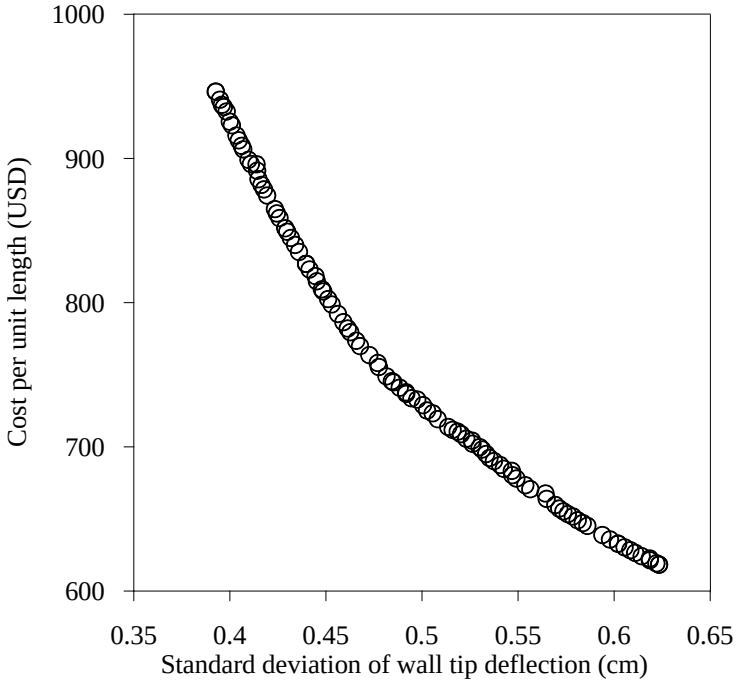

Figure 3.11 Pareto front optimized to cost and standard deviation using TSFD method

To determine the optimum design with respect to cost and standard deviation of

wall tip deflection of the retaining wall problem, the knee point on resulted Pareto fronts were identified using two approaches; normal boundary intersection (NBI) approach and minimum distance approach. In the former method, the distances between each point on Pareto front and the boundary line, which connects the upper point and lower point of Pareto front, are computed in normalized space and the point corresponding to the maximum distance is found which is known as knee point as illustrated in Figure 3.12(a). The second approach utilizes the concept of utopia point and determines the minimum distance among calculated distances between each point on Pareto front and the defined utopia point. Therefore, the knee point is the point on Pareto front corresponding to the minimum distance as illustrated in Figure 3.12(b). The utopia point is originated from the concept of ideal unreal design in which all objectives are at their minimum value and the closest design point to the utopia point is considered as optimum design (Khoshnevisan et al. 2014). Using these approaches, the same knee point characteristics were obtained for both Pareto fronts presented. Moreover, the knee points identified as optimal designs resulting from optimization with methods of MC and TSFD were in good agreement as summarized in Table 3.8. The table represents the optimal values of design parameters of retaining wall backfilled with shredded tire with their corresponding cost and robustness measure. The results are consistent with each other due to the fact that different statistical methods led us into similar design sets and it can be an evidence for appropriateness of response surface.

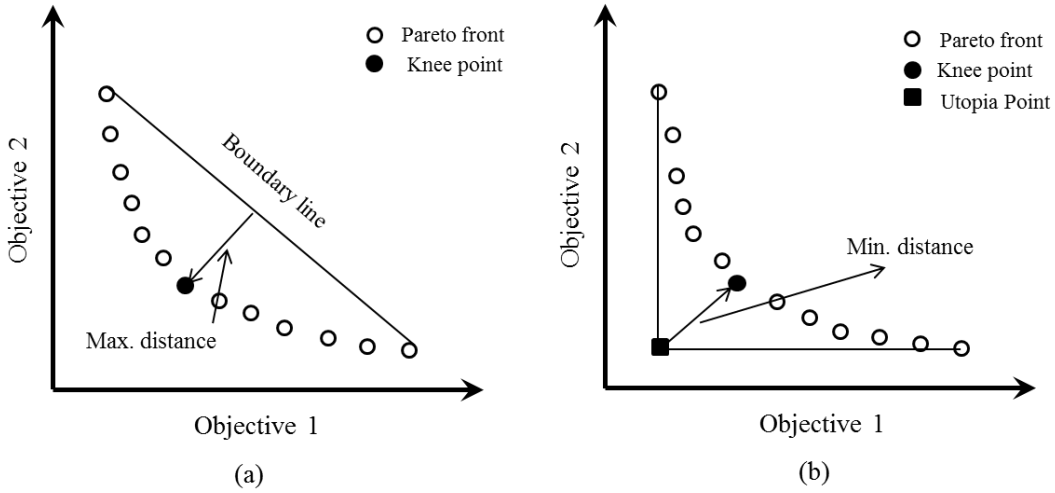

Figure 3.12(a) NBI approach and (b) minimum distance approach

Table 3.8 Knee point parameters obtained from Pareto fronts

Method	Cost (USD)	Standard Deviation (cm)	X_1 (m)	X_2 (m)	X_3 (m)	X_4 (m)
MC	788	0.49	4.74	3	0.87	0.6
TSFD	749	0.48	4.5	3	0.84	0.6

3.9 CONCLUSION

The robust design optimization of retaining wall backfilled with lightweight material and subjected to seismic load was carried out through coupling of finite element dynamic analysis and bi-objective optimization. The robustness of design was satisfied by minimization of standard deviation of wall tip deflection. Along with standard deviation of response, the expenses contributed to construction and operation of this type of wall was another objective to be minimized. On the other hand, the reliability of design was assessed and met using the concept of target reliability index and defining a performance function due to an allowable deflection. Therefore, the uncertainty in backfill parameters and in seismic loading was considered in this methodology which

leads the designers to more efficient designs so as not to overdesign because of safety satisfaction, or not to underdesign because of cost concerns.

In summary, despite the advantages associated to use of shredded tire as backfill for retaining walls, the presented robust design methodology can be introduced as an efficient tool for geotechnical dynamic design of retaining structures that considers safety, robustness and cost simultaneously. Moreover, the knee point concept can be utilized to aid in selection of best design in a design pool.

REFERENCES

Eldin, N. N. and Senouci, A. B. (1992). "Use of scrap tires in road construction." *Journal of Construction Engineering and Management*, 118(3), 561-576.

Bosscher, P. J., Edil, T. B. and Kuraoka, S. (1997). "Design of highway embankments using tire chips." *Journal of Geotechnical and Geoenvironmental Engineering*, 123(4), 295-304.

Reddy, K. R., Stark, T. D., & Marella, A. (2009). Beneficial use of shredded tires as drainage material in cover systems for abandoned landfills. *Practice Periodical of Hazardous, Toxic, and Radioactive Waste Management*, *14*(1), 47-60.

Humphrey, D.N., Sandford, T.C., Cribbs, M.M. and Manion, W.P. (1993). "shear strength and compressibility of tire chips for use as retaining wall backfill." *Transportation Research Record*, 14, 433-451

Cecich, V., Gonzales, I., Hoisaeter, A., Williams, J. and Reddy, K. (1996). "Use of shredded tire as lightweight backfill material for retaining structures." *Wast Management & Research*, No. 14, pp. 433-451

Tweedie, J. J., Humphrey, D. N. and Sandford, T. C., (1998). “Tire shreds as lightweight retaining wall backfill: active conditions.” *Journal of Geotechnical and Geoenvironmental Engineering*, No. 124, pp. 1061-1070.

Lee, J.H., Salgado, R., Bernal, A. and Lovell, C.W. (1999). “Shredded tires and rubber sand as lightweight backfill.” *Journal of Geotechnical and Geoenvironmental Engineering*, 125 (2), pp. 132-141

Ravichandran, N. and Huggins, L. (2013). “Seismic response of gravity-cantilever retaining wall backfilled with shredded tire.” *Geotechnical engineering Journal of the SEAGS & AGSSEA,* Vol. 44 No. 3 14-24

Reddy, S. B. and Krishna, A. M. (2015). “Recycled Tire Chips Mixed with Sand as Lightweight Backfill Material in Retaining Wall Applications: An Experimental Investigation.” *International Journal of Geosynthetics and Ground Engineering*, 1(4), 1-11.

Shrestha, S., Ravichandran, N., Raveendra, M. and Attenhofer, J. A. (2016). “Design and analysis of retaining wall backfilled with shredded tire and subjected to earthquake shaking.” *Soil Dynamics and Earthquake Engineering*, 90, 227-239.

Saribas, A. and Erbatur, F. (1996). “Optimization and sensitivity of retaining structures.” *Journal of Geotechnical Engineering*, 122(8), 649-656.

Ceranic, B., Fryer, C. and Baines, R.W. (2001). “An application of simulated annealing to the optimum design of reinforced concrete retaining structures.” *Computers & Structures*, 79(17), 1569-1581.

Yepes, V., Alcala, J., Perea, C. and González-Vidosa, F. (2008). A parametric study of optimum earth-retaining walls by simulated annealing." *Engineering Structures*, 30(3), 821-830.

Camp, C.V. and Akin, A. (2011). "Design of retaining walls using big bang–big crunch optimization." *Journal of Structural Engineering*, 138(3), 438-448.

Pei, Y. and Xia, Y. (2012). "Design of reinforced cantilever retaining walls using heuristic optimization algorithms." *Procedia Earth and Planetary Science*, 5, 32-36.

Papazafeiropoulos , G., Plevris , V. and Papadrakakis , M. (2013). "Optimum design of cantilever walls retaining linear elastic backfill by use of genetic algorithm." *COMPDYN 2013*

Babu, G. L. S. and Basha, B. M. (2008). "Optimum design of cantilever retaining walls using target reliability approach." *International Journal of Geomechanics*, 8, 240-252

Phoon, K. K. and Kulhawy, F. H. (1999). "Characterization of geotechnical variability." *Canadian Geotechnical Journal*, 36(4), 612-624.

Juang, C. H., Liu, Z. and Atamturktur, H. S. (2013). "Reliability-based robust geotechnical design of retaining walls." *Sound Geotechnical Research to Practice*, pp. 514-524

Liu, Z., Juang, C. H. and Atamturktur, S. (2013). "Confidence level-based robust design of cantilever retaining walls in sand." *Computers and Geotechnics*, No.52, pp. 16-27

Juang, C.H., Wang, L., Liu, Z., Ravichandran, N., Huang, H. and Zhang, J. (2013). "Robust geotechnical design of drilled shafts in sand: New design perspective." *Journal of Geotechnical and Geoenvironmental Engineering*, 139(12), 2007-2019.

Wang, L., Juang, C. H., Atamturktur, S., Gong, W., Khoshnevisan, S. and Hsieh, H. S. (2014). "Optimization of design of supported excavations in multi-layer strata." *Journal of Geoengineering*, Vol. 9, No. 1, pp. 1-12

Balunaini, U., Yoon, S., Prezzi, M. and Salgado, R. (2009). "Final report: Tire shred backfill in mechanically stabilized earth wall application." *FHWA/NA/JTRP*, 2008/17

Bressette, T. (1984). "Used tire material as an alternate permeable aggregate." State of California, Department of Transportation, Division of Engineering Services, Office of

Garegrat, H. (1993). "Finite element analyses of pavements underlain by a tire chip layer and of retaining walls with tire chip backfill." M.S. Thesis, Department of Civil Engineering, University of Maine

Ahmed, I., and Lovell, C.W. (1993). "Rubber soil as light weight geomaterials." *Transportation Research Record*, 61-70

Edil, T. B. and Bosscher, P. J. (1994). "Engineering properties of tire chips and soil mixtures." *Geotechnical Testing Journal*, 17(4), pp. 453-464.

[29] Black, B.A., and Shakoor, A. (1994). “A geotechnical investigation of soil-tire mixtures for engineering applications.” *Proceedings of the First International Conference on Environmental Geotechnics*, Bitech Publications, pp. 617-623

Duffy, D. P. (1995). “Using tire chips as a leachate drainage layer,” *Waste Age*, Vol. 26, No. 9, pp. 113-122.

Cosgrove, T. A. (1995). "Interface strength between tire chips and geomembrane for use as a drainage layer in a landfill cover," *Proceedings of Geosynthetics'95*, Industrial Fabrics Association, St. Paul, MN, Vol. 3, pp. 1157-1168.

Andrews, D.W., and Guay, M. A. (1996). “Tire chips in a superfund landfill cap: A case history of the first use of a tire chip drain layer.” *Nineteenth International Madison Waste Conference*, Dept. of Engineering Professional Development, University of Wisconsin-Madison.

Foose, G.J., Benson, C.H. and Bosscher, P.J. (1996). “Sand reinforced with shredded waste tires.” *Journal of Geotechnical Engineering*, 122: 760-767

Masad, E., Taha, T., Ho, C. and Papagiannakis, T. (1996). “Engineering Properties of Tire/Soil Mixtures as a Lightweight Fill Material.” *Geotechnical Testing Journal*

Wu, W., Benda, C. and Cauley, R. (1997). “Triaxial determination of shear strength of tire chips.” *Journal of Geotechnical and Geoenvironmental Engineering, ASCE*, Vol. 123, No. 5, pp. 479-482.

Gebhardt, M. A. (1997). “Shear strength of shredded tires as applied to the design and construction of a shredded tire stream crossings.” MS Thesis, Iowa State University.

Tatlisoz, N., Edil, T.B., and Benson, C. (1996). “Interaction between Reinforcing Geosynthetics and Soil-Tire chip mixtures.” *Journal of Geotechnical and Geoenvironmental Engineering*, No. 124, pp. 1109-1119

Yang, S., Lohnes, R.A., and Kjartanson, B.H. (2002). “Mechanical properties of shredded tires.” *Geotechnical Testing Journal*, 25 (1), pp. 44-52

Youwai, S., and Bergado, D.T. (2003). “Strength and deformation characteristics of shredded rubber tire-sand mixtures.” *Canadian Geotechnical Journal*, 40(2), pp. 254-264

Moo-Young, H., Sellasie, K., Zeroka, D. and Sabins, G. (2003). “Physical and chemical properties of tire shreds for use in construction.” *Journal of Environmental Engineering*, 129 (10), 921-929

Shalaby, A. and Khan, R.A. (2005). “Design of unsurfaced roads constructed with large-sized shredded rubber tires: a case study.” *Resources, Conservation and Recycling*, No. 44, pp. 318-332.

Warith, M.A., Evgin, E. and Benson, P.A.S. (2004). “Suitability of shredded tires for use in landfill leachate collection systems.” *Waste Management*, No. 24, pp. 967-979

Hataf, N., and Rahimi, M.M. (2006), “Experimental investigation of bearing capacity of sand reinforced with randomly distributed tire shreds.” *Construction and Building Materials*, No. 20, pp. 910–916

Cornell, C. A., Banon, H., and Shakal, A. F. (1979). “Seismic motion and response prediction alternatives.” *Earthquake Engineering & Structural Dynamics*, 7(4), 295-315.

Khuri, A.I., and Mukhopadhyay, S. (2010). “Response surface methodology.” *WIREs Computational Statistics*, Vol. 2, pp. 128-149

Moriasi, D.N., Arnold, J.G., Van Liew, M.W., Bingner, R.L., Harmel, R.D. and Veith, T.L. (2007). “Model evaluation guidelines for systematic quantification of accuracy in watershed simulations.” *Transactions of the ASABE*, 50(3), 885-900.

Deb, K., Pratap, A. and Agarwal, S. (2002). “A fast and elitist multiobjective genetic algorithm NSGA-II.” *Evolutionary Computation*, 6(2), pp. 182-197.

Song, L. (2011). “NGPM -- A NSGA-II program in Matlab.” Aerospace Structural Dynamics Research Laboratory, College of Astronautics, Northwestern Polytechnical University, China

www.recyclenet.com

www.vecoplanllc.com

Head, D., Picornell, M. and Nash, P.T. (2001). “Report: El Paso embankment fill with shredded tire.”

Dwyer, D.F. (2008). “Technical report: tire shred initiative: summary report.” State of New York Department of Transportation, Geotechnical Engineering Bureau

Khoshnevisan, S., Gong, W., Wang, L. and Juang, C. H. (2014). “Robust design in geotechnical engineering–an update.” *Georisk: Assessment and Management of Risk for Engineered Systems and Geohazards*, 8(4), 217-234.

CHAPTER 4

UNCERTAINTY-BASED DESIGN OF I-WALL LEVEE SYSTEM RESTING ON SAND FOUNDATION

ABSTRACT

Levees are integral part of the storm surge and flood protection systems that run along rivers or shore lines. Per the investigations after the Hurricane Katrina and the events thereafter, failures of the I-wall levee systems were found to be the major cause of the extensive flooding. These events suggest that the current design procedures must be revised to reduce the overall probability of failure of the system and its variations through accounting for uncertainties systematically and explicitly in the system. The possible variations in uncertainties such as soil properties due to construction and geological conditions, and the flood water level during flood events can cause high variations in overall performance of I-wall levee systems resulting in unforeseen malfunctions. In this paper, a framework to perform the design optimization of a typical I-wall levee made of clay resting on a sand foundation is proposed. For this purpose, the uncertainties of the system including undrained shear strength of levee fill, friction angle of sand foundation, and flood water level behind I-wall were considered as random variables. The design variables used in optimization setting were the penetration depth of I-wall from the levee crown, width of levee crown and landside slope of levee. Considering the upper and lower limits of design variables, several design cases were generated, then modeled, and analyzed for overall stability regarding the variations in the random variables. Considering the global factor of safety of the system as the response of concern, a

response surface was developed to represent the factor of safety as a function of random and design variables and implemented in optimization procedure. In the design optimization, total cost of I-wall levee system (material and construction) was minimized to reach cost-efficient designs and at the same time the variation in probability of failure was evaluated and minimized to obtain robust designs (a design insensitive to uncertainties). Finally, the optimization yielded a set of preferred designs known as Pareto front from which the optimal design can be selected.

4.1 INTRODUCTION

Levee systems are typically designed using conventional deterministic approaches for site specific hydrological and geotechnical conditions to prevent damage during extreme events. The conventional procedures for design of such flood protection systems are component-performance based approaches and the uncertainties are implicitly accounted for through concept of factor of safety (Sills et al. 2008). Therefore, to consider the interaction and integration of the components of the system, and to explain the uncertainties lying in the system more comprehensive and probabilistic approaches are required in design procedures. To this aim, a robust probabilistic design approach was implemented in this study to systematically take the uncertainties into account and quantify the probability of failure of the system and its variations. Application of this approach in optimization helps evaluate and balance the reliability, robustness, and cost of the design in an explicit manner.

The sudden and uncontrolled failure of critical levee systems may result in severe flooding which causes significant economical and human losses. The failure of such systems usually occurs due to the exceedance of water level from levee crown and/or overestimation of the strengths of levee and foundation soils. Increasing the capacity of such flood protection systems and protecting the landside from overflow of water can be achieved through expanding the levee section or floodwall installation. Expanding the levee section is not considered as a reasonable option where there is limited right of way on the landside or the existing foundation is not suitable for additional levee load. It is displayed in Figure 4.1 that additional space is needed which may not be available for expanding the levee section. Therefore, a floodwall is commonly used in urban areas in these situations.

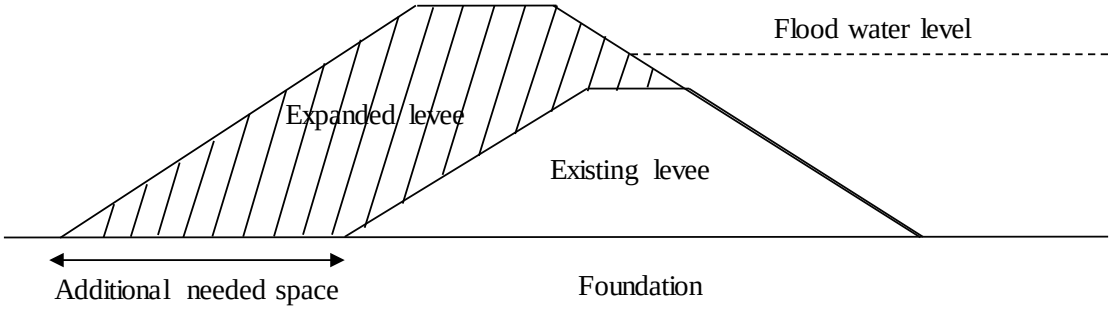

Figure 4.1 Expanding levee section

There are two types of floodwalls (Figure 4.2): I-wall, which is an I-shaped wall typically consisting of sheet pile wall driven into the levee and a concrete cap fixed to the top of sheet pile above the levee crown, and T-wall, which resists the load from flood by cantilever beam action. Because the construction of T-wall is complex and time

consuming compared to the I-wall, adding I-wall to the levee system is usually preferred due to the ease of installation and rehabilitation.

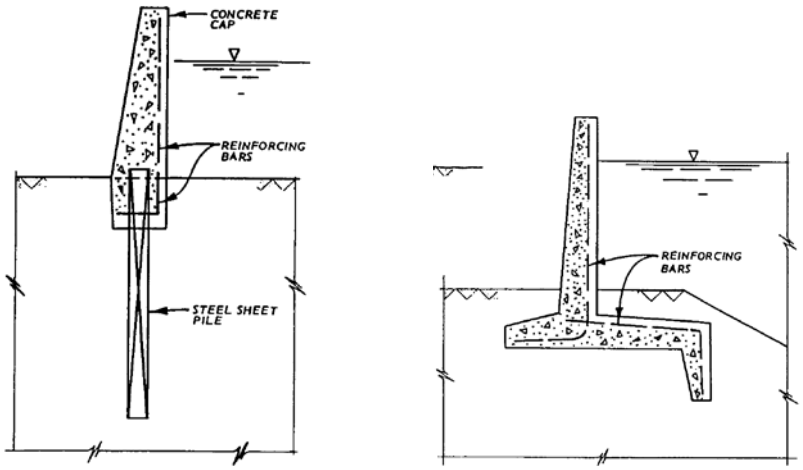

Figure 4.2 (a) I-wall and (b) T-wall (from USACE manual)

Failure of I-wall levee systems in large metropolitan areas can cause loss of life and damages to residential properties and infrastructure due to flooding. Hurricane Katrina in August 2005 caused catastrophic failure of New Orleans levee system and hence massive flooding in the areas. At some locations, the flooding occurred due to the failure of levee I-wall systems with sand foundation prior to being subjected to overtopping. Sills et al. (2008) and Duncan et al. (2008), the IPET (Interagency Performance Evaluation Taskforce) team, investigated on failures of I-wall levee systems in Hurricane Katrina and reported that the south breach of London Avenue I-wall levee system occurred mostly due to the seepage and piping in the sand foundation. For the north breach, the most likely cause of failure was sliding instability in the sand layer due to high uplift pressures acting against the base of the marsh layer. Sasanakul et al. (2008)

and Ubilla et al. (2008) performed centrifuge modeling of the failed levee systems during Hurricane Katrina on sand foundation (on London Avenue canal). The centrifuge model consisted initial phase (consolidation and pore water pressure stabilization) and flood phase (increasing the water level and monitoring the wall movement). They concluded that geometry of levee, penetration depth of the I-wall, and soil profiles were the key factors that contributed to the failure of the levee and recommended the penetration of the sheet pile into the foundation to increase the lateral support of wall along and decrease the flow of water in sand foundation. In addition to IPET, the ILIT (Independent Levee Investigation Team), also conducted a comprehensive site investigation and computer analyses on levee sections from several locations where I-wall levee system failures were observed (Seed et al. 2008). The two teams (IPET and ILIT) developed two-dimensional cross sections of the I-wall levees at the breach locations based on independent interpretations of the levee geometries, soil profiles, and storm-surge data. Similar approaches were adopted by both teams to analyze the performance of the levee systems using displacement-based finite element method (PLAXIS software used by both groups) as well as conventional limit equilibrium methods (SLIDE and UTEXAS used by IPET; SLOPE/W used by ILIT). The major focus of these studies on I-wall levee systems as mentioned above are the numerical and experimental analysis of the cases subjected to Hurricane Katrina and design of I-wall levee systems considering the system uncertainties has not been conducted. However, risk-based optimization of the levee system has been performed by researchers and engineers in the past considering hydraulic and hydrological uncertainties related to flooding. Moreover, the primary focus of most

of the levee design optimizations in the past is overtopping failure and few studies have included geotechnical failure of the levees (Tung and Mays 1981; Hui 2014).

A reliable and robust design approach must not only consider I-wall, levee, and foundation as a combined system, but also consider uncertainties in the system. Therefore, an uncertainty-based design approach needs to be implemented to ensure reliability and robustness of the system. The reliability of the system can be achieved using target (allowable) probability of failure so that designs of higher probability of failure will not be considered. Also, the robustness of the system refers to reduction of design sensitivity to effect of uncertainties in the system (Juang et al. 2013). Furthermore, to obtain an economic design the cost of construction should be considered as one of the objectives. Generally, the cost is balanced with safety requirements using factor of safety of the system in conventional deterministic design approaches and using allowable probability of failure in probabilistic design approaches. In this study, the I-wall levee system design was optimized to cost and robustness considering the uncertainties in soil properties and flood water level behind the I-wall and the robust design was compared with the non-robust design (typical optimal design). In addition, for demonstrating the effect of variation of flood water level on the I-wall levee system design several parametric studies were carried out considering factor of safety of the system and probability of failure.

4.2 I-WALL LEVEE SYSTEM DESIGN OPTIMIZATION APPROACH OF THE STUDY

4.2.1 Defining the Problem and the Variables of the Study

For demonstrating the proposed design approach, an I-wall levee system consisting of an earthen levee made of clay resting on sand was used in this study (Figure 4.3). The variables of the system are categorized into two types: design variables and random variables. The design variables considered in this study are the penetration depth of I-wall (D), the width of levee crown (X), and landside slope of the levee (S). The design exposed height of wall above the levee crown (H_{ex}) and floodside slope of the levee were assumed to be 2 m and 1V:2H, respectively. The uncertain parameters (also known as random variables) considered in the I-wall levee system of the study are flood water level behind I-wall (wl), undrained shear strength of the clay levee fill (s_u), and friction angle of the sand foundation (ϕ). Further details of the ranges and statistical properties of the variables are discussed in the following sections.

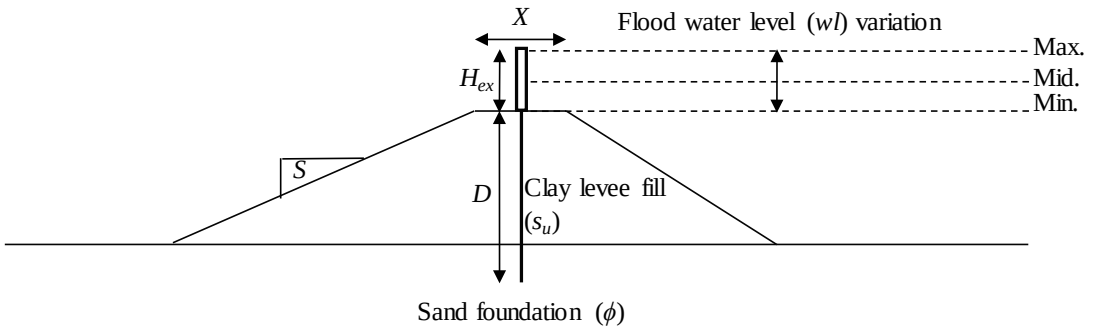

Figure 4.3 The schematic of the I-wall levee system of the study

4.2.1.1 Design variables

One of the important design parameters in I-wall levee system is the penetration depth of the I-wall which has a significant effect on the stability of slope, seepage and cost of construction. Per I-wall design regulation (EC 1110-2-6066) to ensure that adequate penetration will account for variations in soil properties in deterministic design approach the minimum penetration depth (D) of the sheet pile wall shall be the greatest of: 2.5 times the exposed height of the I-wall (H_{ex}) and 3 m below the levee crown. However, the theoretical required penetration in probabilistic design approach can be minimal as is considered in this study. The maximum value of H_{ex} is typically limited to 2 m for I-walls on levees or in soft soils (EC 1110-2-6066). Thus, in this study H_{ex} remained constant as 2 m and the lower limit and upper limit of D were assumed to be 2 m (equal to 1 times H_{ex}) and 8 m.

The levee crown width (X) was considered as a design variable due to its effect on slope stability and size of the levee with lower and upper limit of 3 m and 6 m, respectively. It should be noted that the same elevation was assumed for flood side and landside of the levee crown in this study. The other design variable of the study is the landside slope of the levee. For clay levee fill, steeper slopes can be applied. For riverine levees in which the wave action is not significant compared to coastal levees a steeper flood side can be used in the design (EM-1110-2-1913). Therefore, in this study the flood side slope of the levee was assumed to be 1V:2H and the land side slope (S) varied

between 1V:2H and 1V:4H. The design variables of the study and their ranges are tabulated as below:

Table 4.1 Design variables of the study

Design variable	Wall penetration depth, D (m)	Levee crown width, X (m)	Levee landside slope, S
Range	2-8	3-6	0.25-0.5

4.2.1.2 Random variables

The uncertainties in I-wall levee system design arise from strength of levee and foundation which is controlled by soil properties and from loading on the I-wall which is controlled by flood level. Since the soil profile in the system consists of different layers, uncertainty can be considered for each assumed soil strata. In this study for an I-wall levee system consisting of clay levee and sand foundation, undrained shear strength (s_u) of the levee fill and the friction angle of the sand foundation (ϕ) were considered as the soil-related uncertain parameters. The variation in the water level behind the wall can represent the destabilizing force exerted on the system. Therefore, the flood water level (wl) from the levee crown was considered as the loading-related random variable in this study. Regarding the investigations on I-wall levee systems after Hurricane Katrina, several failures were found to be occurred before the flood water raised high enough to flow over the I-wall. As mentioned earlier, without considering the failure due to overtopping in this study, the flood water level was assumed to vary between levee crown level and the top of the I-wall. Thus, having H_{ex} of 2 m the limiting range of the flood water level was assumed vary between 0 and 2 m. The statistical proprieties assumed for

the random variables are shown in Table 4.2. The standard deviations of the soil-related random variables are assumed so that 3 times the standard deviation covers the limiting range.

Table 4.2 Random variables of the study

Random variable	**Desirable range**	**Mean value**	**Standard deviation** (if using Normal distribution)
ϕ (°)	28-38	33	1.67
s_u (kPa)	20-42	31	3.67
wl (m)	0-2	1	-

4.2.2 Stability Analysis Methods

Several limit equilibrium methods have been developed for evaluating the potential failure and are expressed using factor of safety concept (Coduto 1999). Generally, two different approaches are used in limit equilibrium (LE) analysis of slopes: mass procedure and method of slices. In the method of slices, which is applicable to non-homogenous soil profile in the system, the soil mass is divided into a number of vertical slices and equilibrium equations are solved for each slice. Several methods of slices have been developed and can be used in slope stability analysis such as Ordinary Method of Slices, Simplified Bishop, Spencer, Janbu, Morgensten-Price and Sarma. Out of LE procedures the Spencer's method, which is a common method, can be selected and applied in the slope stability analysis of I-wall levee system.

The LE procedures and especially methods of slices are commonly used by researchers and engineers in slope engineering practice due to their significant computational efficiency compared to finite element (FE)-based procedures. However, Finite Element Method is widely accepted recently as a powerful alternative approach for slope stability analysis which can provide more realistic results in terms of system deformation and slope failure mechanism. In other words, FE analyses are useful when it is necessary to capture the behavior of the soil and wall together to assess stability or when displacements are critical. In FE-based programs the slope failure occurs naturally in the system where the soil shear strength is unable to resist the shear stress (Griffiths and Lane 1999). One of the main FE-based slope stability analysis methods is known as strength reduction method in which the critical slip surface is sought based on shear strain increase due to the reduction in shear strength of soil.

Therefore, to analyze the overall stability and performance of the I-wall levee system resting on sand foundation, both LE-based and FE-based methods were adopted in this study. The comparison of results obtained from these methods allows for evaluating the accuracy of the FS values, which can accordingly guarantee the accuracy of probability of failure computations. Thus, several design combinations of I-wall levee system were selected based on the feasible design domain, and were simulated using the FE-based program PLAXIS 2D and the LE-based program SLIDE. The overall stability using PLAXIS 2D is computed through safety analysis in which the strength reduction method is applied for obtaining FS following the consolidation and plastic analyses. On the other hand, Spencer's method can be used for FS calculation in SLIDE (Rocscience

2016*)*, which is a LE-based slope stability software with built-in finite element groundwater seepage analysis.

4.2.3 Stability Analyses Using LE and FE Procedures

In this study, the overall stability of the I-wall levee system resting on sand foundation was evaluated performing LE and FE procedures. Using the LE-based SLIDE, the overall factor of safety of the system was computed by Spencer's method which is an appropriate method of slices for the defined problem in this study. In SLIDE models, the stress-strain behavior of levee fill and the foundation soil was represented using Mohr-Coulomb material model and the Infinite Strength material type was used for I-wall, assuming it as a rigid wall. For the steady state seepage analysis, hydraulic boundary conditions were applied by setting total heads at floodside and landside of the levee system and the mesh of simulation domain included about 1000 6-node triangular elements. A sample SLIDE model of I-wall levee system is shown in Figure 4.4.

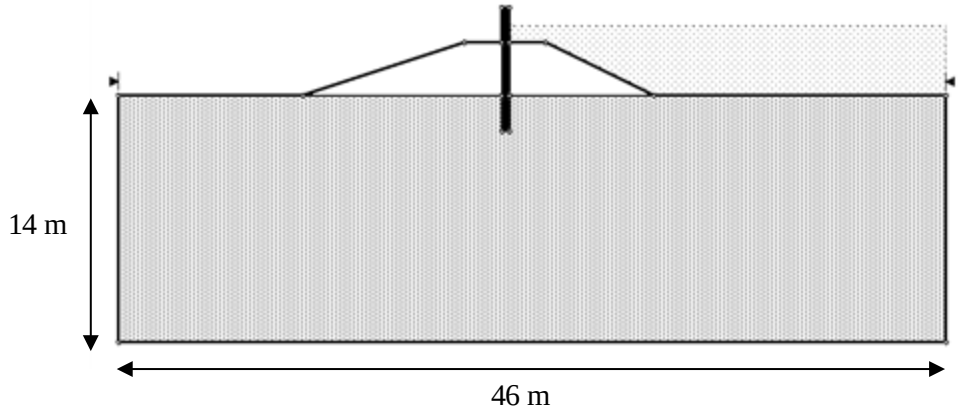

Figure 4.4 A sample SLIDE model of I-wall levee system

Performing safety analysis in PLAXIS 2D, the global factor of safety and the slip surface was obtained. In the safety approach using strength (phi-c) reduction method the shear strength parameters (*tan* ϕ and *c* or s_u) of the soil are successively reduced until failure of the system occurs. The total multiplier ∑Msf is used to define the value of the soil strength parameters at a given stage in the analysis.

$$\sum Msf = \frac{\tan \phi_{input}}{\tan \phi_{reduced}} = \frac{s_{u,input}}{s_{u,reduced}} \tag{4.1}$$

where the strength parameters with subscript *input* refer to the properties entered in the material sets and those with subscript reduced refer to the *reduced* values used in analysis. ∑Msf is set to 1 at the start of the calculation to set all material strengths to their input values. The value of ∑Msf at failure is considered as the FS of the system. Selecting a point in failure zone of the system, the FS curve can be plotted and the global FS can be determined (Brinkgreve et al. 2015: PLAXIS 2D Manual).

In FE simulation with PLAXIS 2D, Mohr-Coulomb and linear elastic material models were used for representing the stress-strain behavior of the soils in the system and the I-wall, respectively. For demonstration of the I-wall components, plate element was used for the sheet pile wall section and the concrete cap covering the exposed height of the I-wall was modeled using soil polygon in this study. To accurately take the wall-soil interaction into account, interface elements were applied in the model. The concrete cap dimensions were obtained from the reports on Levee I-wall of London Ave. canal in New Orleans, as shown in Figure 4.5, which was also constructed on the sand foundation

(Burk & Associates, Inc. 1986). For the sheet pile wall material, properties of PZ-27 sheet pile were used and the plate parameters in PLAXIS 2D were computed accordingly as listed in Table 4.3. Using the Young's modulus (*E*) of steel, moment of inertia (*I*) value and the cross-sectional area (*A*) of the section PZ-27, the equivalent thickness (*d*) of wall can be calculated to be implemented in PLAXIS 2D, considering *h* as plate thickness and *b* as plate width (=1m).

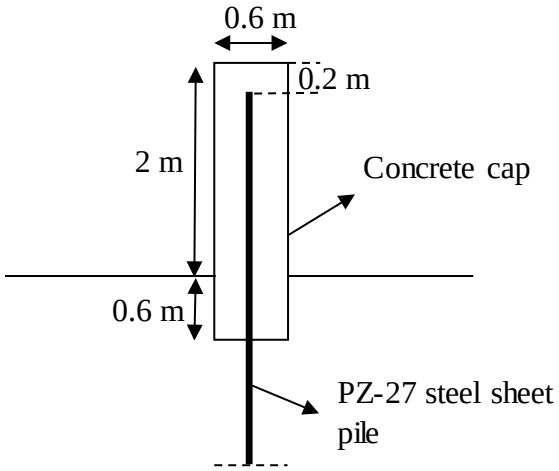

Figure 4.5 Dimensions of concrete cap of the I-wall

Table 4.3 Material properties of the sheet pile wall using PZ-27

PZ-27	Parameter	Unit	Value
From Bethlehem steel corporation	*h*	mm	305
	A	cm^2/m	168.1
	weight	kg/m^2	131.8
	I	cm^4/m	25200
Used in PLAXIS 2D	$EA\ (=E(hb))$	kN/m	3.362E6
	$EI\ (=E\left(\frac{bh^3}{12}\right))$	$kN.m^2/m$	5.04E4

	$d\ (=h=\sqrt{12\left(\frac{I}{A}\right)})$	m	0.4241
	$w\ (=weight\times g\times 10^{-3})$	kN/m/m	1.293

Moreover, a very fine mesh consisting of 1200-1600 15-node triangular elements was adopted in the models as shown in Figure 4.6. The same dimensions for simulation domain were used as in LE models. The regular boundary conditions were also applied to the model so that the vertical sides of the simulation domain were fixed to prevent horizontal translation and the base of the domain was fixed against both horizontal and vertical movements.

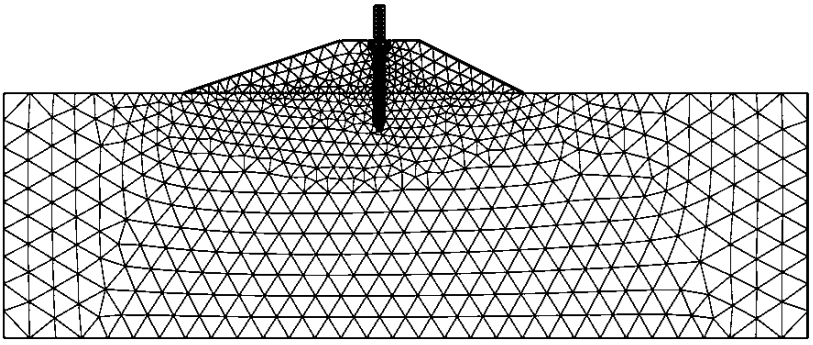

Figure 4.6 Sample of PLAXIS 2D model mesh of the I-wall levee system

It should be noted that prior to performing the stability analysis using LE and FE procedures, nine subset designs as listed in Table 4.4 were selected based on the design domain determined in previous sections for design variables. Regarding the simulation setups, the FS values of the I-wall levee system were obtained using both methods for variations of random variables (min., mean, max.) and compared as shown in Figure 4.7. It can be observed that the two methods are in good agreement with each other. However,

the results of PLAXIS 2D were adopted in optimization approach of this study as is discussed in the following sections.

Table 4.4 Selected design combinations for parametric study

Design	**Combination**	***D* (m)**	***X* (m)**	***S***
1	D_{min}, X_{min}, S_{min}	2	3	0.25
2	D_{max}, X_{max}, S_{max}	8	6	0.5
3	D_{mid}, X_{mid}, S_{mid}	5	4.5	0.33
4	$\boldsymbol{D_{min}}$, X_{mid}, S_{mid}	2	4.5	0.33
5	$\boldsymbol{D_{max}}$, X_{mid}, S_{mid}	8	4.5	0.33
6	D_{mid}, $\boldsymbol{X_{min}}$, S_{mid}	5	3	0.33
7	D_{mid}, $\boldsymbol{X_{max}}$, S_{mid}	5	6	0.33
8	D_{mid}, X_{mid}, $\boldsymbol{S_{min}}$	5	4.5	0.25
9	D_{mid}, X_{mid}, $\boldsymbol{S_{max}}$	5	4.5	0.5

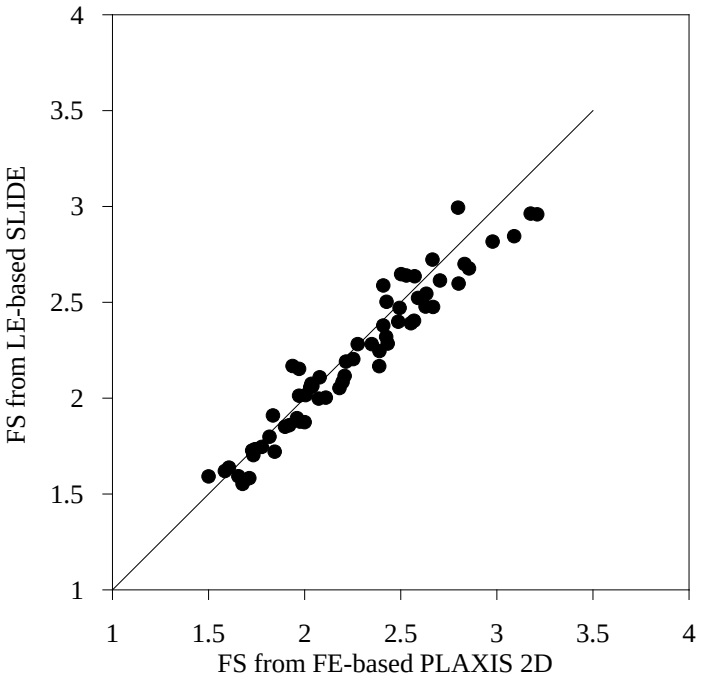

Figure 4.7 Comparison of FS from FE: PLAXIS 2D and FS from LE: SLIDE (Spencer)

4.2.4 Evaluating the Effect of Uncertainties on Overall Stability of the System

The effect of uncertainties (random variables) of the system (wl, ϕ and s_u) on the factor of safety (FS) of I-wall levee system was investigated considering the design parameters to demonstrate the importance of the uncertainties. Therefore, for subset designs 2 to 9 in Table 4.3 the variations of FS with change in each random variable are displayed in Figures 4.8-4.10.

It can be observed from these Figures that the FS value is greater than the assumed minimum FS of 1.5 in all selected design combinations. However, the worst design combinations are not considered here for monitoring the effect of limiting values of each design variable independent from other two design variables. Overall, Figures 4.8-4.10 show that I-wall levee systems were more stable with greater depth of wall

penetration, wider crown levee, and milder landside levee slope. Figure 4.8 shows that increase in flood water level from levee crown to the top of wall results in decrease in FS value. From Figure 4.8(c) it can be concluded that the steeper the landside slope of levee is, the design experiences lower factor of safety and at high water level the FS values are approximately close for variations of landside levee slope.

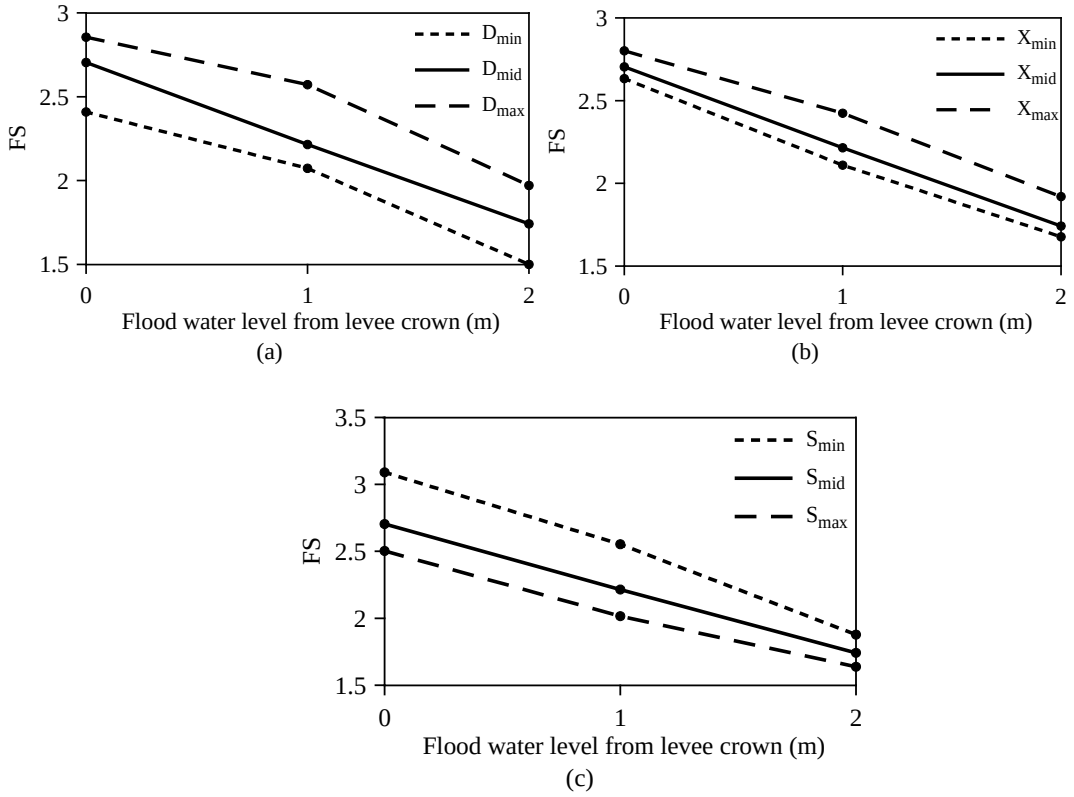

Figure 4.8 Variation of FS with flood water level

Figures 4.9 and 4.10 show that the effects of the soil-related random variables, s_u of levee fill and ϕ of sand foundation, on FS are opposite to that of flood water level. With levee fill of higher s_u, the FS of designs with D_{mid} and D_{min} are similar, as shown in Figure 4.9(a). Figure 4.9(b) shows that the I-wall levee system with wider levee crown gives a slightly greater FS, however by increasing s_u the increase in FS is not significant

for the three design cases (X_{min}, X_{mid}, X_{max}). Generally, Figure 4.9 indicates that the variation in s_u of the levee fill has minor effect on overall stability of the system comparing to the other random variables. As shown in Figure 4.10(a), at low ϕ the FS of design with minimum wall depth is close to that of with medium depth. From Figures 4.10(b) and 10(c), it can be noticed that in terms of levee crown width and landside slope variation of FS with variation of ϕ follow similar trends. Overall, along with evaluating the variation of FS with random variables, the observed variations of FS itself due to variations of uncertainties can provide reasonable justification for selecting those governing random variables.

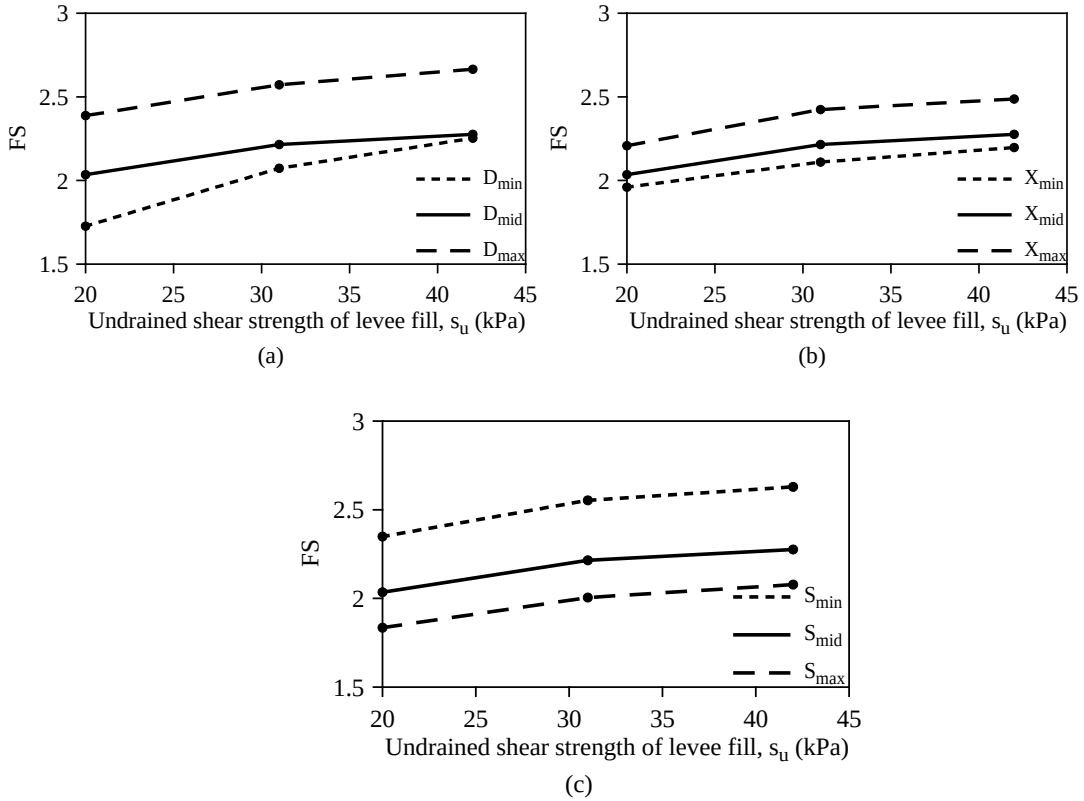

Figure 4.9 Variation of FS with undrained shear strength of levee fill

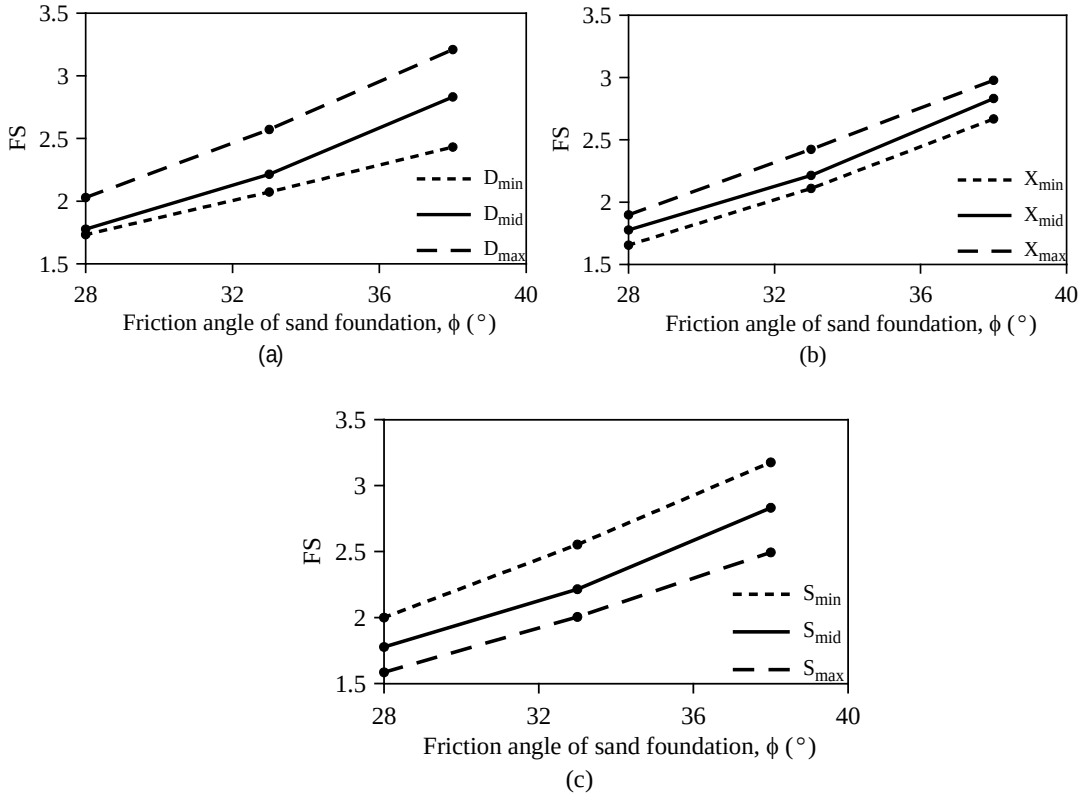

Figure 4.10 Variation of FS with friction angle of sand foundation

4.2.5 Developing Response Surface of the System

To compute FS of I-wall levee system for any possible combinations of design variables with possible variations of random variables and avoid thousands of time-consuming analyses, response surface method was adopted in this study. The response surface method, pioneered in the field of geotechnical engineering by Wong (1985), can be considered as an effective approach for mathematically representing the behavior of geotechnical structures in an approximate manner. Thus, a response surface was developed performing nonlinear regression analysis to represent FS as a function of random variables and design variables. Among the common models used in response

surface method (Khuri and Mukhopadhyay 2010), the second-order polynomial model was used as shown below in this study:

$$y = b_0 + \sum_{i=1}^{n} b_i x_i + \sum_{i=1}^{n} b_{ii} x_i^2 \tag{4.2}$$

where y and x_i denote the response and variables respectively and b_0, b_i and b_{ii} are the coefficients. Using the model in Eq. 4.2, the response surface of the study was established as displayed below with R^2 (coefficient of determination) equal to 0.968:

$$\begin{aligned} FS = {} & 0.7756 + 0.0134\phi + 0.0513 s_u - 0.3324 wl + 0.0554 D + 0.0451 X - 6.7437 S \\ & + 0.0013\phi^2 - 0.0006 s_u^{\,2} - 0.0559 wl^2 + 0.0033 D^2 + 0.0050 X^2 + 5.4571 S^2 \end{aligned} \tag{4.3}$$

Approximating the factor of safety, the above response surface can represent the overall stability of the I-wall levee system consisting of an I-wall with a given exposed height, clay levee fill with a given height supported by sand foundation. However, the validity of the response surface needs to be evaluated prior to using it in the study. For validating the response surface, a number of random design sets combined with randomly selected uncertain parameters were generated and analyzed for system stability. The calculated FS from response surface were compared with those obtained from PLAXIS 2D as shown in Figure 4.11, and the results are in good agreement with each other.

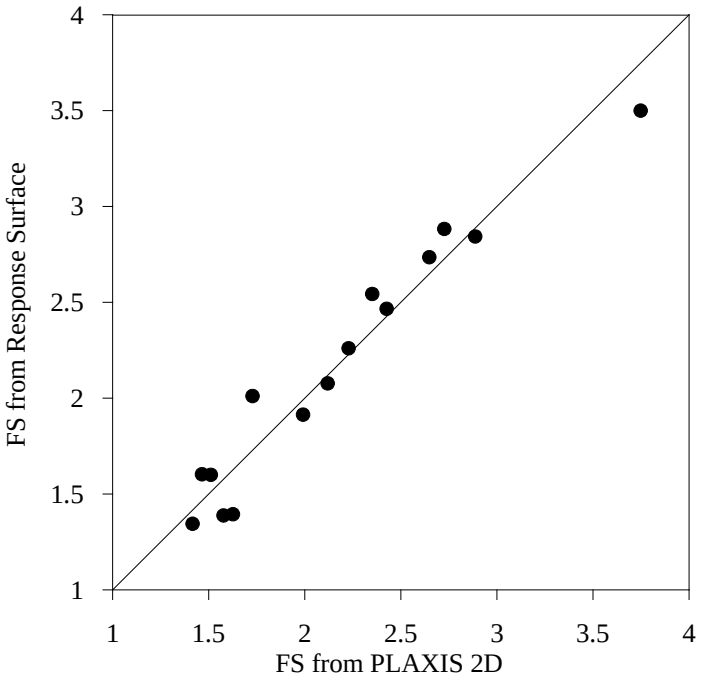

Figure 4.11 Graph of FS obtained from PLAXIS 2D and the response surface

To evaluate the validity of the response surface in a quantitative manner, three quantitative indicators recommended by Moriasi et.al (2007) were adopted for comparing the simulation results (i.e. results from SLIDE) with the observed results (i.e. results from response surface). The indicators used in this study are the Nash-Sutcliffe efficiency (NSE), the percent bias (PBIAS), and the ratio of the root mean square error to the standard deviation of measured data (RSR) that are shown in Eqs. 4.4, 4.5, and 4.6, respectively.

$$NSE = 1 - \left[\frac{\sum_{i=1}^{n} \left(Y_i^{obs} - Y_i^{sim} \right)^2}{\sum_{i=1}^{n} \left(Y_i^{obs} - Y_i^{mean} \right)^2} \right] \tag{4.4}$$

$$PBIAS = \left[\frac{\sum_{i=1}^{n} \left(Y_i^{obs} - Y_i^{sim} \right) * 100}{\sum_{i=1}^{n} Y_i^{obs}} \right] \tag{4.5}$$

$$RSR = \frac{\left[\sqrt{\sum_{i=1}^{n} \left(Y_i^{obs} - Y_i^{sim} \right)^2} \right]}{\left[\sqrt{\sum_{i=1}^{n} \left(Y_i^{obs} - Y_i^{mean} \right)^2} \right]} \tag{4.6}$$

where Y^{obs} is the observation (FS from PLAXIS 2D), Y^{sim} is the simulated value (FS from response surface) and Y^{mean} is the mean of observed data. These validation statistics were computed and the performance of the response surface was rated per Table 4.5. The overall performance was described as Very Good and therefore the mathematical model presented in Eq. 4.3 can be applied for computing FS for any combination of random and design variables.

Table 4.5 Performance ratings for recommended statistics (After Moriasi et al. 2007)

Performance rating	RSR	NSE	PBIAS
Very Good	0-0.5	0.75-1	<±15
Good	0.5-0.6	0.65-0.75	±15 - ±30
Satisfactory	0.6-0.7	0.5-0.65	±30 - ±55
Unsatisfactory	>0.7	<0.5	> ±55
Response surface rating	0.24	0.94	-0.36

4.2.6 Quantifying the Probability of Failure of the System

In probabilistic design approach, probability of failure or other concepts such as reliability index are used as a measure of safety. In this study, probability of failure was computed using the FS response surface presented in Eq. 4.3 through Monte Carlo

simulation and the variation of the probability of failure was evaluated for selected subset designs (listed in Table 4.4). N (=1,000,000) samples were generated for the soil-related random variables based on their distribution, and therefore N number of factors of safety (FS) were calculated. Assuming minimum acceptable FS of 1.5 and m as the number of factors of safety less than 1.5, probability of failure (P_f) of the system was calculated as below:

$$P_f = \frac{m}{N} \tag{4.7}$$

In the first attempt (Figures 4.12-4.14), the soil-related random variables (ϕ, s_u) were assumed to be uniformly distributed as ϕ = U (28,38), s_u= U (20,42); and in the second attempt (Figures 4.15-4.17), ϕ and s_u were assumed to be normally distributed as ϕ= N (33,1.67) and s_u= N (31,3.67) to evaluate the effect of distribution type of random variables on P_f computation. It should be noted that in both attempts, the flood water level varies between levee crown (0 m) and top of wall (2 m) and the variation of probability of failure was monitored with flood water level as the loading-related random variable.

As shown in Figures 4.12-4.14, the probability of failure of design cases (D_{min}, X_{mid}, S_{mid}), (D_{mid}, X_{min}, S_{mid}), and (D_{mid}, X_{mid}, S_{max}) increased to about 0.4-0.6 when the flood water level reached the top of wall. In similar flood situation, the P_f value of the design (D_{mid}, X_{mid}, S_{mid}) increased to about 0.2 and the P_f was found to be acceptable when the water level increased up to 1.2 m. The maximum water levels in which the P_f was considered acceptable for cases including D_{max}, D_{mid} and D_{min} (X and S at mid. value)

were 1.8 m, 1.2 m and 0.8 m, respectively. These water levels were found to be 1.5 m, 1.2 m and 1.0 m for cases including X_{max}, X_{mid} and X_{min} (D and S at mid. value), and 1.6 m, 1.2 m and 0.5 m for cases including S_{min}, S_{mid} and S_{max} (X and S at mid. value), respectively. The Figures 4.12-4.14 show that the P_f is the lowest when having the cases: (D_{max}, X_{mid}, S_{mid}) or (D_{mid}, X_{mid}, S_{min}).

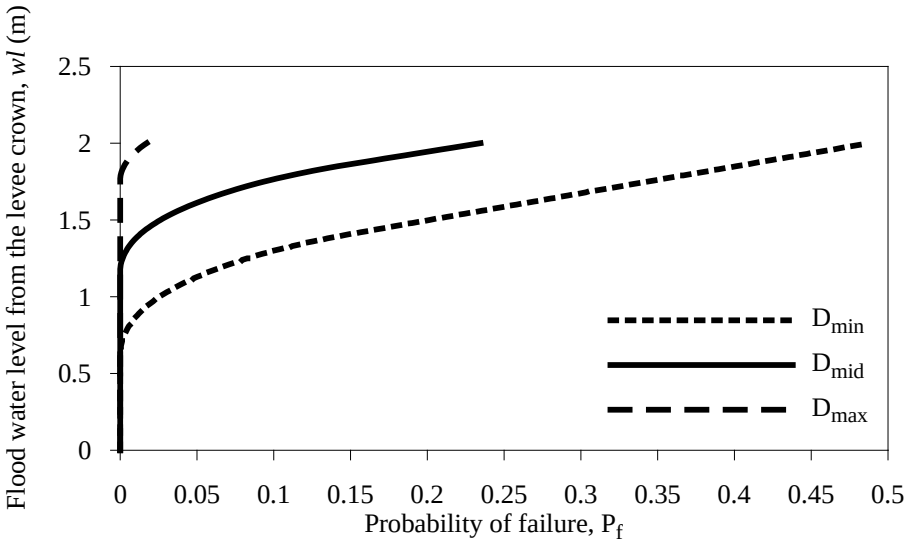

Figure 4.12 Variation of P_f with flood water level considering D using uniform dist. for ϕ and s_u

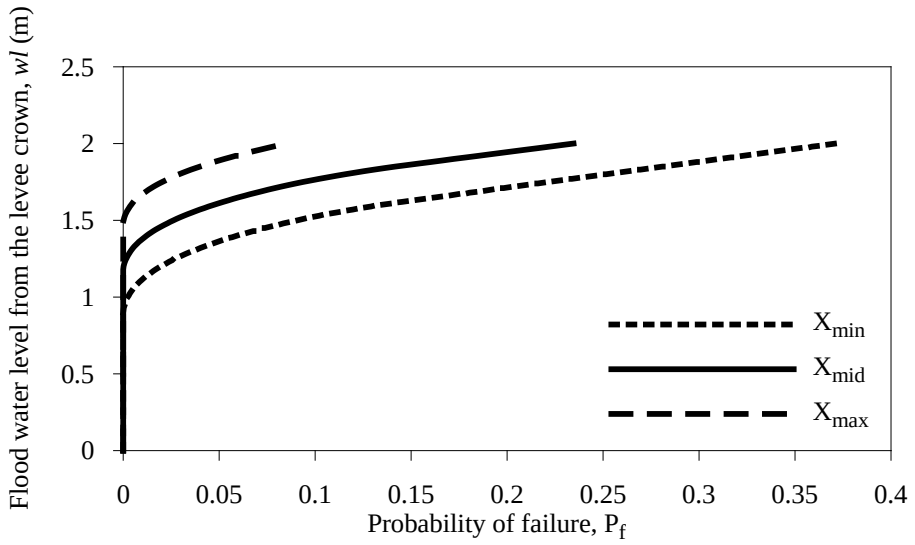

Figure 4.13 Variation of P_f with flood water level considering X using uniform dist. for ϕ and s_u

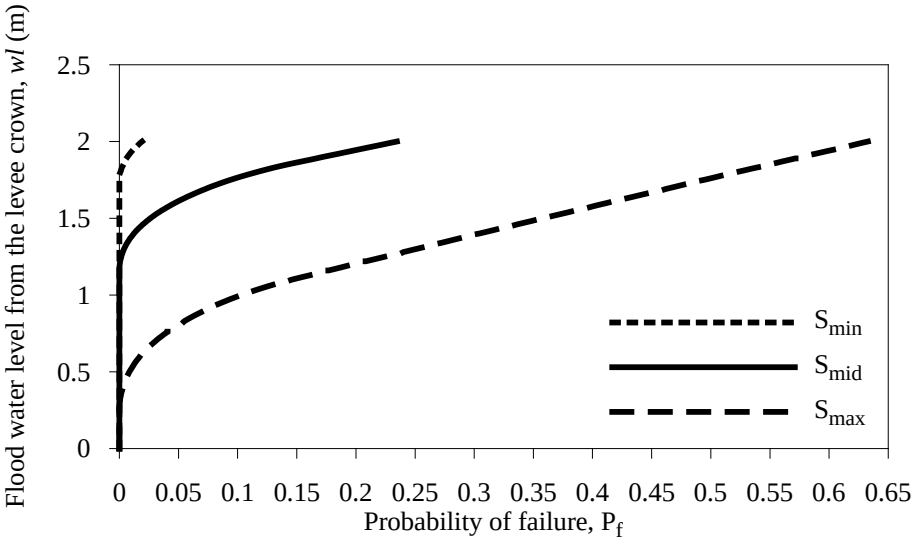

Figure 4.14 Variation of P_f with flood water level considering S using uniform dist. for ϕ and s_u

The results assuming normal distribution for ϕ and s_u are displayed in Figures 4.15-4.17. The P_f values resulting from normally distributed soil-related random variables were found to be mostly less than those from uniformly distributed variables and this is due to considering same probability of occurrence for all the random values in the

desirable range of the random variables when using uniform distribution. Shown in Figures 4.15-4.17, the maximum water levels with acceptable P_f were 2 m, 1.7 m and 1.3 m for cases D_{max}, D_{mid} and D_{min} (X and S at mid. value), respectively; 2 m, 1.8 m and 1.5 m for cases X_{max}, X_{mid} and X_{min} (D and S at mid. value); and 2 m, 1.7 m and 1.1 m for cases S_{min}, S_{mid} and S_{max} (D and X at mid. value), respectively.

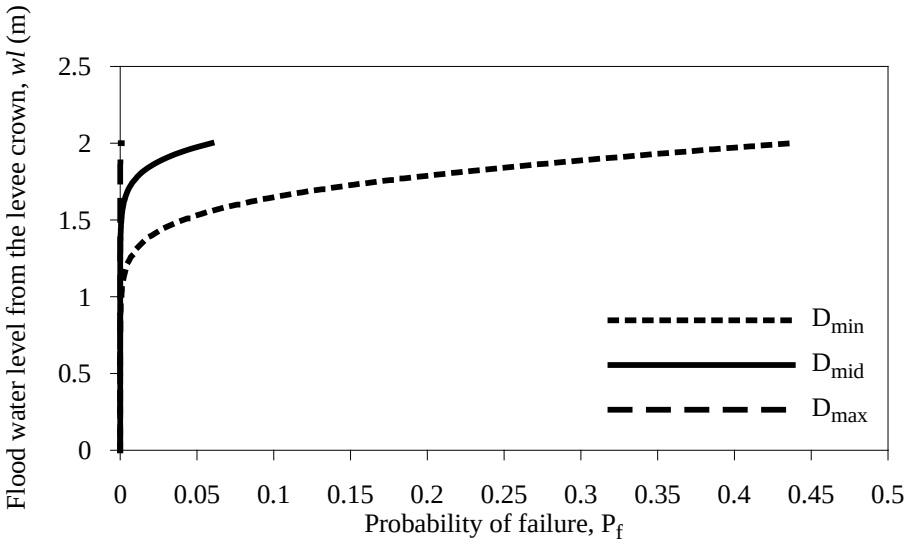

Figure 4.15 Variation of P_f with flood water level considering D using normal dist. for ϕ and s_u

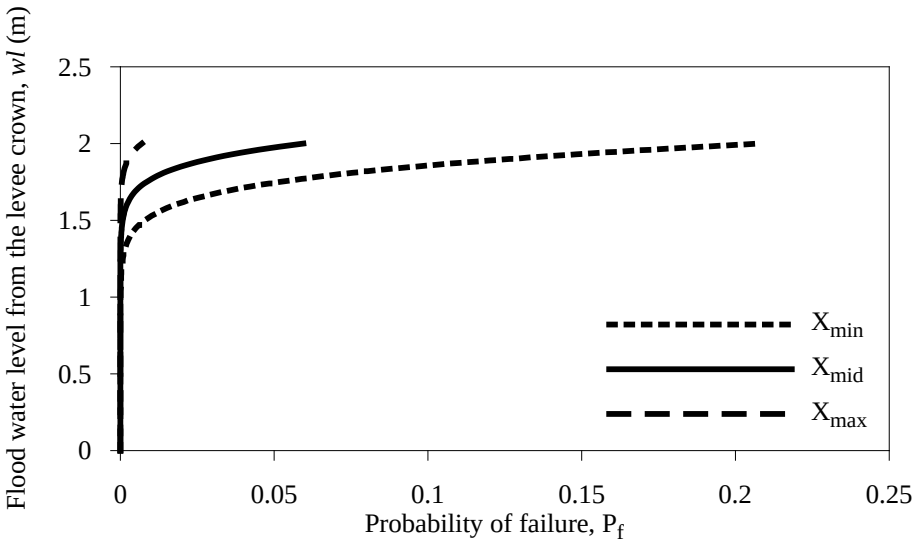

Figure 4.16 Variation of P_f with flood water level considering X using normal dist. for ϕ and s_u

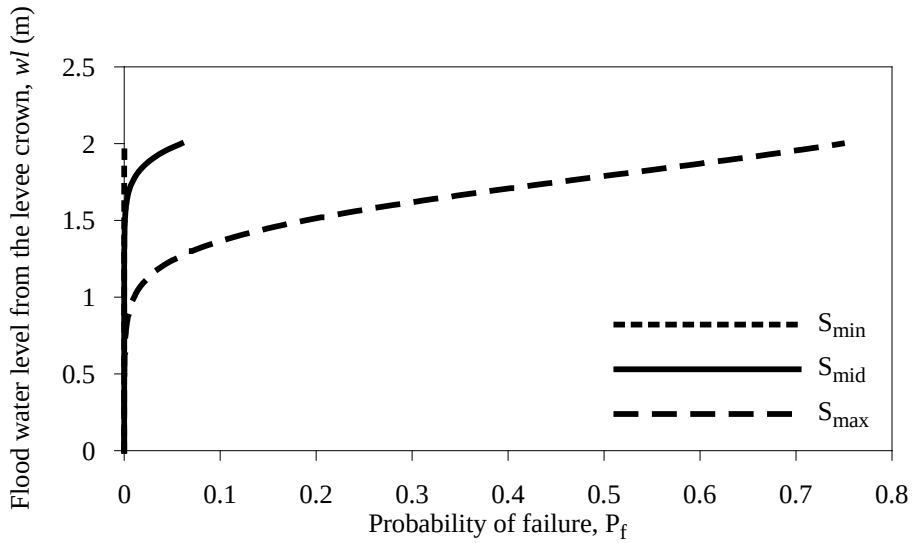

Figure 4.17 Variation of P_f with flood water level considering S using normal dist. for ϕ and s_u

Overall, it can be concluded from Figures 4.12-4.17 that P_f of the I-wall levee system decreases with increasing D, increasing X and decreasing S. Moreover, regardless of type of distribution used for representing the variations of the random variables, design combinations which satisfy the safety constraint of allowable probability of failure of 0.01 are: (D_{max}, X_{mid}, S_{mid}), (D_{mid}, X_{max}, S_{mid}), (D_{mid}, X_{mid}, S_{min}). However, more design sets

can be generated that meet the safety criteria through adjusting the design variables. For example, although D_{min} in a design set causes the probability of failure of the system exceeding the allowable one, the combination of D_{min} with X_{max} and S_{min} can result in a satisfactory performance of the system.

It is worth noting that as reported by Jonkman et al. (2009) based on Congress authorization a flood protection system needs to withstand a hurricane event with an annual probability of occurrence of 1% (0.01) and the probability of failure of the system can be assumed equal to the probability of exceedance of design condition. Thus, the maximum allowable P_f of 0.01 was considered in this study.

4.2.7 Design Optimization of I-wall Levee System of the Study

4.2.7.1 Determination of cost function

Cost is the other constraint that influences the design and consequently the probability of failure, therefore it must be considered as one of the objectives in the design. The cost of I-wall levee system was defined considering the cost of those components in the system that include the design variables. Thus, a sheet pile wall of PZ-27 section with depth of D and a levee with crown width of X and landside slope of S contributed in cost function. The cost function for new construction is expressed as following:

$$C^{(USD/m)} = \left(H_{ex} + D\right)^{(m)} \times \left(\frac{W_{spw}^{(kg/m^2)}}{1000}\right) \times C_{sp}^{(USD/ton)} + \left(2X + 2H_l + \frac{H_l}{S}\right)^{(m)} \times H_l^{(m)} \times C_f^{(USD/m^3)}$$

(4.8)

where H_{ex} is the exposed height of I-wall (=2m), W_{spw} is the weight of sheet pile wall with PZ-27 section (=131.8 kg/m^2) and C_{sp} is the unit cost of sheet pile wall. In the second part, H_l is the height of levee(=3m), and C_f is the unit cost of levee fill. It should be noted that the slope of 1V:2H was assumed for flood side of levee.

Using the manual of RSmeans Building Construction Cost Data for determining the unit cost of sheet piling (C_{sp}) the total cost was defined based on "sheet piling steel, 20' deep excavation, 27 psf, left in place: drive, extract and salvage" equal to $2000/ton. The total cost for levee fill (C_f) was defined based on "Fill by borrow, load, 1 mile haul, spread with dozer for embankment" equal to $14.33 per cubic yard (=$11 per cubic meter) which includes costs of material, labor and equipment.

4.2.7.2 Non-robust design optimization results

The optimization setting was established to balance the probability of failure with cost through minimizing both objectives simultaneously using Non-dominated Sorting Genetic Algorithm (NSGA-ii) developed by Deb et al. (2002). It should be noted that in this type of design optimization the robustness was not considered and the I-wall levee design was optimized based on cost and safety. In the optimization process for each design set, created by NSGA-ii based on the upper and lower limits of design variables, the probability of failure (P_f) was computed using Monte Carlo simulation with N=5000. As a safety constraint, an allowable P_f equal to 0.01 was assumed in the optimization setting. In the first attempt, all the random variables, friction angle of sand foundation (ϕ), undrained shear strength of clay levee fill (s_u) and flood water level (wl) were

assumed uniformly distributed. The Pareto front optimized to cost and P_f is displayed in Figure 4.18.

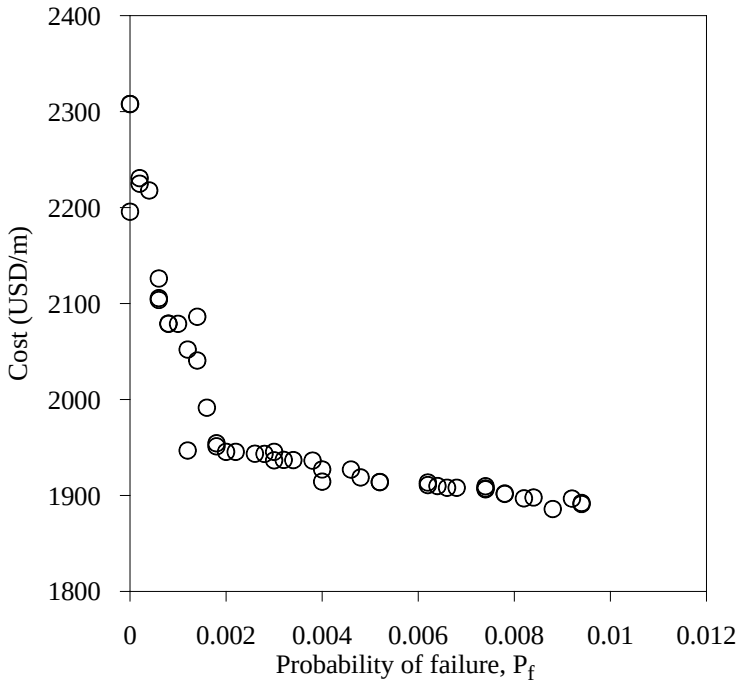

Figure 4.18 Non-robust Pareto front with uniformly distributed random variables

In the second attempt (Figure 4.19) the soil-related random variables (ϕ and s_u) were assumed to be normally distributed. It is observed from the Pareto fronts shown in Figures 4.18-4.19 that the range of cost decreased from \$1,900/m-\$2,300/m in the first Pareto front to about \$1,750/m-\$1,900/m in the second Pareto front. The cause of this reduction in cost can be due to the adjustment of design variables so that the design meet the safety constraint depending on the distribution type of random variables.

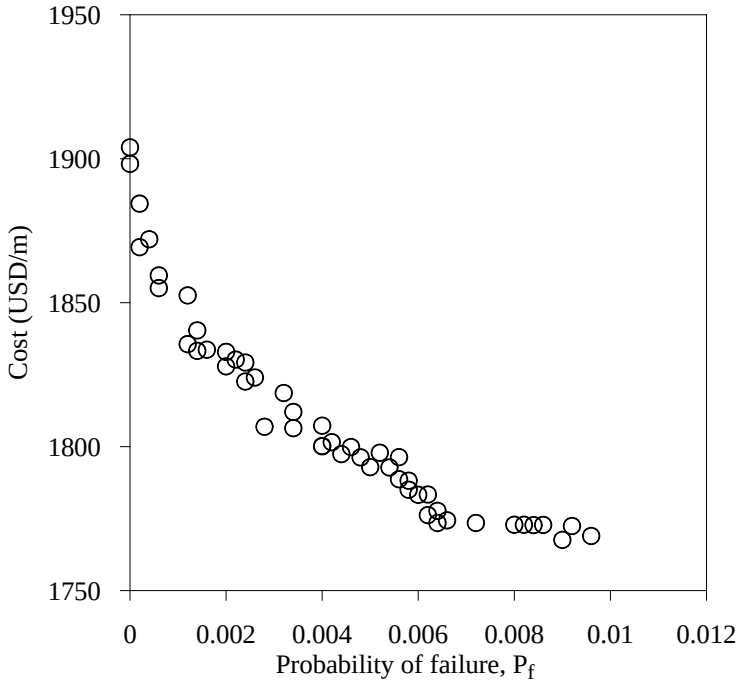

Figure 4.19 Non-robust Pareto front with normally distributed ϕ and s_u

4.2.7.3 Robust design optimization results

Certainty in computation of probability of failure of the system may be guaranteed by using high quality data of the soil profile in the model. However, uncertainties exist in assumed statistical characterization of soil properties due to insufficient sample size, measurement errors, and human errors and the computed probability of failure will not be a certain value and vary under the effect of these variations (Juang et al. 2012; Juang et al. 2013). Therefore, in this section the coefficient of variations (COV) of the soil-related random variables (ϕ and s_u) were also considered as uncertain parameters in optimization setting as: COV_{ϕ} = N (0.05, 0.01), COV_{su}= N (0.12, 0.024).

For each design set, N number of P_f were calculated. Considering P_f as the response of concern, the standard deviation of P_f was taken as the measure of robustness (Wang et al. 2015; Peng et al. 2016). The design optimization was performed by minimizing the cost and maximizing the robustness. Reducing the variation of response (standard deviation of probability of failure, here) leads to increasing the robustness of design. The Pareto front optimized to cost and standard deviation of P_f is shown in Figure 4.20 (for N=1000). It can be observed from the Figure that as the standard deviation of P_f increased from 0 to about 0.0017, the cost decreased from \$2800 to \$1900. This indicates that higher robustness for design demands higher cost.

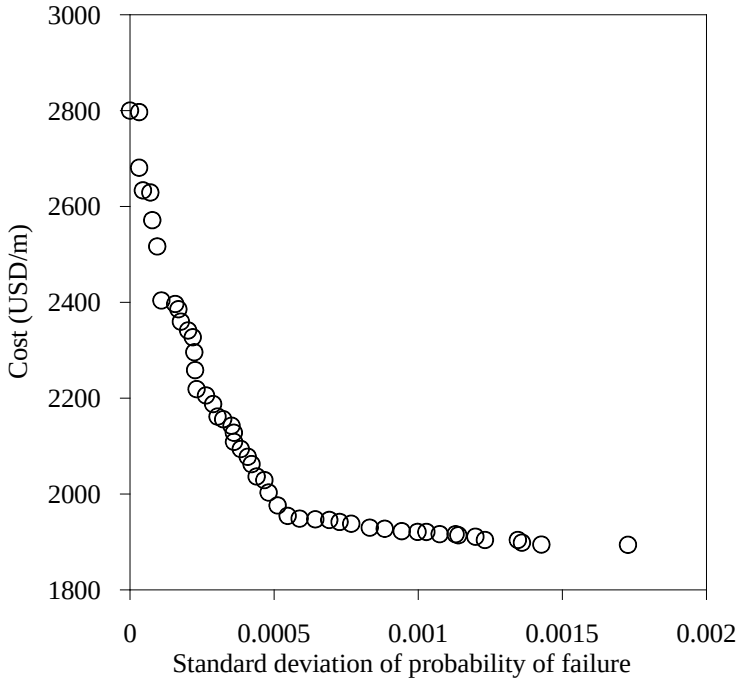

Figure 4.20 Robust Pareto front with normally distributed ϕ and s_u and varying COV

4.2.7.4 Comparison of robust and non-robust design optimization

In this section the Pareto front resulted from robust design optimization is compared with the one resulted from non-robust design optimization as shown in Figure 4.21. The non-robust Pareto front is located below the robust Pareto front showing lower cost of design when robustness of the system is not considered. In other words, robust design optimization may lead to costlier designs than non-robust design, but reducing the sensitivity of the design and the variation of the response (probability of failure) is the key to obtain designs of higher robustness.

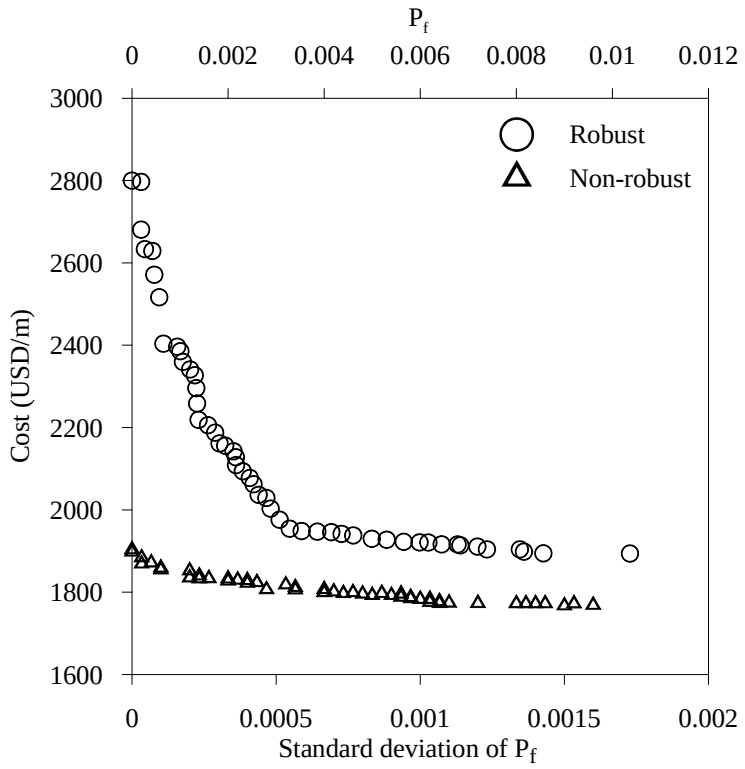

Figure 4.21 Comparison of robust and non-robust Pareto fronts

4.2.7.5 Determination of final design

For determining the optimal design with respect to cost and robustness, the normal boundary intersection (NBI) (Das and Dennis, 1998) approach was used to compute the knee points on the robust Pareto front. As shown in Figure 4.22, for each point of the Pareto front, the distance from the boundary line, which connects the highest point of the Pareto front to the lowest point, is computed in the normalized space of Pareto front. Then, the point with maximum distance from the boundary line is sought and selected as the knee point which corresponds to the optimal design of the study.

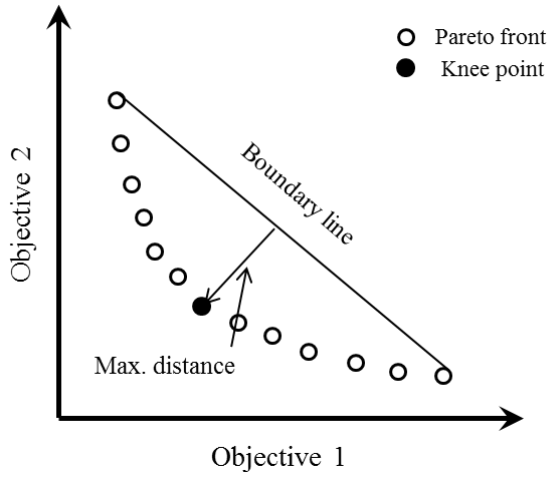

Figure 4.22 Normal boundary intersection approach

The results of optimal designs using the knee point properties of robust and non-robust design Pareto fronts are summarized in Table 4.6, listing the design parameter values of the I-wall levee system. As it is observed, the optimal robust design included a levee with wide crown and mild slope on the landside, and short wall. On the other hand, the optimal non-robust design included a levee with a middle value crown width. Based on the results, a mild slope (about 1V:4H) for landside slope of the levee is recommended

for the final I-wall levee system. The increased width of levee crown in optimal robust design increased cost of the system, but the robustness of the design increased at the same time. This higher cost may seem unreasonable comparing to conventional designs but it helps reducing the unexpected variations of the system response. In conventional designs of I-wall levee systems, the deeper wall may be desired to prevent seepage in sand foundation which leads to costly designs, but from the robust Pareto front of this study a system with deep wall resulted in a design with the least robustness.

Table 4.6 Optimal design properties for robust and non-robust optimization

Optimization type	D (m)	X (m)	S	Cost (USD/m)
Robust	2.00	6.00	0.25	1954
Non-robust	2.00	3.55	0.28	1807

Pareto fronts can also be used to obtain the final design based on the engineering preferences and available budget and desired level of robustness or cost can also be specified for designers. Moreover, additional constraints can be applied to the optimization setting and minimum FS and allowable P_f can be modified based on engineering judgments. These features increase the flexibility of this framework in ensuring the robust design optimization.

4.3 CONCLUSION

In this paper, the authors proposed a framework for design optimization of I-wall levee systems resting on sand considering the uncertainties in levee and foundation soils

and in flood water level. Through the adopted design approach, an I-wall levee system on sand foundation and the random and design variables were demonstrated; the overall stability of the system was analyzed using finite element and limit equilibrium methods and the effect of uncertainties was evaluated; then based on a developed response surface for FS the probability of failure was computed using Monte Carlo simulation. Bi-objective design optimizations were performed to obtain non-robust (cost vs. probability of failure) and robust (cost vs. standard deviation of probability of failure) Pareto fronts. In the robust optimization, the robustness and cost-efficiency of the design were satisfied and balanced by minimizing the standard deviation of probability of failure and the cost, respectively. The proposed approach can be introduced and implemented in design of flood protection systems in which the variations in soil properties and water elevation may lead to catastrophic failures.

REFERENCES

Sills, G. L., Vroman, N. D., Wahl, R. E., & Schwanz, N. T. (2008). Overview of New Orleans levee failures: lessons learned and their impact on national levee design and assessment. *Journal of Geotechnical and Geoenvironmental Engineering*, *134*(5), 556-565.

Duncan, J. M., Brandon, T. L., Wright, S. G., & Vroman, N. (2008). Stability of I-walls in New Orleans during hurricane Katrina. *Journal of Geotechnical and Geoenvironmental Engineering*, *134*(5), 681-691

Interagency Performance Evaluation Task Force IPET. (2007). Performance evaluation of the New Orleans and Southeast Louisiana Hurricane protection system. *Final Rep. of the Interagency Performance Evaluation Task Force*, U.S. Army Corps of Engineers

Sasanakul, I., Vanadit-Ellis, W., Sharp, M., Abdoun, T., Ubilla, J., Steedman, S., & Stone, K. (2008). New Orleans levee system performance during Hurricane Katrina: 17th Street Canal and Orleans Canal North. *Journal of geotechnical and geoenvironmental engineering*, *134*(5), 657-667

Ubilla, J., Abdoun, T., Sasanakul, I., Sharp, M., Steedman, S., Vanadit-Ellis, W., & Zimmie, T. (2008). New Orleans levee system performance during hurricane Katrina: London Avenue and Orleans canal south. *Journal of Geotechnical and Geoenvironmental Engineering*, *134*(5), 668-680.

Seed, R. B., Bea, R. G., Abdelmalak, R. I., Athanasopoulos, A. G., Boutwell Jr, G. P., Bray, J. D., ... & Collins, B. D. (2006). Investigation of the Performance of the New Orleans Flood Protection System in Hurricane Katrina on August 29, 2005. *Independent Levee Investigation Team: Final Report*

Tung, Y. K., & Mays, L. W. (1981). Risk models for flood levee design. *Water Resources Research*, *17*(4), 833-841.

Hui, R. (2014). Optimal design of levee and flood control systems. *Doctoral dissertation, University of California, Davis.*

Juang, C. H., Wang, L., Liu, Z., Ravichandran, N., Huang, H., & Zhang, J. (2013). Robust geotechnical design of drilled shafts in sand: New design perspective. *Journal of Geotechnical and Geoenvironmental Engineering*, *139*(12), 2007-2019.

Coduto, D. P. (1999). Geotechnical engineering: principles and practices. *Pearson College Division*.

Das, B. (2010). Principles of Geotechnical Engineering. *Cengage Learning*.

Wright, S. G., & Duncan, J. M. (2005). Soil Strength and Slope Stability. *John Wiley & Sons*

Griffiths, D. V., & Lane, P. A. (1999). Slope stability analysis by finite elements. *Geotechnique*, *49*(3), 387-403.

Brinkgreve, R. B. J., Kumarswamy, S., & Swolfs, W. M. (2015). Plaxis 2D Manual. *PLAXIS bv, The Netherlands.*

Burk & Associates, Inc (1986). London avenue canal floodwalls and levees – General design memorandum.

USACE. (2011). EC 1110-2-6066, Engineering and design: Design of I-walls.

USACE. (2000). EM-1110-2-1913, Engineering and design: Design and construction of levees.

Wong, F.S. (1985). Slope reliability and response surface method. *Journal of Geotechnical Engineering*, 111(1), 32-53.

Moriasi, D.N., Arnold, J.G., Van Liew, M.W., Bingner, R.L., Harmel, R.D. and Veith, T.L. (2007). Model evaluation guidelines for systematic quantification of accuracy in watershed simulations. *Transactions of the ASABE*, 50(3), 885-900.

Waier, P. R., Babbitt, C., Baker, T., Balboni, B., & Bastoni, R. A. (2010). RSMeans: Building Construction Cost Data 2010.

Jonkman, S. N., Kok, M., Van Ledden, M., & Vrijling, J. K. (2009). Risk-based design of flood defence systems: a preliminary analysis of the optimal protection level for the New Orleans metropolitan area. *Journal of Flood Risk Management*, *2*(3), 170-181.

Peng, X., Li, D. Q., Cao, Z. J., Gong, W., & Juang, C. H. (2016). Reliability-based robust geotechnical design using Monte Carlo simulation. *Bulletin of Engineering Geology and the Environment*, 1-11.

Das, I., and Dennis, J. E. (1998). Normal-boundary intersection: A new method for generating the Pareto surface in nonlinear multi-criteria optimization problems. *SIAM Journal on Optimization*, *8*(3), 631-657.

CHAPTER 5

A PROBABILISTIC GEOTECHNICAL DESIGN OPTIMIZATION FOR I-WALL LEVEE SYSTEM SUPPORTED BY CLAY FOUNDATION

ABSTRACT

This paper presents a probabilistic design framework for design of I-wall levee systems supported by clay foundations. Failure of I-wall levee systems, typically due to misestimation of soil properties and flood water level, can cause massive economical and human losses. To account for uncertainties systematically and explicitly, a robust geotechnical design optimization approach was adopted in this study. The variations in input uncertain parameters such as strength and flow properties of soil and flood water level may result in high variations in overall response of I-wall levee systems. In this study, undrained shear strengths of clay foundation and clay levee fill and flood water level were considered as random variables while the penetration depth of I-wall, width of levee crown and landside slope of levee were considered as design variables. Several design cases were generated, then modeled and analyzed using limit equilibrium and finite element methods for overall stability in terms of factor of safety. Considering the global factor of safety of the system as the response of concern, a response surface was developed to represent the factor of safety as a function of random and design variables and used in optimization procedure. Total cost of I-wall levee system and standard deviation of probability of failure of the system (as a measure of robustness) were considered as the objectives of robust optimization constrained to allowable probability of failure. Additionally, non-robust optimization was conducted and compared to the

robust one. Finally, the optimizations yielded a set of preferred designs known as Pareto front from which the optimal design can be selected based on engineering preferences.

5.1 INTRODUCTION

Levee systems as well as other geotechnical systems involve unavoidable uncertainties due to insufficient data and measurement errors (Phoon and Kallhawy 1999), compensating for these uncertainties cannot be achieved by conventional deterministic approaches which use single set of site specific hydrological and geotechnical parameters. Therefore, to take the uncertainties in key parameters into account systematically and explicitly probabilistic approaches are commonly used. In this study, such a robust probabilistic design approach is proposed to reduce the variation in probability of failure due to variation in soil properties and flood water level. Application of this approach in optimization helps evaluate and balance the reliability, robustness, and cost of a design in an explicit manner (Juang et al. 2013).

Overestimation of the strengths of levee and foundation soils and/or exceedance of the flood water from the levee crown were found to be causes of failure of the levee system which may result in significant economical and human losses due to severe flooding. The capacity of levee systems can be increased by floodwall installation. Floodwalls, vertical structural elements, are commonly used in urban areas where there is limited right of way on landside of the levee. Two common types of floodwalls are: I-wall, an I-shaped wall typically consisting of sheet pile wall driven into the levee and a concrete cap fixed to the top of sheet pile above the levee crown (Figure 5.1), and T-wall,

which resists the load from flood by cantilever beam action. Generally, adding I-wall to the levee system is usually preferred due to the ease of installation and rehabilitation. Increasing the capacity of the levee system can also be achieved by expanding the levee section, as shown in Figure 5.1, which needs huge amount of soil and space that may not be available on landside of the levee. This method is not an interest of this study and therefore not is discussed in detail.

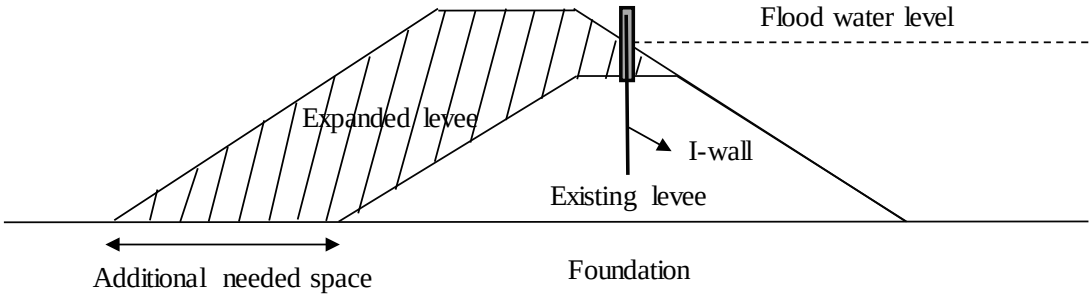

Figure 5.1 Installing I-wall vs. expanding levee section

The design of I-wall levee system may look simple but the past failures show that the current design procedure must be revised. Hurricane Katrina in August 2006 caused catastrophic failure of New Orleans I-wall levee systems and hence massive flooding in the areas. At some locations, the flooding occurred due to the failure of levee I-wall systems resting on clay foundation prior to being subjected to overtopping that was observed at the 17th Street Canal and Inner Harbor Navigation Canal (IHNC) east bank I-wall levee systems. Sills et al. (2008) and Duncan et al. (2008) (Interagency Performance Evaluation Taskforce, IPET) investigated the failures of I-wall levee systems on clay foundation during Hurricane Katrina and reported that translational sliding and deep-seated movements occurred in the weak clay foundation. Sasanakul et al. (2008) and

Ubilla et al. (2008) performed centrifuge modeling of the failed levee systems on clay foundation (a section from 17th Street Canal), and found that the major cause of the breach in the system was the foundation failure. In addition, they emphasized that soil profile, geometry of levee, and penetration depth of the I-wall were the key factors contributing to the failure of the I-wall levee system. IPET and ILIT (Independent Levee Investigation Team) analyzed the performance of levee systems using finite element method and limit equilibrium method to investigate the performance of various sections from breached areas in New Orleans. Moreover, the uncertainties in input parameters (geotechnical properties and loading) for modeling the I-wall levee system were not explicitly considered in their approaches. Risk-based optimizations of the levee system that have been performed by researchers and engineers in the past only consider hydraulic and hydrological uncertainties related to flooding event. In addition, the primary focus of most of the levee design optimizations in the past was overtopping failure and few studies have included geotechnical failure (such as slope stability) of the levees before the flood water reaches top of the wall (Tung and Mays 1981; Hui 2014).

In this study, the I-wall levee system design was optimized to cost and robustness considering the uncertainties in soil properties and flood water level behind the I-wall and the robust design was compared with the non-robust design (typical design optimization). In addition, for demonstrating the effect of variation of flood water level on the I-wall levee system design several parametric studies were carried out considering factor of safety of the system and probability of failure.

5.2 CONTRIBUTING VARIABLES OF THE STUDY

The key components of an I-wall levee system are: I-wall, clay levee fill, and clay foundation (Figure 5.2). The material properties and the geometry of these components affect the safety and the cost of construction.

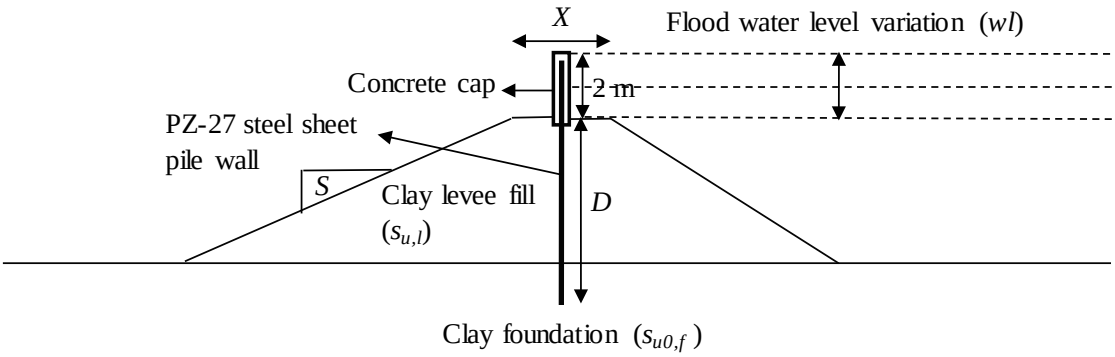

Figure 5.2 The schematic of the I-wall levee system of the study

Penetration depth of the I-wall (*D*), levee crown width (*X*), and the landside slope of levee (*S*), marked on Figure 5.2, are the key design parameters and were considered as the design variables in this study. The flood side slope of the levee was assumed to be 1V:2H as per USACE regulations steeper slopes can be applied for riverine levees made of clay (EM-1110-2-1913). The I-wall consists of sheet pile wall of PZ-27 section and concrete cap and the design exposed height of wall above the levee crown (H_{ex}) was also assumed to be 2 m (shown in Figure 5.2). The lower and upper limits of the design variables are tabulated in Table 5.1.

The uncertainties in the design of I-wall levee system supported by clay foundation arise from strengths of clay levee fill, clay foundation and flood water level. The shear strength parameters and the flood water level are associated with capacity and load on the system, respectively. Therefore, undrained shear strength of the clay levee fill

($s_{u,l}$), undrained shear strength of the clay foundation ($s_{u0,f}$) and flood water level (wl) were considered as the random variables. $s_{u0,f}$ is the reference undrained shear strength of clay and it is assumed to increase with depth at a rate of 1.7 kPa/m (IPET 2008). The statistical proprieties used for the random variables are shown in Table 5.1. The standard deviations of the soil-related random variables are considered so that the limiting range will be covered by 3 times the standard deviation covers. It should be noted that overtopping failure was not considered in this study and the design flood water level was assumed to vary between levee crown level and the top of the I-wall.

Table 5.1 Design and random variables of the study

Variable type	**Variable**	**Desirable range**	**Mean value**	**Standard deviation** (if using Normal distribution)
Design	D (m)	2-8	5	N/A
	X (m)	3-6	4.5	N/A
	S	0.25-0.5	0.33	N/A
Random	$s_{u0,f}$ (kPa)	10-20	15	1.67
	$s_{u,l}$ (kPa)	20-42	31	3.67
	wl (m)	0-2	1	-

5.3 EVALUATING OVERALL STABILITY OF THE SYSTEM

Generally, the possible failure modes of a levee system can be categorized into: overtopping, sliding, piping-underseepage, piping-throughseepage, surface erosion, and slope instability. In this study, the slope failure mode was considered and the overall stability of the I-wall levee supported by clay foundation was analyzed using limit

equilibrium (LE) and finite element (FE) methods. Furthermore, the effect of uncertainties on the overall stability was evaluated. The factors of safety obtained from these methods were compared for accuracy and verification purpose. The FE method demands significantly longer computational time compared to LE method. The LE methods and especially method of slices are commonly used in slope engineering practice due to simple and easy to understand theory and less computational time. However, FE method is recently widely accepted as a powerful alternative approach for slope stability analysis and provides more realistic results in terms of deformation and slope failure mechanism.

Several subset of designs of I-wall levee system were selected based on the ranges of design variables in Table 5.2, and were simulated using the LE-based program SLIDE and the FE-based program PLAXIS 2D.

Table 5.2 Subset designs selected for stability analysis

Design	**Combination**	***D* (m)**	***X* (m)**	***S***
1	D_{min}, X_{min}, S_{min}	2	3	0.25
2	D_{max}, X_{max}, S_{max}	8	6	0.5
3	D_{mid}, X_{mid}, S_{mid}	5	4.5	0.33
4	$\boldsymbol{D_{min}}$, X_{mid}, S_{mid}	2	4.5	0.33
5	$\boldsymbol{D_{max}}$, X_{mid}, S_{mid}	8	4.5	0.33
6	D_{mid}, $\boldsymbol{X_{min}}$, S_{mid}	5	3	0.33
7	D_{mid}, $\boldsymbol{X_{max}}$, S_{mid}	5	6	0.33

8	D_{mid}, X_{mid}, $\boldsymbol{S_{min}}$	5	4.5	0.25
9	D_{mid}, X_{mid}, $\boldsymbol{S_{max}}$	5	4.5	0.5

Using the LE-based SLIDE, the overall FS of the system was computed by Spencer's method. In SLIDE models, the stress-strain behavior of levee fill and the foundation soil was represented using Mohr-Coulomb model and the 'Infinite Strength' material type was used for I-wall, assuming it as a rigid wall. Steady state seepage condition was assumed and was imposed by setting total heads at floodside and landside of the levee system. The mesh of simulation domain included about 1000 6-node triangular elements. A sample SLIDE model of I-wall levee system is shown in Figure 5.3. The simulation domain (depth and width of foundation) was obtained using simplified domain of I-wall levee system on 17th Street Canal.

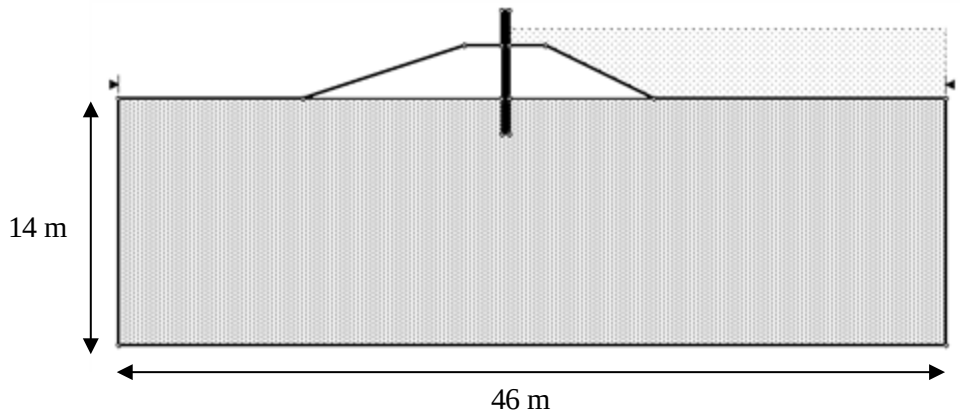

Figure 5.3 A sample SLIDE model of I-wall levee system

The overall stability of the system using PLAXIS 2D was computed through safety analysis in which the strength reduction method is applied for obtaining the global

FS. In strength (phi-c) reduction method the shear strength parameters (ϕ and c or s_u) of the soil are successively reduced until failure of the system occurs. The total multiplier ∑Msf which defines the value of the soil strength parameters at a given stage in analysis, is considered as the FS of the system in PLAXIS 2D and is computed as below:

$$\sum Msf = \frac{\tan\phi_{input}}{\tan\phi_{reduced}} = \frac{s_{u,input}}{s_{u,reduced}} \tag{5.1}$$

where the strength parameters with subscript *input* refer to the properties entered in the material setting and those with subscript reduced refer to the *reduced* values in analysis (Brinkgreve et al. 2015: PLAXIS 2D Manual). In PLAXIS 2D models, Mohr-Coulomb and linear elastic material models were used for representing the stress-strain behavior of the soils in the system and the I-wall, respectively. For the I-wall components, plate element was used for the sheet pile wall section and the concrete cap covering the exposed height of the I-wall was modeled using soil polygon. Interface elements were also applied in the model considering the wall-soil interaction. Moreover, a very fine mesh consisting of 1200-1600 15-node triangular elements was adopted in the models as shown in Figure 5.4. The regular boundary conditions were also applied to the model so that the vertical sides of the simulation domain were fixed to prevent horizontal translation and the base of the domain was fixed against both horizontal and vertical movements.

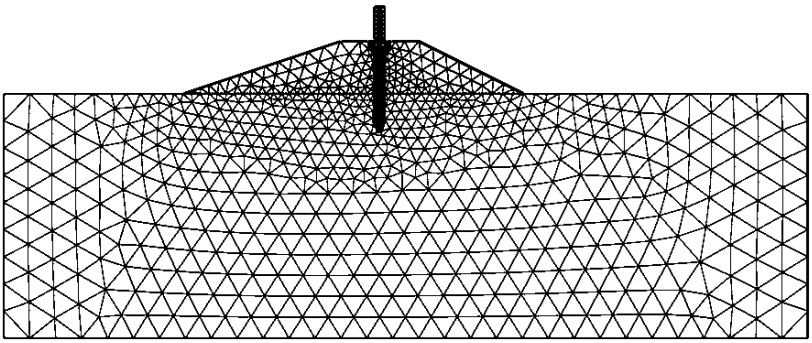

Figure 5.4 Sample of PLAXIS 2D model mesh of the I-wall levee system

Regarding the simulation setups, the FS values of the I-wall levee system were obtained using both methods for variations of random variables (min., mean, max.) and compared as shown in Figure 5.5. It was observed that FS values obtained by FE analysis were about 0.25 (on average) lower than those obtained by LE analysis. Therefore, the results of PLAXIS 2D were adopted for further analysis.

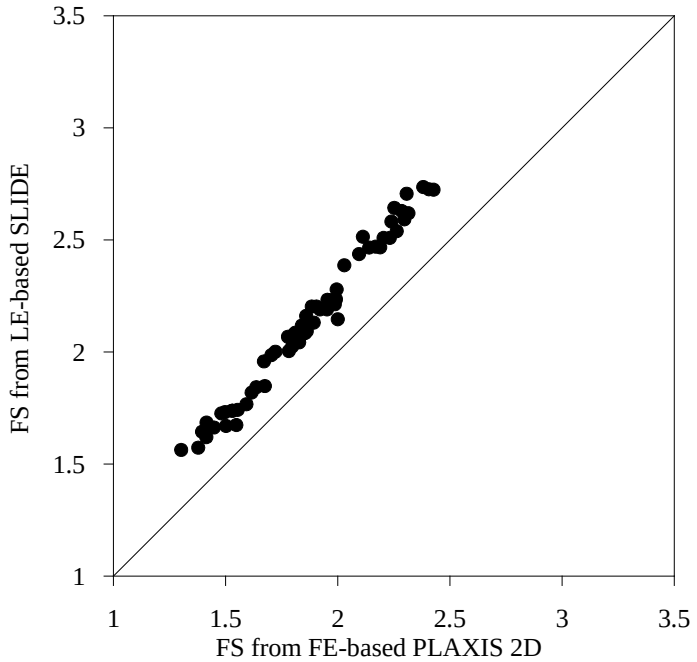

Figure 5.5 Comparison of FS from FE: PLAXIS 2D and FS from LE: SLIDE

5.4 EFFECT OF UNCERTAINTIES ON OVERALL STABILITY

Using the FS results from PLAXIS 2D, the effect of uncertain parameters (random variables) of the system ($s_{u0,f}$, $s_{u,l}$, wl) on overall stability of I-wall levee system resting on clay was evaluated to demonstrate the significance of the uncertainties on design. Therefore, the variation in FS is shown in Figures 5.6-5.8 for subset designs 2-9 of Table 5.2 due to variations of random variables. Figure 5.6 shows that increase in reference undrained shear strength of clay foundation ($s_{u0,f}$) from 10 kPa to 20 kPa results in increase in FS from about 1.4 kPa to about 2.5 kPa (while other random variables are at their mean value). Figure 5.6(a) shows a similar variation in FS with $s_{u0,f}$ variation for both designs (D_{mid}, X_{mid}, S_{mid}) and (D_{min}, X_{mid}, S_{mid}). As shown in Figure 5.6(b), regardless of the levee crown width (X) FS increases with $s_{u0,f}$ increase. From Figure 5.6(c) it can be concluded that the design experienced less stability with steeper landside slope of levee.

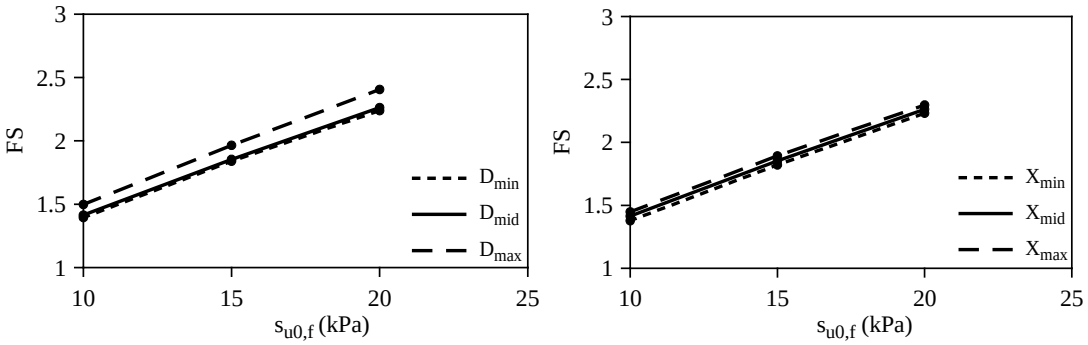

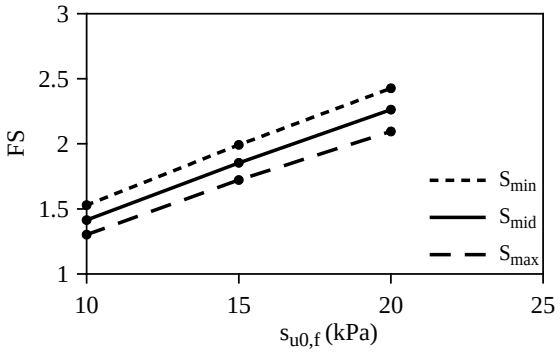

Figure 5.6 Variation of FS with undrained shear strength of clay foundation ($s_{u0,f}$)

The effect of undrained shear strength of levee fill ($s_{u,l}$) on FS of the system is shown in Figure 5.7, and unlike results of Figure 5.6, increase of FS with increase of $s_{u,l}$ is not observed except for design case (D_{mid}, X_{mid}, S_{min}) (Figure 5.7(c)). Similar to what the design cases experienced with $s_{u0,f}$, as shown in Figure 5.7(a), designs (D_{mid}, X_{mid}, S_{mid}) and (D_{min}, X_{mid}, S_{mid}) experienced similar FS values. Moreover, change in levee crown width was not effective on overall stability of system as seen in Figure 5.7(b). Overall, Figure 5.7 indicates that the variation of $s_{u,l}$ of the levee fill has minor effect on stability of the system comparing to the other random variables. This may be due the relatively deep failure surface along which the levee fill has a small share of cohesion.

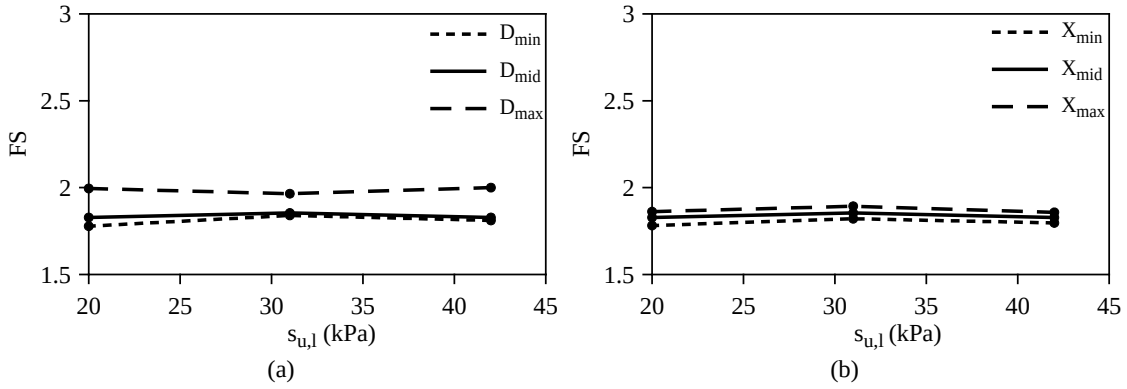

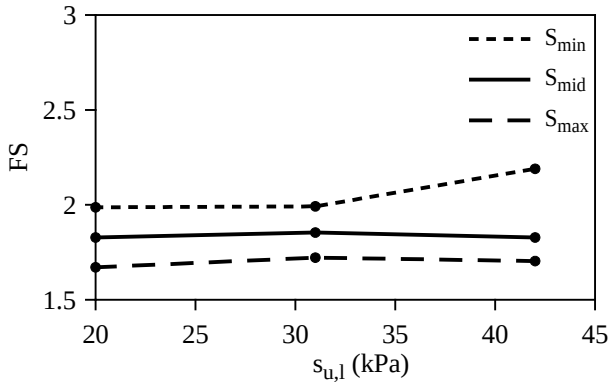

(c)

Figure 5.7 Variation of FS with undrained shear strength of levee fill ($s_{u,l}$)

Figures 5.8 show that the FS decreases with increasing the flood water level (*wl*), as it was expected. The FS of the system decreased from about 2.2 to about 1.5 when the flood water rised from levee crown to top of wall. As shown in Figure 5.8, design sets have experienced similar trend as in Figures 5.6 and 5.7.

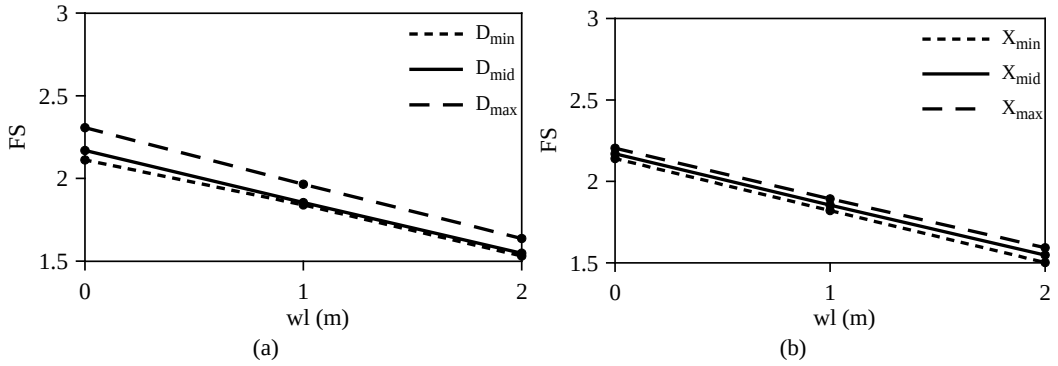

(a) (b)

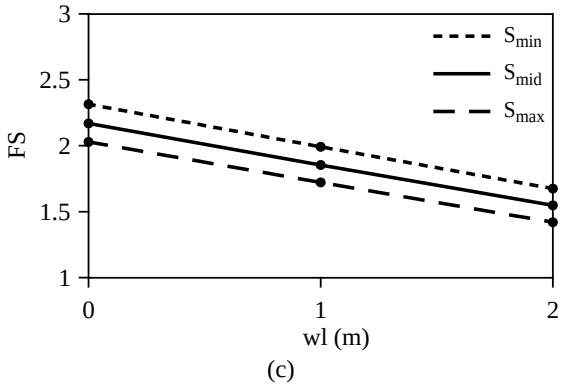

(c)

Figure 5.8 Variation of FS with flood water level (*wl*)

It can be concluded from Figures 5.6-5.8 that the random variables $s_{u0,f}$ and *wl* have significant influence on overall stability of the I-wall levee system supported by clay foundation, while $s_{u,l}$ has minor influence. It was also observed that similar FS values were obtained with variations of random variables from systems with walls of minimum and medium depth (when *X* and *S* were at mid. value), and levees of minimum, medium and maximum crown width (when D and S were at mid. value). However, the I-wall levee system supported by clay foundation was overall more stable with greater depth of wall penetration, wider crown levee, and milder landside levee slope. Moreover, the observed variations of FS due to variations of random variables can provide reasonable justification for selecting the key uncertainties.

5.5 FS RESPONSE SURFACE AND VALIDATION

Using the FS results from previous section, a response surface was developed through nonlinear regression analysis to represent FS as a function of random variables and design variables. Application of response surface method in this study provides the possibility of computing FS of I-wall levee system resting on clay foundation efficiently

for any combinations of design variables and variations of random variables. Among the common models used in response surface method (Khuri and Mukhopadhyay 2010), the second-order polynomial model was adopted as shown in Eq. 5.2.

$$y = b_0 + \sum_{i=1}^{n} b_i x_i + \sum_{i=1}^{n} b_{ii} x_i^2 \tag{5.2}$$

where b_0, b_i and b_{ii} are the coefficients of model, and y and x_i are the response and variables respectively. The established response surface of the study (displayed in Eq. 5.3) with R^2=0.997 represents the overall stability of the I-wall levee system supported by clay foundation consisting of an I-wall with a given exposed height and clay levee fill with a given height.

$$\begin{aligned} FS = {} & 1.3322 + 0.1073 s_{u0,f} + 0.0122 s_{u,l} - 0.3126 wl - 0.0302 D + 0.0247 X - 3.9512 S \\ & - 0.0007 s_{u0,f}^2 - 0.0002 s_{u,l}^2 - 0.0004 wl^2 + 0.0055 D^2 - 0.0003 X^2 + 3.7587 S^2 \end{aligned} \tag{5.3}$$

To ensure the accurate representation of overall stability of the system, the developed response surface was validated. To this aim, several randomly generated values for design and random variables were used for PLAXIS 2D simulation and the response surface. The results were compared as shown in Figure 5.9 and a very good agreement was observed between the two the FS values obtained from response surface and those obtained from PLAXIS 2D.

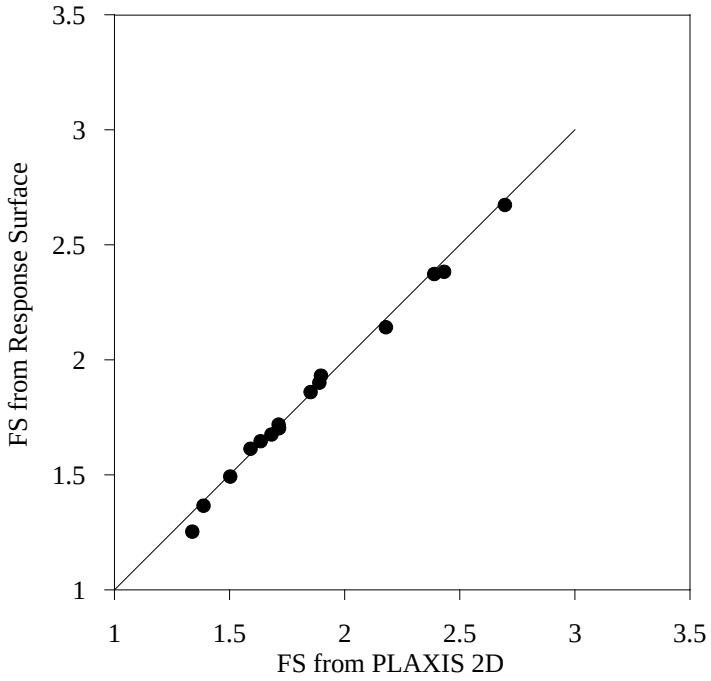

Figure 5.9 Graph of FS obtained from PLAXIS 2D and the response surface

5.6 COMPUTING PROBABILITY OF FAILURE OF THE SYSTEM

Probability of failure is typically used as a measure of safety in probabilistic design method and, in this study it was computed through Monte Carlo simulation based on the FS response surface presented in Eq. 5.3. In this step, for subset designs 3-9 listed in Table 5.4 N=1,000,000 samples were generated for the soil-related random variables which were assumed to be normally distributed ($s_{u0,f}$ = N (15,1.67) and $s_{u,l}$ = N (31,3.67)), and therefore N number of factors of safety (FS) were calculated. Assuming minimum acceptable FS of 1.5 and m as the number of factors of safety less than 1.5, probability of failure (P_f) of the system was calculated as below.

$$P_f = \frac{m}{N} \tag{5.4}$$

It should be noted that the flood water level varies between levee crown (0 m) and top of wall (2 m) and the variation of probability of failure was monitored with variation of flood water level as the loading-related random variable. As shown in Figures 5.10-5.12, the probability of failure of design cases (D_{min}, X_{mid}, S_{mid}), (D_{mid}, X_{min}, S_{mid}), and (D_{mid}, X_{mid}, S_{max}) increased to about 0.4-0.6 when the flood water level reached the top of wall. In similar flood situation, the P_f value of the design (D_{mid}, X_{mid}, S_{mid}) increased to about 0.4 and the P_f was found to be acceptable when the water level increased up to 1.0 m. The maximum water levels in which the P_f was considered acceptable for cases including D_{max}, D_{mid} and D_{min} (X and S at mid. value) were about 1.5 m, 1.0 m and 1.0 m, respectively. These water levels were found to be about 1.0 m for all cases including X_{max}, X_{mid} and X_{min} (D and S at mid. value), and 1.5 m, 1.0 m and 0.5 m for cases including S_{min}, S_{mid} and S_{max} (X and S at mid. value), respectively.

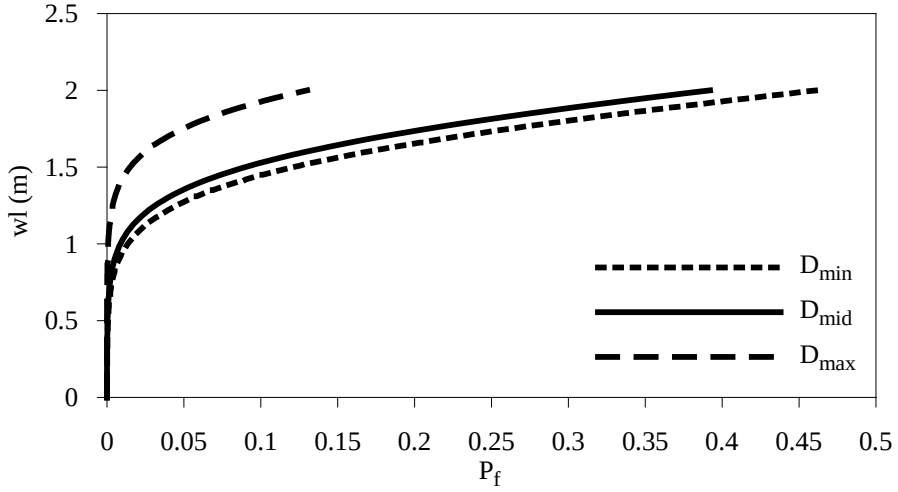

Figure 5.10 Variation of P_f with flood water level considering D

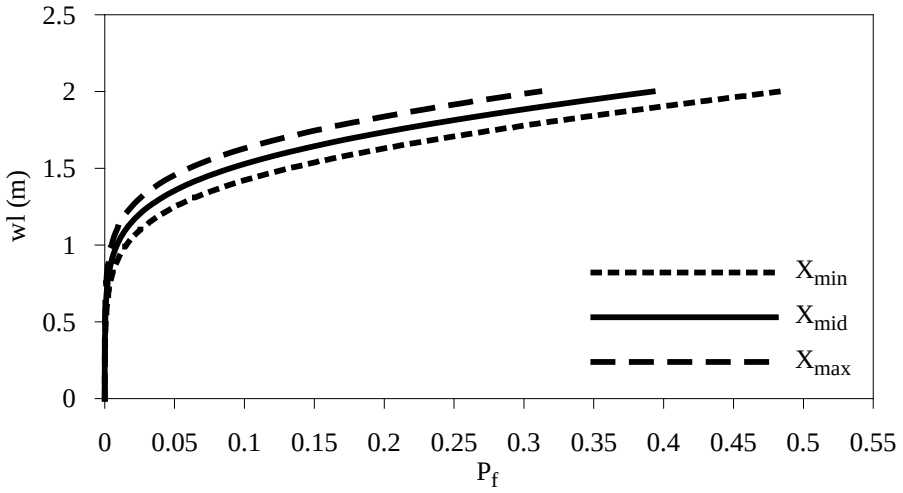

Figure 5.11 Variation of P_f with flood water level considering X

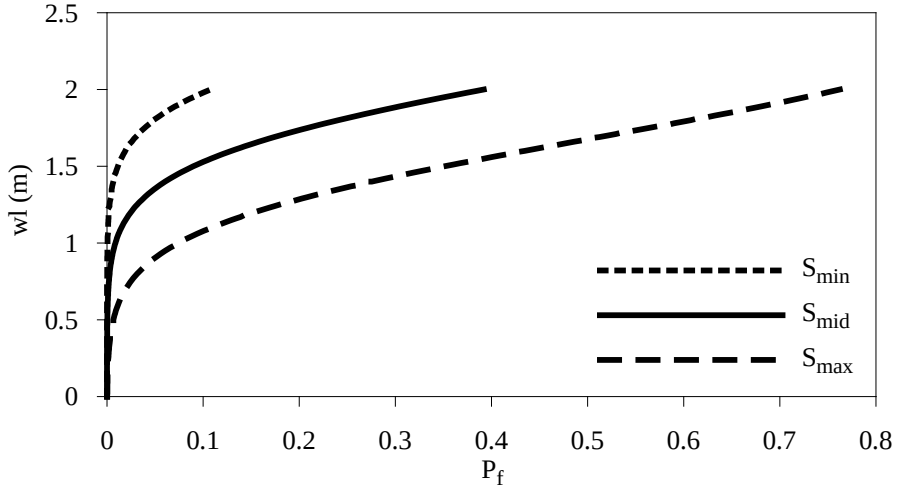

Figure 5.12 Variation of P_f with flood water level considering *S*

Overall, it can be concluded from Figures 5.10-5.12 that P_f of the I-wall levee system supported by clay foundation decreases with increasing *D*, increasing *X* and decreasing *S*. Moreover, P_f is the lowest when having the cases: (D_{max}, X_{mid}, S_{mid}) or (D_{mid}, X_{mid}, S_{min}). However, the allowable P_f (assumed to be 0.01) was exceeded and there may be more design cases that would meet the safety criteria through adjusting the

combination of design variables. It is worth noting that as reported by Jonkman et al. (2009) based on Congress authorization a flood protection system needs to withstand a hurricane event with an annual probability of occurrence of 1% (0.01) and the probability of failure of the system can be assumed equal to the probability of exceedance of design condition. Thus, the allowable P_f of 0.01 was considered in this study.

5.7 DESIGN OPTIMIZATION OF THE SYSTEM

5.7.1 Determination of Cost Function

The cost of I-wall levee system was considered as one of the objectives in the design optimization due to its influence on design and consequently the probability of failure. The cost function was defined considering the cost of those components in the system that include the design variables. Thus, a sheet pile wall of PZ-27 section with depth of D and a levee with crown width of X and landside slope of S contributed in cost function. The cost function for new construction is expressed as following:

$$C^{(USD/m)} = \left(H_{ex} + D\right)^{(m)} \times \left(\frac{W_{spw}{}^{(kg/m^2)}}{1000}\right) \times C_{sp}{}^{(USD/ton)} + \left(2X + 2H_l + \frac{H_l}{S}\right)^{(m)} \times H_l{}^{(m)} \times C_f{}^{(USD/m^3)}$$

(5.8)

where H_{ex}=2 m, W_{spw} is the weight of sheet pile wall (=131.8 kg/m^2), H_l is the height of levee (=3 m). C_{sp} is the unit cost of sheet pile wall (=\$2000/ton), and C_f is the unit cost of levee fill (= \$11/m^3), which include material, labor and equipment per RSmeans Building Construction Cost Data.

5.7.2 Non-robust Design Optimization

In this step, probability of failure was also considered as one of the objectives of the optimization along with the cost. The bi-objective optimization setting was established to balance the probability of failure with cost through minimizing both simultaneously using Non-dominated Sorting Genetic Algorithm (NSGA-ii) developed by Deb et al. (2002). It should be noted that in this type of design optimization the robustness was not considered and the I-wall levee design was optimized only based on cost and safety. In the optimization process for each design set, created by NSGA-ii based on the upper and lower limits of design variables, the probability of failure (P_f) was computed using Monte Carlo simulation with N=5000 and allowable P_f = 0.01 was assumed as a safety constraint. The soil-related random variables were assumed to be normally distributed ($s_{u0,f}$ = N (15,1.67) and $s_{u,l}$ = N (31,3.67)) and the flood water level was assumed to be uniformly distributed as wl=U (0,2). The Pareto front optimized to cost and P_f is displayed in Figure 5.13 and it is observed from that the probability of failure of the system increased from 0 to about 0.009 as the cost decreased from $3,500/m to $2,200/m.

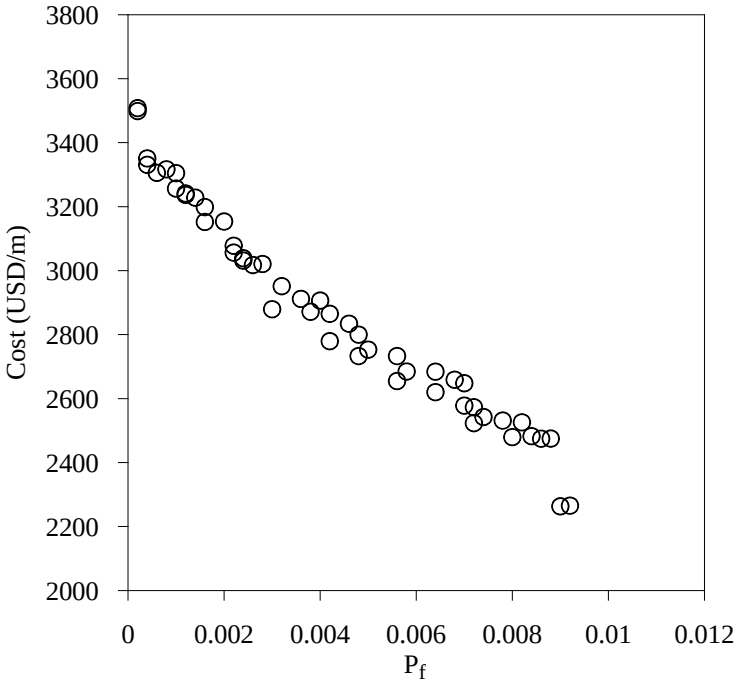

Figure 5.13 Non-robust Pareto front optimized to cost and P_f

5.7.3 Robust Design Optimization

The probability of failure of the system can be considered as a certain value when high quality data are used for soil properties in the system. But typically, due to insufficient sample size, measurement errors, and human errors uncertainties exist in assumed statistical characterization of soil properties and the computed probability of failure will vary under the effect of these variations (Juang et al. 2012; Juang et al. 2013). Therefore, in this step the standard deviation of probability of failure was considered as the measure of robustness and objective of optimization along with cost (Wang et al. 2015; Peng et al. 2016). Thus, the coefficient of variations (COV) of the soil-related random variables ($s_{u0,f}$ and $s_{u,l}$) were considered as uncertain parameters in optimization setting as: COV$s_{u0,f}$ = N (0.11, 0.022), COVs_u^l = N (0.12, 0.024).

In the optimization process, N number of P_f and their standard deviation were calculated using Monte Carlo simulation for each design set generated in NSGA-ii. The design optimization was performed by minimizing the cost, and maximizing the robustness which was achieved by minimizing the standard deviation of probability of failure. The Pareto front optimized to cost and standard deviation of P_f is shown in Figure 5.14 (for N=1000). A trade-off relationship can be observed between the two objectives as the standard deviation of P_f increased from 0 to about 0.0017, the cost decreased from about $3,500/m to $2,500/m. This indicates that higher robustness for design demands higher cost.

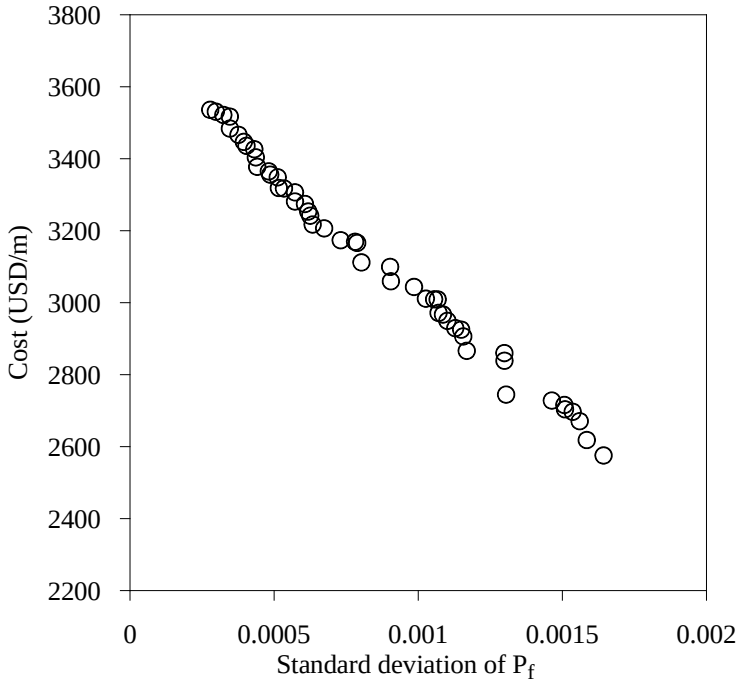

Figure 5.14 Robust Pareto front optimized to cost and standard deviation of P_f

5.7.4 Comparison of Robust and Non-robust Design Optimization

In this step, the Pareto front resulted from robust design optimization was compared with the one resulted from non-robust design optimization as shown in Figure 5.15. The robust Pareto front is located above the non-robust Pareto front showing slightly higher cost when robustness is considered in design. In other words, non-robust design optimization may lead to more cost-efficient designs than robust design, but reducing the sensitivity of the design via decreasing the variation of the response of the system (probability of failure, in this study) is the key to prevent the system from experiencing unexpected responses.

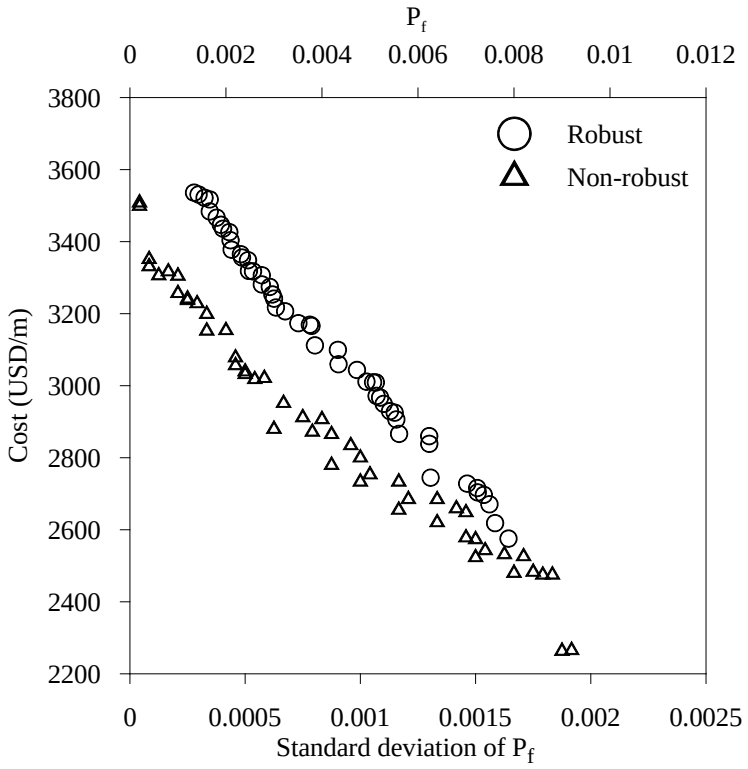

Figure 5.15 Comparison of robust and non-robust Pareto fronts

A better comparison was conducted by calculating the probability of failure of the captured robust designs obtained from robust Pareto front. Illustrated in Figure 5.16, the probability of failure of robust and non-robust designs are in a similar range 0-0.01, and the cost of robust designs are about $200/m higher than that of non-robust designs. It can be also observed from the figure that for a desired P_f of 0.005 the non-robust design costs about $2700/m while the corresponding cost of robust design is about $3000/m.

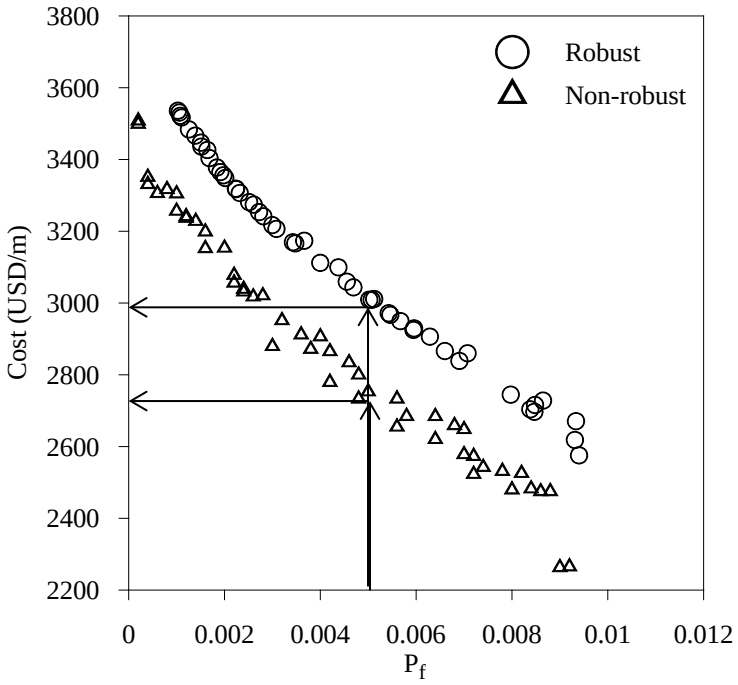

Figure 5.16 Comparison of robust and non-robust designs regarding P_f

5.7.5 Application of Pareto Fronts for Selecting Final Design

For determining the final optimal design with respect to cost and robustness, the minimum distance approach was used in this study regarding the straight-line shape of the Pareto front. As shown in Figure 5.17, the concept of utopia point, which is the ideal

unreal design with all objectives at their minimum, was implemented and the distance between each point on Pareto front and the utopia point was computed (Khoshnevisan et al. 2014). The point on Pareto front corresponding to the minimum distance was considered as the optimal design.

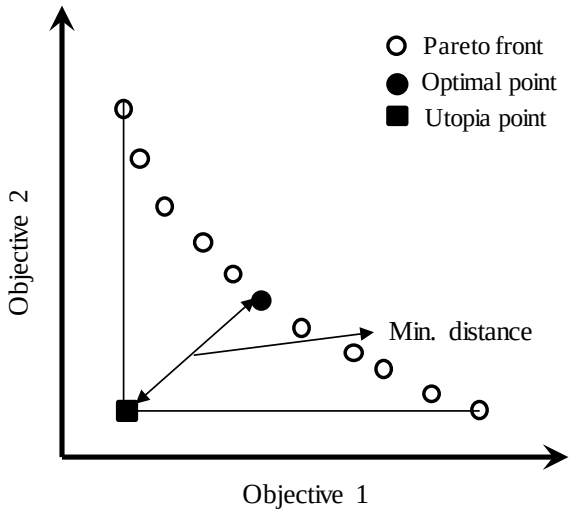

Figure 5.17 Minimum distance approach

The design parameters of optimal designs of I-wall levee system resting on clay foundation were obtained and summarized in Table 5.3 using robust and non-robust Pareto fronts. As it is observed, the optimal robust design included a levee with wide crown and mild slope on the landside, and a wall with depth of 6.39 m, which is considered as medium-deep wall per the ranges. On the other hand, the optimal non-robust design included an I-wall of medium depth. Based on the results, a mild land side slope (1V:4H) and wide levee crown is recommended for the final I-wall levee system supported by clay foundation. The increased depth of I-wall in optimal robust design increased cost of the system, but the robustness of the design increased at the same time.

This higher cost may seem unreasonable comparing to conventional designs but it helps reducing the unexpected variations of the system response.

Table 5.3 Optimal design properties for robust and non-robust optimization

Optimization type	***D* (m)**	***X* (m)**	***S***	**Cost (USD/m)**
Robust	6.39	6.00	0.25	3,112
Non-robust	5.54	5.87	0.25	2,879

Pareto fronts can also be used to obtain the final design based on the engineering preferences and available budget and desired level of robustness or cost can also be specified for designers. Moreover, additional constraints can be applied to the optimization setting and minimum FS and allowable P_f can be modified based on engineering judgments. These features increase the flexibility of this framework in ensuring the robust design optimization.

5.8 CONCLUSION

In this paper, the authors proposed a framework for probabilistic design optimization of I-wall levee systems resting on clay foundation considering the associated uncertainties in levee and foundation soils and in flood water level. The overall stability of the system was analyzed using finite element and limit equilibrium methods, and the effect of uncertainties was evaluated. It was found that the reference undrained shear strength of clay foundation and the flood water level had the most influence on factor of safety of the system among random variables and the width of

levee crown was the least effective among design variables. Based on a developed response surface for FS the probability of failure was computed using Monte Carlo simulation and it was concluded that design cases including maximum depth of I-wall or minimum landside slope experienced lowest probability of failures. Moreover, bi-objective design optimizations were performed to obtain non-robust (cost vs. probability of failure) and robust (cost vs. standard deviation of probability of failure) Pareto fronts. In the robust optimization, the robustness and cost-efficiency of the design were balanced by minimizing the standard deviation of probability of failure and the cost simultaneously and the results were compared with results of non-robust optimization. The obtained final optimal designs I-wall levee system consisted of medium to deep wall penetration, wide levee crown, and mild landside slope. The proposed approach can be introduced and implemented in design of flood protection systems in which the variations in soil properties and water elevation may lead to catastrophic failures.

REFERENCES

Phoon, K. K., & Kulhawy, F. H. (1999). “Evaluation of geotechnical property variability.” *Canadian Geotechnical Journal*, *36*(4), 625-639.

Juang, C. H., Wang, L., Liu, Z., Ravichandran, N., Huang, H., & Zhang, J. (2013). Robust geotechnical design of drilled shafts in sand: New design perspective. *Journal of Geotechnical and Geoenvironmental Engineering*, *139*(12), 2007-2019.

Sills, G. L., Vroman, N. D., Wahl, R. E., & Schwanz, N. T. (2008). Overview of New Orleans levee failures: lessons learned and their impact on national levee design and

assessment. *Journal of Geotechnical and Geoenvironmental Engineering*, *134*(5), 556-565.

Duncan, J. M., Brandon, T. L., Wright, S. G., & Vroman, N. (2008). Stability of I-walls in New Orleans during hurricane Katrina. *Journal of Geotechnical and Geoenvironmental Engineering*, *134*(5), 681-691

Interagency Performance Evaluation Task Force IPET. (2007). Performance evaluation of the New Orleans and Southeast Louisiana Hurricane protection system. *Final Rep. of the Interagency Performance Evaluation Task Force*, U.S. Army Corps of Engineers

Sasanakul, I., Vanadit-Ellis, W., Sharp, M., Abdoun, T., Ubilla, J., Steedman, S., & Stone, K. (2008). New Orleans levee system performance during Hurricane Katrina: 17th Street Canal and Orleans Canal North. *Journal of geotechnical and geoenvironmental engineering*, *134*(5), 657-667

Ubilla, J., Abdoun, T., Sasanakul, I., Sharp, M., Steedman, S., Vanadit-Ellis, W., & Zimmie, T. (2008). New Orleans levee system performance during hurricane Katrina: London Avenue and Orleans canal south. *Journal of Geotechnical and Geoenvironmental Engineering*, *134*(5), 668-680.

Seed, R. B., Bea, R. G., Abdelmalak, R. I., Athanasopoulos, A. G., Boutwell Jr, G. P., Bray, J. D., ... & Collins, B. D. (2006). Investigation of the Performance of the New

Orleans Flood Protection System in Hurricane Katrina on August 29, 2005. *Independent Levee Investigation Team: Final Report*

Tung, Y. K., & Mays, L. W. (1981). Risk models for flood levee design. *Water Resources Research*, *17*(4), 833-841.

Hui, R. (2014). Optimal design of levee and flood control systems. *Doctoral dissertation, University of California, Davis.*

Brinkgreve, R. B. J., Kumarswamy, S., & Swolfs, W. M. (2015). Plaxis 2D Manual. *PLAXIS bv, The Netherlands.*

Khuri, A.I., and Mukhopadhyay, S. (2010). "Response surface methodology." *WIREs Computational Statistics*, Vol. 2, pp. 128-149

Jonkman, S. N., Kok, M., Van Ledden, M., & Vrijling, J. K. (2009). Risk-based design of flood defence systems: a preliminary analysis of the optimal protection level for the New Orleans metropolitan area. *Journal of Flood Risk Management*, *2*(3), 170-181.

Waier, P. R., Babbitt, C., Baker, T., Balboni, B., & Bastoni, R. A. (2010). RSMeans: Building Construction Cost Data 2010.

Deb, K., Pratap, A. and Agarwal, S. (2002). "A fast and elitist multiobjective genetic algorithm NSGA-II." *Evolutionary Computation*, 6(2), 182-197.

Juang, C. H., Wang, L., Atamturktur, S., & Luo, Z. (2012). Reliability-based robust and optimal design of shallow foundations in cohesionless soil in the face of uncertainty. *Journal of GeoEngineering*, *7*(3), 75-87.

Wang, L., Gong, W., Luo, Z., Khoshnevisan, S., & Juang, C. H. (2015). Reliability-based robust geotechnical design of rock bolts for slope stabilization. In *IFCEE 2015* (pp. 1926-1935).

Peng, X., Li, D. Q., Cao, Z. J., Gong, W., & Juang, C. H. (2016). Reliability-based robust geotechnical design using Monte Carlo simulation. *Bulletin of Engineering Geology and the Environment*, 1-11.

Khoshnevisan, S., Gong, W., Wang, L. and Juang, C. H. (2014). "Robust design in geotechnical engineering–an update." *Georisk: Assessment and Management of Risk for Engineered Systems and Geohazards*, 8(4), 217-234.

Coduto, D. P. (1999). Geotechnical engineering: principles and practices. *Pearson College Division*.

USACE. (2000). EM-1110-2-1913, Engineering and design: Design and construction of levees

CHAPTER 6

SUMMARY AND CONCLUSION

6.1 SUMMARY OF DISSERTATION

In this dissertation, a robust geotechnical design optimization framework was developed for retaining walls subjected to earthquake load and I-wall levee systems subjected to flood. Through the framework, the uncertainties in engineering properties of soils (backfill in retaining walls, levee fill and foundation in I-wall levee systems), also called as random variables, were considered along with the uncertainty in the external load (earthquake in retaining walls and flooding in I-wall levee systems). The key design variables of these two systems were determined and based on their ranges several design cases were generated. For computing the respective responses of concern numerically finite element analyses were performed and appropriate response surfaces were developed and validated for the respective responses of concern. Using the response surface and suitable optimization setting (in terms of objective functions and constraints), the designs of these critical geotechnical systems were optimized to cost and robustness while satisfying the safety constraints simultaneously. Sets of preferred designs, known as Pareto fronts, were captured through the bi-objective robust optimizations that can be used as a decision-making tool in engineering practice. The characteristics of the systems are summarized in Table 6.1.

Table 6.1 Summary of framework characteristics for retaining wall and I-wall levee system

Characteristic	Cantilever retaining walls		I-wall levee systems	
	Sand backfill	**Shredded tire backfill**	**Sand foundation**	**Clay foundation**
Uncertainties	- Friction angle of backfill - PGA of earthquake load	- Friction angle of backfill - Cohesion of backfill - PGA of earthquake load	- Friction angle of sand foundation - Undrained shear strength of clay levee fill - Water level of flood load	- Undrained shear strength of clay foundation - Undrained shear strength of clay levee fill - Water level of flood load
Design variables	- Width of the wall footing - Width of the wall toe - Thickness of wall stem - Thickness of wall footing		- Depth of penetration of I-wall - Width of the levee crown - Landside slope of the levee	
Analysis type	Dynamic deformation analysis		Stability Analysis	
Response of concern	Wall tip deflection		Factor of safety of the system	
Response surface model	Logarithmic		2^{nd} order polynomial	
Safety and serviceability constraint	- Target reliability index - Allowable wall tip deflection		Allowable probability of failure	
Robustness measure	- Standard deviation of wall tip deflection - Signal-to-noise ratio		- Standard deviation of probability of failure	

6.2 MAJOR FINDINGS

The dissertation's major findings are listed as below:

- The robust geotechnical design optimization framework that considers the uncertainties in the engineering properties of soil and load is unique and can be considered as a beneficial tool for design of retaining walls and levees preventing overdesign and underdesign of these critical systems because of safety and cost, respectively.
- The uncertainties in loading due to natural disasters such as earthquake and flooding were found to be as important as the uncertainties in the soil properties of the system, and must be taken into account in the design of critical systems especially in earthquake-prone and flood-prone areas.
- The robust design Pareto fronts obtained from bi-objective optimization, which are optimized to robustness and cost, can be readily used by engineers to select a suitable design based on cost limitations and performance requirements.
- Depending on the type of geotechnical system, different robustness measures are considered based on the safety and serviceability aspects of the system. For example, in this study as the robustness measure, standard deviation of wall tip deflection was used in optimization of retaining walls and standard deviation of probability of failure was adopted in optimization of I-wall levee systems.

- Depending on the statistics of random variables, different methods such as Monte Carlo simulation (MCS), Taylor Series Finite Difference (TSFD) and First Order Second Moment (FOSM) are used for computation of robustness measures for which the variations in response due to the variations in random variables need to be calculated.
- The constraints of the optimization setting are included based on engineering preferences in terms of safety and serviceability criteria and their acceptable values, and the range of design variables (new range must be a subset of original range based on which the response surface was established).
- The response surface approach can be considered as an efficient method to predict the response of a system without the need of performing hundreds of advanced (and time-consuming) simulations. Response surface of a system as used in this study simplifies the link between the complex analyses and the optimization process.

6.3 RECOMMENDATIONS FOR FUTURE WORK

- Geotechnical design optimization of various critical systems subjected to various loadings due to natural disasters may be performed using the proposed framework in this dissertation.
- Uncertainties in earthquake load can be considered systematically in other seismic parameters such as frequency content, duration of the ground motion.
- In retaining wall design, the uncertainties in in-situ soil properties can be considered along with the uncertainties in backfill material. The inclination of

the backfill material in contact with in-situ soil can be considered as a design variable in design optimization. In addition, if sloping backfill surface is used in design, the slope of backfill can also contribute in optimization as a design variable.

- In I-wall levee systems, if complicated soil profile is used in foundation, the uncertainties in material of different of layers can be considered. In addition, their effect on overall stability of the system can be investigated.
- For design optimization of coastal I-wall levee systems that run along the shoreline the wave action of the water load need to be considered.